2006

Analysis of hot rolling events that lead to ridge-buckle defect in steel strips

Wanda Maria Carolina Melfo
University of Wollongong

Analysis of hot rolling events that lead to ridge-buckle defect in steel strips

A thesis submitted for the award of the degree of

Doctor of Philosophy

from

UNIVERSITY OF WOLLONGONG

by

WANDA MARIA CAROLINA MELFO

BEng (Mech), MEng (Mat)

School of Mechanical, Materials and Mechatronics Engineering

2006

Certification

I, Wanda Melfo, declare that this thesis, submitted in fulfilment of the requirements for the award of Doctor of Philosophy, in the School of Mechanical, Materials and Mechatronics Engineering, University of Wollongong, is wholly my own work unless otherwise referenced or acknowledged. The document has not been submitted for qualifications at any other academic institution.

Wanda Melfo

August 2006

Acknowledgements

I wish to express my deep gratitude to my supervisor Prof. Rian Dippenaar for his support, patience and guidance throughout all these years. My thanks are also due to the team at BlueScope steel, specifically to Chris Killmore, Chris Carter and Jim Williams for their continuous interest and contribution to my studies.

To the students of the engineering faculty, good friends and excellent professionals, thank you for make each day a nice day. To the staff of the roll workshop and the hot strip mill research in BlueScope steel, for coping with my requests with patience and a smile. Many thanks to all the staff at the Engineering Faculty especially to Lorelle, Greg, Nick, Jose and David Wexler for their help and attentions

To my mum, one of the special women the world had. To my family, for their love that make me strong and free; and to all the friends in this and the other part of the world for being always present and make feel special. And most of all, thanks to Chris Brown for all his care, sharing and patience.

Finally, thanks to the Australian Research Council (ARC linkage grant LP0348927), BlueScope Steel and the University of Wollongong for funding the project.

Thank you all,

Wanda

Abstract

Thinly cold-rolled steel sheet, following hot-rolling, sporadically present a defect known in industry as ridge-buckle. The defect is only detected in the last stage of production of thin rolled strips, after they have been hot rolled, cold rolled, annealed and tempered. Ridge-buckle consists of sinusoidal waveforms located in one or two bands near the central region of the strip width and in most cases, affecting the full length of the strip. Coils with such a defect have to be discarded or degraded. The aim of this manuscript is to present our contribution towards an elucidation of the origins of ridge-buckle defect by experimental and theoretical approaches combined with analysis of plant data.

We explored two of the main factors that in the past, has been regarded as possible origins of ridge-buckle defect: a) the occurrence of microstructural variations along the width of the hot rolled strip, which could lead to different extents of deformation during cold rolling and subsequent operations; and b) the presence of a protuberance (also called ridge) on the hot rolled strip, which will directly affect the shape of the cold rolled strip.

The possibility that variations in grain size or crystallographic texture along the width of the strip could contribute to the formation of ridge-buckle defect was explored by studying samples extracted from strips hot-rolled in the industrial process. We determined experimentally and compared quantitatively, the ferrite grain sizes and the crystallographic orientations of grains along the width of the strip. In the strips studied, no evidence was found of any statistically significant variations in these two microstructural variables.

Empirical models of recrystallization were used in an attempt to gain a better understanding of the quantitative impact of minor temperature variations (of the order experienced in practice) on the strip strength and hence, its mechanical behaviour within the rolling process. This exploratory exercise confirmed that the strip strength during hot rolling varies very little as a result of relatively small variations in temperature along the width of the strip. Furthermore, the ferrite grain size developed following hot-rolling and cooling on the run-out table, also varies very little due to the temperature variations measured. Therefore, the strength of the hot rolled strip along its width is not affected to the extent that can have a significant influence on the deformation in the subsequent rolling processes. These calculations led us to conclude that ridge in the hot rolled strip is not related to uneven deformation during rolling due to strength variations and hence, ridge-

buckle defect cannot be attributed to strength differences along the width of the hot-rolled strip.

In industrial practice, the occurrence of ridge-buckle in subsequent cold rolling operations has been linked to the presence of ridges in the hot rolled strip. Moreover, a modelling study conducted in parallel with this investigation confirmed this link. Having established that variations in microstructure, texture or strength along the hot-rolled strip width are unlikely causes of the occurrence of ridge-buckle defect we attempted to link ridge occurrence in hot rolled strips and to uneven roll-wear in the finishing mill. By collecting data of 40 consecutive schedules, we were able to determine that ridge formation in hot rolled strips is a common occurrence. Moreover, uneven roll-wear was frequently observed, at least in the period and in the schedules over which our data were collected. A significant finding was the establishment of a strong link between ridge occurrence on the hot-rolled strips and uneven roll wear occurring close to the centre of the work-rolls in the finishing-mill.

The evidence of uneven wear on the work-rolls in the hot strip mill led our study to an assessment of the possible causes of uneven roll-wear. A thorough review of the available literature in conjunction with the evidence we found of excessive ridge formation in steels containing silicon, led to the hypothesis that the integrity of the tertiary strip scale in the roll bite could be a major contributing factor to uneven roll-wear.

We developed a method to study in-situ the formation of oxides on the hot steel substrate, by adapting a High Temperature Microscope with means to introduce air instantaneously onto the surface of the sample. This technique enabled us to study oxidation of the steel surface under conditions closely simulating the oxygen potential pertaining to the rolling temperatures in industrial finishing rolling practice (excluding the complicating effects of water cooling). The in-situ experimentation was complemented with a thorough characterisation of the oxides remaining on the samples after cooling by using relevant metallographic techniques.

The experiments were conducted on two types of steel, low carbon steel and silicon containing steel. The results show distinctive differences in the oxidation behaviour of the two types of steel. The low carbon steel form a typical three-layered structure of iron oxides although with very little (almost undetectable) hematite formation. On the other hand, the silicon steels, which apart from silicon also

contain aluminium and manganese in small amounts, formed a thick interface layer of complex oxides and intermetallics between the substrate and a layer of magnetite followed by a hematite layer at the gas/oxide interface. It was evident that in silicon steels, the formation of the interface layer interfered with the diffusion of iron species as the final oxide layer was significantly thinner than the oxide layer that formed on low-carbon steel.

Another significant finding in the case of low carbon steel was the tendency of the oxide to detach or “spall” from the surface during oxide growth. We were able to observe the detachment of the oxide in-situ with precise account of the time and temperature of occurrence. The relevance of this finding is that if sufficient time elapsed between spallation of the scale and the strip entering the roll-bite, brittle scale would form (due to isolation of the oxide layer from the iron source). The scale then will fracture under the loads applied in the roll-bite, affecting the heat transfer to the rolls and hence, its thermal fatigue resistance. Furthermore, we were able to observe and determine the time to nucleation of new oxides that form on top of already existing oxides on low carbon steel substrate. The time required to nucleate the new oxide is related to the austenite grain size of the steel substrate. Further studies are proposed to elucidate the exact nature of this interesting sequence of events.

Finally, early oxidation events were linked to uneven roll-wear due to fracture of the scale in the roll-bite, an increase in the heat transfer rate to the work-roll surface and friction in the roll-bite. An assessment of the possible causes that may affect the integrity of the tertiary scale led us to conclude that whenever uneven changes occur in the cooling patterns of the strip or roll, in descaling efficiency or in the lubrication systems, uneven roll-wear could result.

Although a definitive solution to the 40-year old problem of ridge-buckle defect is still to be found, we have made advances in narrowing the possible origins of the defect to specific causes or events. Ridge-buckle is originated mainly by the presence of ridge in the hot-rolled strip; in turn, ridge occurrence is related to uneven wear of the work-rolls in the finishing-mill. Uneven wear is most likely caused by failure of the tertiary scale, due most probably to uneven cooling and/or lubrication patterns during the hot rolling process. In addition to these findings, a novel method of studying scale formation during the early stages of the interaction between oxygen and the steel substrate was developed.

Table of contents

Chapter 1
Introduction

Ridge-buckle defect has been afflicting cold rolled steel strip production for more than forty years. Cold rolled coils with such a defect should be discarded or degraded, representing losses of millions to the industry. The main difficulty in determining the root cause of ridge-buckle defect is its sporadic occurrence which impedes a systematic study of the problem. A concise report describing the occurrence of ridge-buckle was presented by Gilbertson in 1965 and almost 40 years after, Blazevic (2002) published an extensive description of his practical experience towards finding a solution to the defect in steel industries world-wide. Despite these and many other efforts, it has not been possible to find unambiguous links between its incidence and specific variations of plant parameters or practices. Definitive answers as to the underpinning cause of the defect occurrence have not been established to date.

The aim of this manuscript is to present our contribution towards an elucidation of the origins of ridge-buckle defect by experimental and theoretical approaches combined with analysis of plant data. We conducted experiments with products from BlueScope Steel and the plant data were extracted from the hot-strip mill located in their Port Kembla Steel-Works in Australia. Although a definitive solution to the 40 year old problem is still to be found, we have made advances in narrowing the origin of the defect to specific causes. In addition, we are presenting studies aimed at a more complete understanding of the fundamentals of the early formation of oxides on steel at high temperature.

1.1 Ridge-buckle defect

Ridge-buckle defect consists of sinusoidal waveforms between 100 and 200mm in width, up to around 3mm amplitude and a pitch of about 200-300mm appearing on the central region of thin strips (~0.4 mm thick) following cold rolling, annealing and tempering. Figure 1.1 shows a photograph of an uncoiled steel strip with the defect manifested after tempering and a schematic illustration depicting the nominal dimensions of the defect and characteristic build-up that evidence its occurrence in a coil.

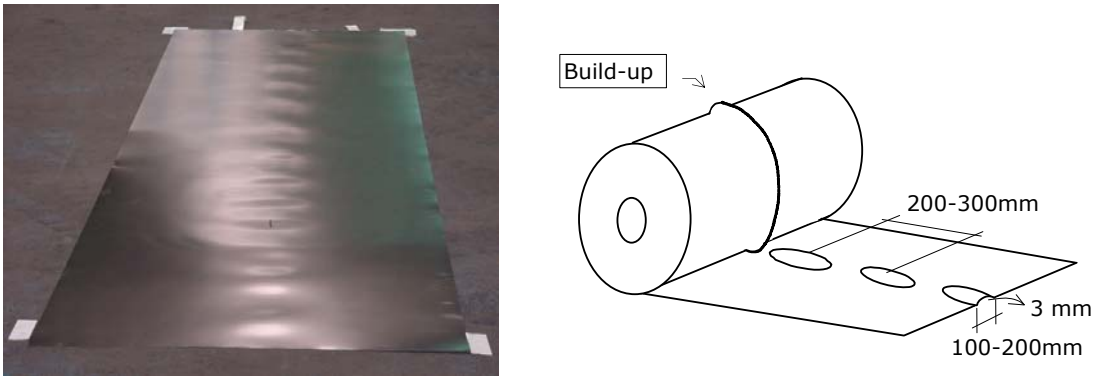

Figure 1.1 Schematic illustration of a coil presenting ridge-buckle defect and a photograph of tinplate strip affected by ridge-buckle. (Photograph was taken by Chris Carter at BlueScope Steel's Port Kembla temper-mill).

Although the defect manifests itself only after tempering, the whole process of thinning the steel from slab into strip depicted in Figure 1.2, can influence its occurrence.

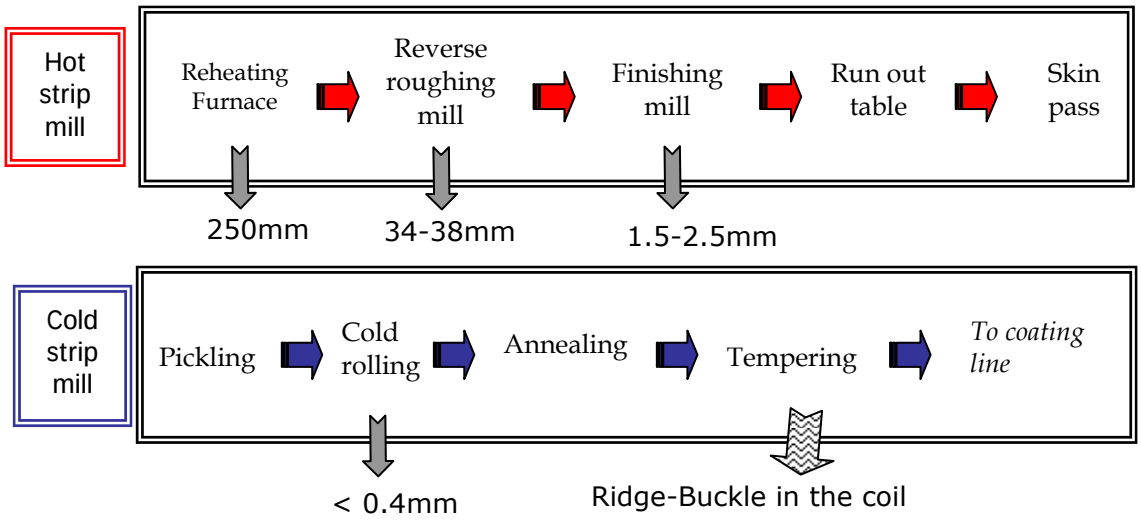

Figure 1.2: Schematic flow-chart of the rolling process from slab to thin-rolled strip coil. The thickness of the steel obtained after each processing is also detailed.

The production process of a cold rolled steel strip of which the Port Kembla Steelworks of BlueScope Steel is an example, starts in the reheating furnace where steel slabs produced by the continuos casting process, with a thickness of 250mm, are heated to approximately 1200ºC. Once extracted from the furnace, slabs are rolled individually in 7 or 9 passes through the reverse roughing-mill until a thickness of 34–38mm is attained. The slab at this stage is referred to as a 'transfer bar' and enters the finishing mill at approximately 1000ºC to be further reduced in

thickness. The finishing-mill consists of 6-stands of 4-high roll, operating in tandem, referred to as F1 to F6 from entry to exit, where the transfer bar is reduced to strips of typically 1.5 to 2.5mm in thickness. The hot-rolled strip is then cooled on the run-out table to approximately 600ºC and coiled. Further reductions to thickness below 0.4mm are executed in a five-stand cold-rolling mill after the strip has been chemically etched (pickling process) to eliminate residues of oxides. The required mechanical properties are achieved by batch or continuous annealing of the coils followed by a final reduction to strictly controlled dimensions in a double-stand temper-mill under tension. It is in the coil of tempered strips with thickness less than 0.4mm where the ridge-buckle defect is manifested.

1.2 On the origins of ridge buckle defect

Different authors (Gilbertson, 1965; Blazevic, 2002; Christoph et al, 1959 and Park et al, 1994) agree that the ridge-buckle defect should originate from inconsistencies in the hot rolled strip, leading to uneven deformation of the strip when cold rolled and tempered. These and other authors have identified two common denominators linked to the origin of uneven deformation:

a) The presence of centre ridges in the hot-strip
b) Localised differences in microstructure or crystallographic texture in the hot-strip

1.2.1 Ridges in hot-rolled strips

The thickness of the strip is measured by a thickness profile-meter consisting of two high-energy X-ray detectors with multiple beams and a linear scintillation based detector array, located at the exit of the finishing-mill as shown in Figure 1.3. The signal generated from the profile-meter, corresponding to the profile of the strip in multiple zones along its length, is averaged and presented as a single curve. A ridge is a protuberance above the ideal thickness profile, located along the width of a hot rolled strip and affecting presumably all its length as shown in Figure 1.4.

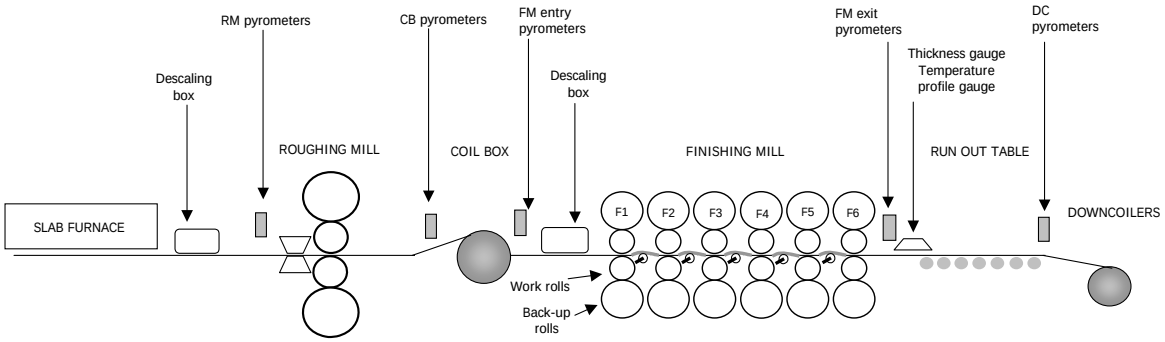

Figure 1.3. Schematic illustration of the hot strip mill located at the BlueScope Steel Port Kembla works.

Ridges can be located at the edges of the strip or alternatively in locations other than the edges; a case called centre ridge, as shown in Figure 1.4. Instead of the contour of the strip, it is the average thickness of the strip that is presented on the profile-meter graph and therefore, the location of the ridge with respect to the bottom or the top of the strip cannot be determined.

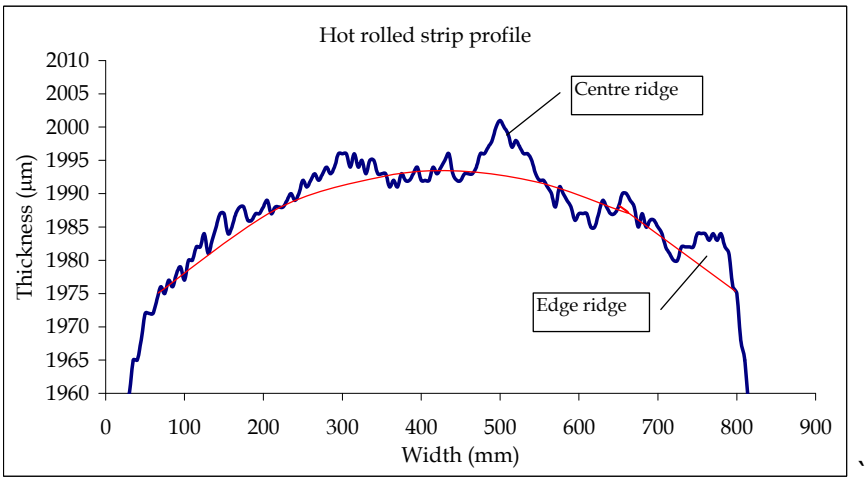

Figure 1.4. Profile of a hot-rolled strip as detected by the X-ray profile-meter. The strip in the figure contains a centre ridge as well as an edge ridge. The thin grey line corresponds to the ideal parabolic shape of the strip

Slabs exiting the reheating furnace are programmed to be rolled in schedules. A schedule is delimited by the exchange of the six sets of finishing-mill work-rolls. Work-rolls, which are the rolls in contact with the strip, are inserted at the start of the schedule following precise grinding to working dimensions, and extracted after a pre-determined number of slabs have been rolled. The rolls are usually extensively worn at this stage. From a minimum of 40 up to a maximum of 150 slabs can be rolled in each schedule. Each strip profile can be monitored on-line by the mill operator, the first occurrence of ridges in a strip of a schedule is only a few

microns in height, and can be detected when it reaches a height of approximately 5μm. In the following strips of the schedule the height of the ridge might increase or disappear. When the height increases or other ridge peaks appear in the following strips, the operator is obliged to intervene. Increasing the delay time between each strip, meaning longer reheating time in the furnace is usually the first measure to be taken. The last resource applied when the height of ridges is evidently increasing from strip to strip, is to change the work-rolls before the programmed end of the schedule.

In an extensive plant trial, Carter (2002) tracked hot rolled strips with ridges through the subsequent processing steps to the final tinplate coil. He demonstrated that ridge-buckle in the final product developed in the same positions where ridge was located on the hot-rolled strip. Carter (2002) furthermore provided convincing evidence that it is this centre ridge, when it exceeds 7μm in height, that is mainly responsible for the development of ridge-buckle defects in subsequent cold rolling of the strip. Other researchers have also acknowledged the fact that ridge-buckle defect originates from ridges present in the hot-rolled strip although few attempts have been made to determine the origin of these ridges (Gilbertson, 1965; Christoph *et al*, 1959 and Park *et al*, 1994). Gilbertson (1965) found excessive cooling in bands of the strip being hot-rolled, leading to uneven roll-wear which in turn affected strip shape causing ridges. Localised thermal-expansion of the rolls has been proposed by Blazevic (2002) as a cause of ridge formation, although he failed to provide convincing evidence of his proposal. Park *et al* (1994) presented arithmetic calculations to illustrate the nature of ridge-buckle describing it as a hump or excess thickness in the material that is stretched in excess to the rest when tempering under tension, therefore it buckles when the coil is uncoiled. Park *et al*'s (1994) conclusions reinforce the premise that ridge buckle defect is related to a ridge originating in the hot-rolling process.

1.2.2 Metallographic differences in the hot rolled strip

The second proposal on the origins of ridge-buckle is the presence of localised differences in microstructure or crystallographic texture in the hot rolled strip. Metallographic studies conducted by Rocquet *et al* (1965) on transverse cuts of hot-rolled strip that developed ridge buckle defect when cold-rolled, revealed differences in grain size at the surface of the strip corresponding to the zones where ridge-buckle occurred. They found that relatively small grain sizes on the strip surface could be linked to the formation of ridge-buckle in further rolling operations. The evidence provided by Rocquet *et al* (1965) has not been confirmed

by other researchers and the origins of the grain size inconsistencies have not been fully evaluated. Differences in grain size on hot rolled strip should be related to recrystallization behaviour during hot-rolling and the factors affecting recrystallization may also generate preferential grain orientation or crystallographic texture on the hot rolled strips which, in turn, may also lead to uneven deformation of the strip when cold rolled. A seemingly related phenomenon is observed in cold-rolling of stainless steel, where preferential orientation in clusters of grains with certain crystallographic orientations leads to uneven deformation during rolling (Takechi *et al*, 1967 and Chao, 1967). Microstructural or perhaps textural differences in bands of the strip may be one of the causes of ridge-buckle defects and we pursued further studies of this possible cause.

In summary, the literature suggests two main different causes which are presented in Figure 1.5.

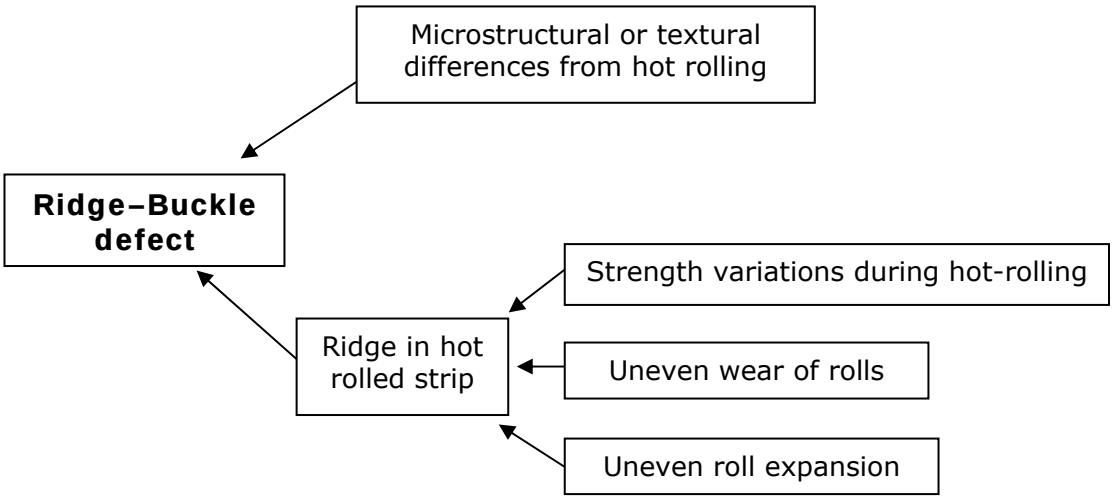

Figure 1.5. Schematic representation of the possible origins of ridge-buckle defect.

In the next chapters two of the proposed possible causes of ridge-buckle defect will be further explored: microstructural or textural differences and uneven wear of finishing-mill work-rolls. Our colleagues at the University of Wollongong (Zhu *et al*, 2006) are in the process of developing physically based mathematical models to predict how ridge-buckle defect can develop due to cold rolling and tempering when the hot-rolled strip contains ridges. In this contribution we shall concentrate on our analysis of in-plant data, the objective of which is to determine if uneven work-roll wear could lead to the formation of ridges in hot-rolled steel strips.

The relative importance of microstructural (or crystallographic textural) differences and the formation of ridge in hot-rolled strip will be further evaluated in the context

of the problems affecting particularly BlueScope Steel rolling plants. Two of their products, which are reduced to thicknesses below 0.4mm, sporadically present ridge-buckle defect: strips to manufacture food and beverage cans (tinplate) and strips for electric motors (commonly called silicon steels). Approximate compositions of those two steels are presented in Table 1.1.

Table 1.1 Approximate composition of the steels presenting ridge-buckle defect

	Composition (%mass, bal.Fe)						
	C	Mn	P	Si	S	Cr	Al
Low-carbon	0.045	0.21	0.012	<0.005	0.014	0.015	0.03
Silicon steels	0.003	0.4	0.034	0.57 - 1	n/a	0.025	0.30

Chapter 2 contains a critical literature analysis on recrystallization during hot-rolling, roll wear studies in hot-rolling mills, and the formation and integrity of scale on the strips and rolls. In chapter 3, hot-rolled strips from the compositions of interest are analysed to determine if the presence of microstructural or textural differences can lead to ridge-buckle defect. In chapter 4, empirical recrystallisation models are applied by using in-plant conditions to calculate the grain size developed during finishing-rolling and the effect that observed temperature variations could have in the microstructure during rolling and after cooling. Chapter 5 contains an analysis of plant data, to determine whether work-rolls from the finishing mill, undergo uneven wear and the relationship with the occurrence of ridge in hot rolled strip. The results from chapters 3, 4 and 5 lead to the experimental approach in chapter 6, which consists on a study of scale formation in the strips on the short times of finishing rolling. Finally, the practical relationship between the experimental results and the origin of ridge-buckle defect is presented in chapter 7.

Chapter 2
Literature analysis

In this chapter a critical analysis will be presented on selected aspects of the extensive literature concerned with hot rolling principles, in order to assess two of the possible causes that may contribute to the formation of ridge-buckle defect: metallographic differences in the hot-strip during hot rolling and uneven roll-wear that may lead to ridge on hot-rolled strips. To begin with, a brief description of the processes of recrystallization occurring during hot rolling and the available empirical models are presented. This description is followed by details of selected existing techniques to analyse microstructure and crystallographic textures. The second part describes mechanisms of roll-wear and possible origins of uneven roll-wear reported on the literature. Finally, as the interaction between roll surface and strip scale induces roll-wear; this chapter concludes with an analysis of literature on scale formation during hot-rolling, factors affecting the integrity of the scale and methods by which scale formation and scale/roll interaction have been studied.

2.1 Recrystallization during hot rolling

During hot rolling, the material is compressed in the normal direction (thickness) while it elongates in the rolling direction. As the hot material is deformed, dislocation density increases with the consequent strain hardening of the metal. Energy is stored in the metal due to accumulated strain around the newly created dislocations. The process of recovery consisting on the relief of the stored energy by virtue of dislocation motion and annihilation is enhanced by the high atomic diffusion at elevated temperature (Callister, 2003, p. 181). The dislocation density is reduced only a little during recovery and in the remaining zones of high dislocation concentration, the high energy accumulated will induce the nucleation or recrystallization of new strain-free grains. New grains are created by the reorganisation of dislocations into high angle grain boundaries. High angle grain boundaries are more mobile than low angle grain boundaries. The size of the newly formed grains will increase with time but tends to approach to a size limit because the mobility of the boundaries decreases with increasing disorientation (Guy, 1960, p. 425). The structure is then fully recrystallised when the grains have achieved their limit size driven by the accumulated strain energy. Nevertheless, because of the high atomic mobility at high temperatures, those grains can continue growing

driven by the reduction of energy occurring when the grain boundary area is reduced. The combined recovery, recrystallization and grain growth processes will reduce the strength of the material, which now can be re-rolled under virtually the same loads applied in the previous deformation.

A simplified stress flow curve of austenite grains being deformed at constant strain rates is depicted in Figure 2.1. The stress increases while the material is deformed due to combined work hardening and recovery (RV); the dislocation density increases and subgrain structures are developed (Sellars *et al*, 1979). When a critical strain at point C (ε_c) is achieved, the material undergoes dynamic recrystallization (DRX). During DRX, as the dynamic recovery is relatively slow, the subgrain boundaries are ill formed and sufficient strain energy is stored to form nuclei of new, stress-free, grains while deformation is still occurring. The work hardening continues, but at a reduced rate due to the slow dynamic recovery and the onset of DRX, until the strain reaches a peak value at point P (ε_p). At this stage the stress is lowered because the rate of DRX is higher than the work hardening. With further deformation, the flow stress reaches a steady-state regime σ_s. On the other hand, if the strain applied is lower than the critical strain (ε_c), the material undergoes static recrystallization (SRX) and it will recrystallise after being deformed (Manohar *et al*, 2001).

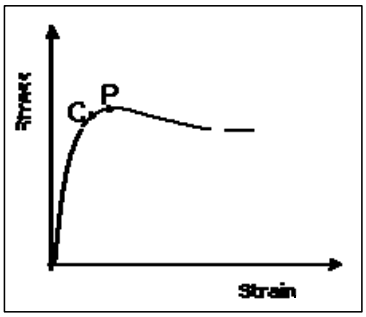

Figure 2.1. Schematic illustration of a flow curve for materials exhibiting dynamic recrystallization (see text) . Adapted from Sakai and Jonas (1984).

The extent to which recovery, recrystallization and grain growth occur is affected by the conditions of rolling and the steel composition. Rolling temperature (T) plays a major role in the mobility of dislocations, while the strain (ε) and strain rate ($\dot{\varepsilon}$) applied determine the accumulation of energy which is the main driving force for

recrystallization. A combination of these three parameters provides the basis for the empirical equations that have been developed by a large number of researchers in an attempt to predict the final grain size and hence, the mechanical properties of the hot-rolled strip.

After grains free of dislocations are formed, either under SRX or DRX, the grains will develop up to certain diameter, restricted by the number of newly formed grains, the activation energy for RX and the time they are allowed to grow. The time required to develop a fully recrystallised structure is referred to as t_{RX}. When new grains form by DRX, grain development is called meta-dynamic recrystallization (MDRX) as opposed to the process occurring in SRX where grains nucleate and grow after deformation. Further grain growth (GG) occurs if more time, at temperature, is allowed after SRX or MDRX. During GG, the smaller grains are eliminated, the larger grains grow and the grain boundaries assume a lower energy configuration (Humphreys, 1999).

Sellars (1979, 1980) defined general recrystallization equations for the calculation of grain size after MDRX or SRX and grain growth (Eq. 2.1 and 2.2).

$$d_{RX} = A d_0^{m} \varepsilon^{n} \dot{\varepsilon}^{b} e^{\left(\frac{Q_{RX}}{RT}\right)^{a}} \qquad \text{Eq. 2.1}$$

$$d_{GG}^{p} = d_{RX}^{p} + Bte^{\left(\frac{Q_{GG}}{RT}\right)} \qquad \text{Eq. 2.2}$$

where, d_{RX}: recrystallised grain size, d_0: initial grain size, Q_{RX}: activation energy for recrystallization, Q_{GG}: activation energy for grain growth R: ideal gas constant; and A, B, a, b, m, n, p: empirical constants that are material specific.

These empirical equations developed by Sellars, imply that the steel composition will have a determining influence on grain development during rolling. Alloying elements and impurities play an important role in the grain size developed during rolling. Tamura *et al* discriminate between microalloying elements such as Nb, V, Ti, Al and B; substitutional elements such as Si, Mn, Mo, Cu, Ni and Cr; and impurities formed by reaction with S, P, Ca and other rare earth metals. Microalloying elements form products such as carbides and nitrides which can be soluble or not under the pertaining rolling temperatures. These products contribute to the refinement of austenite grains and can modify the austenite recrystalization temperature. The substitutional elements can reduce or increase the transformation temperature from austenite to ferrite, refine the ferrite grains and even modify the

transformed microstructure. The inclusions do not influence the grain size developed, but can be detrimental to the mechanical properties of the steel and its deformability.

The effect of microalloying and substitutional elements can be variable along the slab thickness due to segregation. Segregation of microalloying elements to the centre of the slab can occur during solidification in the continuous caster and can affect recrystallization and the uniformity of grain size. Segregation of carbon to the surface during reheating also can play a role on the developed microstructure, mainly by modifying the transformation temperature.

The ferrite grain size after hot rolling is essentially determined by the austenite grain size achieved in the last stand of the hot rolling mill and the cooling rate on the run-out table. Furthermore, incomplete recrystallization as a result of accumulated strain during hot-rolling and prompt cooling will affect the transformation to ferrite, and hence the ferrite grain size.

2.1.1 Recrystallization models

The need to predict and control the mechanical properties of the final rolled product has driven numerous attempts to better understand and model the processes of recrystallization and grain growth. Being able to control the exact combination of chemical composition, temperatures, strain, strain rate and cooling rate that will lead to a desired final product, has been the main driver to develop recrystallization models. Two main approaches have been utilized to predict recrystallization; one may be called an empirical approach while the other is an atomistic approach.

Sellars and co-workers (1979, 1980) were the first to develop empirical modelling techniques for the hot-rolling of steel. They utilized the equations outlined above to calculate the fraction of recrystallised grains in a certain time (X_{RX}), size of the fully recrystallised austenite grains (d_{RX}) and the grain size after a defined growing time (d_{GG}).

Numerous research groups have made contributions to Sellars' empirical model. Samarasekera and co-workers (Devadas *et al*, 1991[a,b,c]; Muojekwu, 1997 and Samarasekera 1997) from the University of British Columbia developed a special project for the understanding of the hot-rolling process. They validated different available equations by single and double-hit hot-compression, and hot-rolling laboratory tests. Jonas and co-workers (Guthrie *et al*, 1990; Jonas, 1997, 2001;

Laasraoui *et al*, 1991; Sakai *et al* 1984 and Siciliano *et al*, 2000) made significant contributions to the dynamic recrystallization theory and proposed the use of rolling loads from industrial data to validate the models. Colas and collaborators (Colas, 1996, 1998; Zambrano *et al*, 2003) validated and adapted the models to industrial trials on C-Mn steels. Hodgson *et al* (1992) also validated the original Sellars equations using torsion tests to predict the properties of C-Mn, C-Mn-Ti and C-Mn-Nb steels following hot-rolling. These groups among others, and also Stumpf (2003), have been successful in predicting the microstructure of the final hot-rolled product in their own trials. Table 2.1 displays the main recrystallization model equations compiled and validated by Siciliano et al (2000), using mean flow stress (MFS) from industrial data, Devadas et al (1991c), using single and double-hit hot-compression tests and Stumpf (2003), by mill log analyses and hot-compression test. The equations in the form shown in Table 2.1 were selected specifically to comply with the conditions pertaining to a finishing-mill, so that they can be applied to the analysis of plain C-Mn steels.

Van Leeuwen (2000) argued that since the empirical models are influenced by variations in processing conditions such as composition and temperature, the empirical constants (Q_{RX}, Q_{GG}, A, B, a, b, m, n, p from equations 2.1 and 2.2) need to be determined experimentally each time. Moreover, it is common to encounter divergences on the constants proposed by different authors (Table 2.1 above) due to the variability on the conditions of the experimental trials. Such a variation is illustrated in the equations to calculate peak strain ε_p displayed in Table 2.1, although the values of the constants values do not appear to be greatly different, calculations using same values of the variables lead to quite different values of peak strain for each proposed equation.

The second approach to predict nucleation, recrystallization, grain growth and phase transformation is based on the mobility of grain boundaries, accumulated energy due to deformation and free energy influenced by the elements present in the alloy. Humphreys and Hatherly (1996) presented in comprehensive detail the fundamentals of recrystallization phenomena in annealing. More recently, Hanlon *et al* (2001) and Humphreys (1999) included the role of plastic deformation during rolling in the kinetics of recrystallization. In addition to that, Van Leeuwen *et al* (2000, 2003) have modelled effectively the austenite-to-ferrite phase transformation.

The atomistic model enriches the understanding of recrystallization mechanisms but its industrial application is still limited mainly due to computational limitations which restrict the simulations to very short time periods and few variables. Both models, empirical and atomistic, are complementary in the perception of the microstructure evolution during hot rolling.

Table 2.1: Recrystallization models and their respective constituent equations relevant to the analysis of plain C-Mn steels. The equations were compiled from the studies of Devadas *et al* (1991), Siciliano *et al* (2000) and Stumpf (2003). (SRX: static recrystallization, DRX: Dynamic recrystallization)

Devadas *et al*	**Siciliano *et al***	**Stumpf**
Strain $\varepsilon = 1.155 \ln\left(\frac{h_0}{h_f}\right)$		
Strain rate $\dot{\varepsilon} = \frac{v\varepsilon}{(r(h_0 - h_f))^{1/2}}$		
Peak strain		
$\varepsilon_p = 4.9 \times 10^{-4} d_0^{0.5} \left(\dot{\varepsilon} \cdot \exp\left(\frac{312000}{RT}\right)\right)^{0.15}$	$\varepsilon_p = \left(\frac{1 + 20Nb}{1.78}\right) 2.8 \times 10^{-4} d_0^{0.5} \left(\dot{\varepsilon} \cdot \exp\left(\frac{375000}{RT}\right)\right)^{0.17}$	$\varepsilon_p = 1.3 \times 10^{-4} d_0^{0.3} \left(\dot{\varepsilon} \cdot \exp\left(\frac{330000}{RT}\right)\right)^{0.2}$
Critical Strain		
$\varepsilon_c = 0.8 \cdot \varepsilon_p$	$\varepsilon_c = \left(0.8 - 13Nb_{eff} + 112Nb_{eff}^2\right) \cdot \varepsilon_p$ $Nb_{eff} = Nb - \frac{Mn}{120} + \frac{Si}{94}$	$\varepsilon_c = 0.8 \cdot \varepsilon_p$
Condition for DRX : $\varepsilon > \varepsilon_c$		
Half recrystallization time		
For SRX		
$t_{0.5}^{SRX} = 3.67 \times 10^{-14} \varepsilon^{-0.86 d_0^{0.24}} \dot{\varepsilon}^{-0.28} d_0^{0.14} \exp\left(\frac{301000}{RT}\right)$	$t_{0.5}^{SRX} = 2.3 \times 10^{-15} \varepsilon^{-2.5} d_0^2 \exp\left(\frac{230000}{RT}\right)$	
For DRX		
$t_{0.5}^{DRX} = 0.4 \cdot \left(\dot{\varepsilon} \cdot \exp\left(\frac{300000}{RT}\right)\right)^{-0.8} \exp\left(\frac{240000}{RT}\right)$		$t_{0.5}^{DRX} = 0.4 \cdot \left(\dot{\varepsilon} \cdot \exp\left(\frac{238000}{RT}\right)\right)^{-0.8} \exp\left(\frac{240000}{RT}\right)$
Recrystallised fraction $X = 1 - \exp\left(-0.693\left(\frac{t}{t_{0.5}}\right)\right)$		
Diameter of grains after RX		
For SRX		
$d_{SRX} = 18.51 \cdot \ln\left(\frac{T}{973}\right) \cdot d_0^{0.374} \varepsilon^u \dot{\varepsilon}^{-0.1}$ $u = -0.5 d_0^{0.267} \left(\frac{973}{T}\right)^{3.933}$	$d_{SRX} = 343 \cdot d_0^{0.4} \cdot \varepsilon^{-0.5} \cdot \exp\left(\frac{-45000}{RT}\right)$	
For MDRX		
$d_{MDRX} = 1.8 \times 10^3 \cdot \left(\dot{\varepsilon} \cdot \exp\left(\frac{312000}{RT}\right)\right)^{-0.15}$	$d_{MDRX} = 2.6 \times 10^4 \cdot \left(\dot{\varepsilon} \cdot \exp\left(\frac{300000}{RT}\right)\right)^{-0.23}$	$d_{MDRX} = 2.6 \times 10^4 \cdot \left(\dot{\varepsilon} \cdot \exp\left(\frac{238000}{RT}\right)\right)^{-0.23}$
Accumulated strain $\varepsilon_i^a = \varepsilon_i + (1 - X_{i-1})\varepsilon_{i-1}$		

<table>
<tr><td colspan="3">Diameter of grains after grain growth</td></tr>
<tr><td rowspan="4">SRX & DRX
$d_\gamma^{7.5} = d_{SRX}^{7.5} + 4.2\times10^{27} t_{ip} \exp\left(\frac{-400000}{RT}\right)$</td><td colspan="2">SRX, $t_{ip} < 1s$
$d_\gamma^2 = d_{SRX}^2 + 4.0\times10^7 (t_{ip} - 4.32t_{0.5}) \exp\left(\frac{-113000}{RT}\right)$</td></tr>
<tr><td>SRX , $t_{ip} > 1s$
$d_\gamma^7 = d_{SRX}^7 + 1.5\times10^{27} (t_{ip} - 4.32t_{0.5}) \exp\left(\frac{-400000}{RT}\right)$</td><td>SRX , $t_{ip} > 1s$
$d_\gamma^7 = d_{SRX}^7 + 1.5\times10^{27} ((t_{ip} - 1) - 4.32t_{0.5}) \exp\left(\frac{-400000}{RT}\right)$</td></tr>
<tr><td colspan="2">DRX , $t_{ip} < 1s$
$d_\gamma^2 = d_{SRX}^2 + 1.2\times10^7 (t_{ip} - 2.65t_{0.5}) \exp\left(\frac{-113000}{RT}\right)$</td></tr>
<tr><td>DRX , $t_{ip} > 1s$
$d_\gamma^7 = d_{SRX}^7 + 8.2\times10^{25} (t_{ip} - 2.65t_{0.5}) \exp\left(\frac{-400000}{RT}\right)$</td><td>DRX , $t_{ip} > 1s$
$d_\gamma^7 = d_{SRX}^7 + 8.2\times10^{25} ((t_{ip} - 1) - 2.65t_{0.5}) \exp\left(\frac{-400000}{RT}\right)$</td></tr>
<tr><td colspan="3">Ferrite grain size</td></tr>
<tr><td></td><td>$d_\alpha^0 = 1.5 + 5\dot{T}^{-0.5} + 22(1 - \exp(-1.5\times10^{-2} d_\gamma))$
$d_\alpha = d_\alpha^0 (1 - 0.45\varepsilon_f^{0.5})$</td><td>$d_\alpha^0 = (6.67 - 10[C] - [Mn])(\dot{T}^{-0.175})(d_\gamma^{0.4})$
$d_\alpha^{urx} = (6.67 - 10[C] - [Mn])(\dot{T}^{-0.175})(d_\gamma^{0.4-0.25\varepsilon})$
$d_\alpha^0 = d_\alpha^0 X_{SRX} + d_\alpha^{urx}(1 - X_{srx})$</td></tr>
<tr><td colspan="3">Terminology
ε: strain
h_o: entry thickness (m)
h_f: exit thickness (m)
$\dot{\varepsilon}$: strain rate [s^{-1}]
v: peripheral roll speed [m s^{-1}]
r: roll radius [m]
ε_p: peak strain for RX
d_o: initial austenite grain size [μm]
R: 8.31 J mol^{-1} K^{-1}
T: strip temperature [K]
ε_c: critical strain for RX
$t_{0.5}^{SRX}$: time for 0.5 RX when SRX [s]
$t_{0.5}^{DRX}$:time for 0.5 RX when DRX [s]
X: Fraction recrystallised after time t
d_{SRX}: diameter of austenite grains after SRX
d_{DRX}: diameter of austenite grains after DRX
ε_i^a: accumulated strain in step i
t_{ip}: interstand time
d_g: austenite grain size after interstand time
d_α^0: Ferrite grain size from fully RX austenite grains [μm]
$\dot{T}$: cooling rate [ºC/s]
d_α: Ferrite grains size from retained strain austenite grains
ε_f: retained strain after leaving the finishing train
[C] [Mn] [Si] [Nb]: wt% C, Mn, Si and Nb into steel
d_α^{urx}: Ferrite grain size from non-RX austenite grains (μm)</td></tr>
</table>

2.1.2 Strength models

The well-known classical work of Hall (1951) and Petch (1953) predicts that strength of a metal at temperatures below recrystallization is a strong function of grain size (Eq. 2.3).

$$\sigma_y = \sigma_i + k_y d^{-1/2} \qquad \text{Eq. 2.3}$$

where, σ_y is the yield strength of the material, σ_i is the lattice yield stress related to the resistance of the crystal lattice to dislocation movement, k_y is a constant depending on the material composition related to the relative hardening contribution of the grain boundaries and d is the average diameter of the grains. According to the Hall-Petch equation, the strength of the material depends on the grain boundaries and density of precipitates disturbing the dislocation movement during deformation in the absence of recrystallization.

Morrison (1966) proposed an equation to calculate the constant k_y as a function of alloy elements in steel, and the modified Hall-Petch equation became:

$$\sigma_y = 70 + 32[Mn] + 84[Si] + 680[P] - 30[Cr] + 33[Ni] + 11[Mo] + 38[Cu] + 5000[N] + 18.1d^{-1/2} \quad \text{Eq. 2.4}$$

with [Mn], [Si], [P], [Cr], [Ni], [Mo], [Cu] and [N] as concentrations in mass percent.

During hot-rolling, grain boundaries move and lattice dislocations move and interact so that the strength at temperature is determined by the mechanism of recrystallization. When dynamic recrystallization occurs during hot-rolling, the effect of the grain size of the material entering the roll is negligible because new grains are forming during deformation. Stumpf (2003) proposed an equation to calculate the mean flow stress of steel during dynamic recrystallization for deformation at temperatures below 1000ºC, which relates the mean flow stress to the Zener-Hollomon parameter (Z) (

Table 2.2~~Table 2.2~~).

Zener and Hollomon (1944) proposed a parameter (Z) that incorporates the effects of changes in strain rate and deformation temperature on the flow stress of metals in general,

$$Z = \dot{\varepsilon} \exp\left(\frac{Q_{def}}{RT_{def}}\right) \quad \text{Eq. 2.4}$$

where, Q_{def} is the apparent activation energy for deformation, and T_{def} is the deformation temperature.

The approach of Sims (1954), to calculate the mean flow stress (MFS) of the strip based on measured roll-force, has been used to predict the strength of the material during rolling by Maccagno (1994), Siciliano *et al* (2000) and Stumpf (2003) and to evaluate their recrystallization equations. It calculates the flow stress based on the force applied by the rolls during industrial rolling and on the geometrical parameters in the roll-bite, which in turn depend on the roll diameter and the reduction in thickness of the hot-rolled strip.

When rolling conditions induce the material to undergo static recrystallization, the former former grains will be work hardened in the roll-bite and recrystallization occurs

following that deformation, therefore the effect of composition besides rolling parameters will define the strength of the strip. The equation for strength during SRX proposed by Misaka (1968) (

Table 2.2~~Table 2.2~~) relates the strength to composition, temperature, strain and strain rate.

Table 2.2. Mean flow stress under conditions of static and dynamic recrystallization

Mean flow stress (MPa)	
SRX	
$MFS_{SRX} = f_1 f_2 9.8 \exp\left[(0.126 - 1.75C) + 0.0594C^2 + \frac{2851 + 2968C - 1120C^2}{T}\right]$ $f_1 = 0.768 + 0.137Mn + 0.51Nb + 4.217Ti$ $f_2 = \varepsilon^{0.21}\dot{\varepsilon}^{0.13}$	
DRX	
$MFS_{DRX} = 69.63 \sinh^{-1}\left(\frac{Z}{1.25 \cdot 10^{13}}\right)^{0.2}$	
Terminology ε: strain $\dot{\varepsilon}$: strain rate [s^{-1}]	T: strip temperature [K] Z: Zener-Hollomon parameter C, Mn, Ti, Nb: wt% C, Mn, Ti and Nb into steel

2.1.3 Crystallographic textures on hot rolling

When austenite is rolled above the recrystallization temperature, the crystals arrange in certain crystallographic texture and the intensity of that texture depends on the amount of strain accumulated prior to recrystallization. Austenite displays the cube {100} <001> texture, which transforms primarily into the rotated cube {001} <110> in ferrite (Ray *et al*, 1994). Conversely, if the austenite is unable to recrystallise totally during or following rolling, it develops relatively sharp texture fibres. Fibres are the name given to a range of orientations limited to a single degree of rotational freedom about a simple axis (Bunge, 1982). Common fibre textures found in non-recrystallised steels are {110}<112>, {112}<111> and {123}<634>. The major components of the resulting ferrite crystallographic texture when fibres are present in austenite are {332}<113> and {113}<110> (Ray, 1996). The resulting microstructure due to the effect of rolling parameters and composition can be studied by metallography and crystallographic texture analysis.

Traditional texture analysis uses diffraction orientation and intensity of neutrons or X-rays from a crystal lattice as main techniques for examination. Pole figures and orientation distribution functions (ODF) are obtained by these methods and

represent the bulk textural distribution or macro-texture of the exposed surface. Pole figures will effectively demonstrate the presence of preferential texture orientation, while ODF describes the frequency of occurrence of particular orientations in a three dimensional (Euler) orientation space (Ray *et al*, 1994).

A recently developed technique, electron back-scattering diffraction (EBSD), is used to determine the relative crystallographic orientation of each grain comprised in a certain area of a metal sample. The sample surface is bombarded with a beam of electrons inside a scanning-electron microscope, and the backscattered electrons are detected on a screen. That allows the digital detection of Kikuchi patterns generated from an array of pixels in the sample surface, which when put together, represent a map of the absolute orientation of each grain (micro-texture) and the orientation relationship between the different grains (meso-texture) including the orientation of boundary planes. Besides the orientation maps, pole figures and ODF can also be obtained by this technique.

It is now recognised that clusters of grains can exist in the material, which have a common specific texture component (Dingley *et al*, 1992). Such clusters will have a different effect on the overall properties than if the grains which compose them had been randomly orientated throughout the material. It was not until the development of the EBSD technique that such clusters have been observed and analysed for the first time. An example of the effect of texture clusters on the deformation properties of the metal is the roping defect occurring on stainless steel.

Roping defect occurs in high chromium stainless steel and consists of multiple buckled areas occurring at regular distances along the width of the cold rolled strip (Takechi *et al*, 1967; Chao, 1967). Park *et al* (2002), by using using EBSD, demonstrated that the occurrence of roping is related to the presence of preferential texture clusters developed along the length of the continuously-cast slab, at regular intervals through the width and at the centre thickness of the slab. To date, the origins of those clusters of crystallographic textures in stainless steel have not been fully explained however, Chao (1967) proposed that the segregation of chromium carbide precipitates might influence the rotation of crystals during casting. Although roping occurs after cold rolling, similar to ridge-buckle, it does not seem to be the same defect since ridge-buckle occurs solely in one or two regions of the strip and in much wider areas. Nevertheless, the effect of possible texture clusters on the formation of ridge buckle cannot be totally dismissed and will be further analysed in this monogram.

2.2 Roll wear on hot rolling mills

Rolls used in hot strip rolling consist of a core of cast iron, coated with a shell of harder material. On the rolls in contact with the strip, called work-rolls, the tough shell consists of a martensite matrix reinforced with carbides of Mo, W, Cr, Fe or V. The carbides precipitate as an eutectic component on grain boundaries or remain as dispersed particles within the matrix. Roll-shell composition and its prior thermal treatment are selected according to the strains and strain rates to which the roll will be submitted. Furthermore, stringent conditions of abrasive, adhesive, thermal and mechanical loads induce constant wear on the roll surface impossible to prevent. Therefore, a compromise between hardness and toughness should prevail in the design of the roll material.

A schematic illustration of the work-roll while strip is being rolled is shown in Figure 2.2. On the roll-bite, the work-roll is in contact with the scale that has formed on the surface of the hot-strip, while compression is being applied on both the scale and the steel. On exit of the roll-bite, a set of nozzles spray water onto the surface of the roll to reduce its surface temperature. Then the roll surface contacts the back-up roll where Hertzian stresses are generated. Finally, another set of nozzles cool the roll surface before re-entering the roll-bite. Note that this coolant distribution refers to the arrange in Port Kembla finishing-mill.

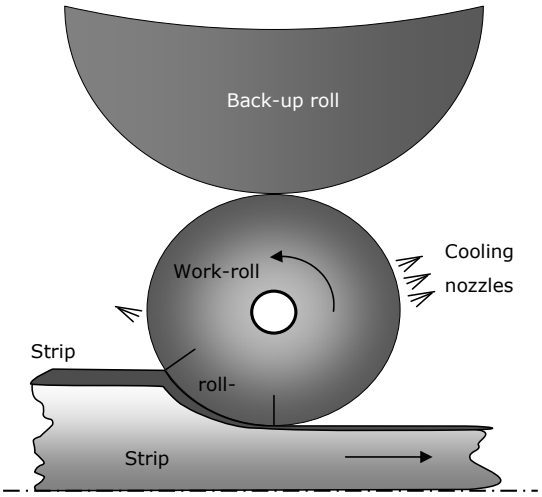

Figure 2.2 Schematic of the load contact and cooling systems for a roll in the finishing-mill in Port-Kembla Steelworks.

2.2.1 Work-roll wear mechanisms

During hot strip rolling, rolls are worn by a combination of various wear mechanisms. Adhesive and abrasive wear occurring while in contact with strip scale and back-up roll; corrosive wear by thermal oxidation and enhanced by the high operating temperature and the humid atmosphere, and surface-fatigue wear occurring by a combination of mechanical and thermal loading cycles (Rabinowicz, 1965; Williams *et al*, 1965; Stevens, 1971; Lee *et al*, 2001; Kato *et al*, 1992).

Abrasion

A number of authors maintain that the major wear mechanism in work-rolls of hot-strip mills is abrasive wear (Williams *et al*, 1965; Stevens, 1971; Lee *et al*, 2001). By definition, abrasion occurs when hard particles slide against a softer surface, digs into it and extracts the material out in the form of fragments (Rabinowicz, 1965). Abrasive wear can occur either because one of the surfaces have hard protuberances or because an external abrasive grit of foreign material is interposed between the surfaces or become imbedded in one of them (Riesz, 1970). In any case, either the surface or the loose fragments should be harder than the material being abraded.

Williams *et al* (1965) suggested that the scale formed on the surface of the strip between stands on the finishing mill is hard enough to cause abrasion of the rolls. Bernard *et al* (1946) argued that at temperatures above 900ºC the oxide layer on the strip surface has proportionally more magnetite with a hardness of HV 420-500, while below 900ºC the major oxide phase will be wüstite which is much softer (HV 270-350). Although other researches agree that magnetite is more abrasive than wüstite, there is considerable debate about the exact proportions of wüstite and magnetite in the tertiary scale that forms in the hot-strip mill (Garnaud, 1977 and Bolt, 2000, 2004). Garnaud (1977) showed convincingly that the fraction of magnetite formed during hot-strip rolling is essentially temperature independent. However, despite this fact the arguments of Bernard *et al* (1946) are still commonly used in the industry in attempts to explain scale-related issues (Roberts, 1983; Williams *et al* 1970 and Mascia, 1998).

In their roll-wear experiments, Kato *et al* (1992) observed the formation of scratches or abrasion marks in the matrix of high-chromium cast-iron but not in the carbides, a demonstration that the abrasive material is softer than the carbides but harder than martensite. They measured the depth of the scratches formed, which

were comparable to the corresponding calculated depth of wear caused by one cycle, concluding that abrasion is probably one of the main mechanisms of wear in rolls. The experiments of Kato *et al* (1992) were conducted at temperatures up to 600ºC in where corrosive and thermo-mechanical wear are also contributing to the total wear; therefore the contributions of pure abrasive wear could not be isolated. Furthermore, they did not attempt to identify the abrasive material and because their experiments comprised multiple cycles, it is not possible to discard the possibility that the carbides themselves act as abrasive fragments once detached from the roll surface. At temperatures above 600ºC Kato *et al* (1992) observed that the surface of the roll material appeared to be covered by an oxide film and the abrasion traces actually disappeared, arguing that the oxide layer prevents abrasion and that roll wear might be caused by a combination of oxidation reactions and mechanical loads.

Adhesion

Rabinowicz (1965) explains that adhesive wear can occur whenever one solid material slides over the surface of another or if it is pressed against it, causing small fragments of the material to detach and adhere to the adjacent surface. Adhesion occurrence is independent of the bulk hardness of the material, because either harder or softer material can get adhered to the parent surface. The relative speed of the strip in the roll bite, in comparison to the peripheral roll speed, changes continuously at the interface roll-strip. The strip and the roll are constantly sliding with respect to each other excepting at the neutral point in the roll bite. Therefore, adhesive wear can certainly occur in the roll-bite.

For oxide-forming metals, it is found that the sliding systems can lead to the formation of either large metal fragments or small oxide particles, whose dimensions depend on the work of adhesion between particle and substrate and the hardness of the particles. The right combination of particle dimensions and load is required to allow the detachment of fragments. According to their adhesion properties, the critical dimension and load for oxide particles are very small, meaning that it is highly plausible that particles of oxides from the scale on the strip surface can detach and contribute to roll-wear (Rabinowicz, 1965).

Thermal fatigue

One distinctive feature observed on the surface of rolls used in hot environments is the presence of micro-cracks, normally referred to as fire-cracks. The micro-cracks formed at the surface of the roll are generally initiated at the carbide-matrix

interface, running parallel and perpendicular to the surface (Kato *et al*, 1992; Lee *et al*, 1997[a]). Thermal cycles produce cracks perpendicular to the surface at the interface between matrix and carbides; while the load applied by the backup-roll forms fatigue cracks parallel to the surface (Kato *et al*, 1992). Fire-cracks will eventually converge causing fragments of the surface to detach and consequently wear the surface of the rolls.

Kato *et al* (1992) determined experimentally that only 500 cycles of thermo-mechanical loads on the surface of the rolls are enough to form fire-cracks, while materials subjected to the same loads at room temperature require more than 100 thousand cycles before the surface experiences micro-fractures. Lee *et al* (1997[b]) asserted that the thermal fatigue life of roll materials is determined by the collective effect of the size and volume fraction of the coarse primary carbides, the frequency of surface crack formation, the increase of internal stress and the softening of the material by cycling.

The following mechanism of fire-crack formation has been proposed by Stevens *et al* (1971) and depicted on Figure 2.3. The main body of the roll that remains cool prevents the thermal expansion of a heated element on the roll surface. This results in development of compression stresses during heating (contact zone with the strip) and tension stresses during cooling (when leaving the roll-bite). Assuming a point on the roll surface entering the roll-bite, the material is compressed elastically along OA while being heated. When the combination of strain and temperature reaches a certain value ($3.3x10^{-3}$ and 370ºC for cast-iron), the compressive yield stress is reached and the material starts to deform plastically. As the material on the roll surface is being deformed plastically the strain continues to increase while stress decreases because the compressive stress required to deform the material at these temperatures corresponds to its yield stress. When the point on the material exits the roll-bite, the temperature is suddenly reduced and the material begins to contract. In order to reach the condition of zero strain the material undergoes higher tensile stresses than at the start and the tensile yield-stress is reached at a certain combination of strain and temperature ($2.1x10^{-3}$ and 104ºC for cast iron), plastic deformation occurs again but on the opposite direction. The cycle will restart with the material having a certain amount of accumulated internal tensile stress, so the hysteresis cycle includes accumulation of internal stresses. Failure, or micro-crack formation, occurs when the accumulation of internal tensile stress exceeds the fracture strength of the material.

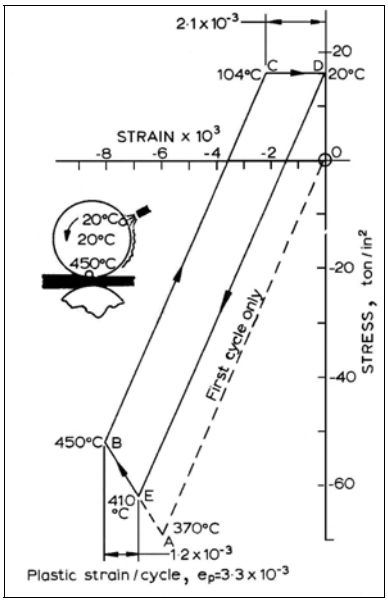

Figure 2.3. Stress-strain hysteresis loop for roll surface during hot-rolling. Roll material is undergoing cycles between 20 and 450ºC. After Stevens *et al* (1971)

2.2.2 The influence of temperature on roll wear

Penetration of the strip-heat into the cylinder surface is extremely small due to the high rotational speed of the rolls (Yuen, 1994). Moreover, it is a very difficult task either to measure during industrial process or to simulate under laboratory conditions the surface temperature changes of the cylinder due to the extremely fast rotation of the rolls. In the finishing mill for example, the speeds are in the order of 2 to 18 revolutions per second. Stevens *et al* (1971) made novel experimental measurements on industrial rolls in a roughing-mill stand using a thermocouple arrangement that re-welds while the roll is being worn during rolling. The results of measured temperatures on the roll when it is in contact with the strip at 1230ºC for one revolution (0.2 rev.s^{-1}) are shown in Figure 2.4.

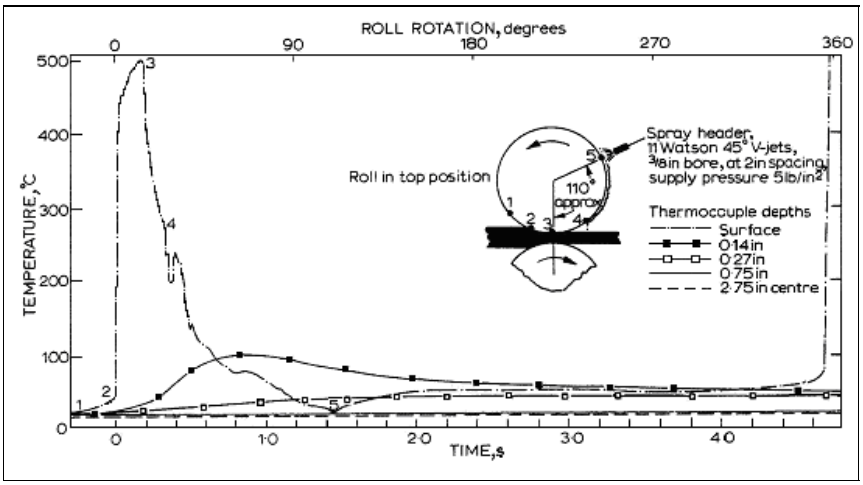

Figure 2.4. Variation of roll temperature in the roughing-mill, during the first roll-revolution. From Stevens *et al* (1971)

As shown in Figure 2.4 roll surface temperature increases almost instantaneously to 500ºC from the time that the strip makes contact with the roll at point 2 until the strip exits the roll-bite where it reaches the maximum temperature. After leaving the roll-bite, the roll surface temperature drops to approximately the initial temperature. The effect on the surface temperature change caused by the roll cooling sprays is also illustrated in Figure 2.4 at the point 5. Inspection of the temperature traces corresponding to thermocouples located deeper into the rolls shows that the roll coolers have an insignificant effect on the temperature of the roll material below the immediate surface and hence, there is almost no heat penetration. It should be borne in mind that the experiments described in Figure 2.4 were conducted on at rotational speed of 0.2 rev.s^{-1} which is very low compared to the typical speeds of industrial finishing rolling mills (2-18 rev.s^{-1}) therefore even less temperature penetration should be experienced in the sub-surface of finishing-mill work rolls.

Numerous mathematical models reported in the literature (for example, Yuen, 1994; Tseng at el, 1995; Horsky *et al*, 1996; Raudensky *et al*, 2002; Perez *et al* 2004; Saboonchi *et al*, 2004) that predict temperature variations on the surface of a rotating cylinder during hot rolling are based on the measurements of Stevens *et al* (1971). Numerical results from these models confirm that the maximum roll-surface temperature occurs at the exit of the roll-bite and the penetration of heat into the roll material decreases exponentially, with the rotation cycles. Pérez *et al*

(2004) calculated a decrease from 540ºC at the surface to 90ºC at a position 1.5mm below the rolls surface. Furthermore, Yuen (1994) calculated that the core temperature of the rolls will increase exponentially until reaching a steady-state of around 80ºC and further found that changes on the location of cooling systems can produce variations of the core roll temperature of 40-50%. Moreover, Lundberg (1997) demonstrated by using mathematical models that the temperature reached by the roll surface is about half the strip temperature and depends on the contact times. At contact times of 63ms (similar to the first roll of Port-Kembla finishing-mill) the maximum temperature calculated by Lundberg (1997) on the roll surface was 530°C from making contact with a strip at 1130°C.

Lee *et al* (1997[b]) demonstrated by tensile thermal fatigue experiments, the influence of cyclic maximum temperature in the life of roll materials (Table 2.3~~Table 2.3~~). The combination of high temperature and a high number of cycles will produce failure of the material at tensile stresses below its fracture strength.

Table 2.3. Number of cycles to fracture for two types of roll materials when varying the maximum temperature (Tmax) in the thermal fatigue cycles, a) for cast iron and b) for high speed steel roll-shells. After Lee S *et al* (1997[b])

a) Cast iron shell						
Composition (%)	C	Si	Mn	Ni	Mo	Fe
	3.20	0.83	0.68	3.60	0.32	bal
Cycle Temperatures (ºC)	min	200	200	200		
	max	**400**	**450**	**500**		
Number of cycles to fracture		**1200**	**400**	**11**		

b) High speed steel							
Composition (%)	CE	W_{eq}	Mn	V	Mo	Cr	Ni
	2.01	11.64	0.2-0.5	3.95	0.32	4-6	0.5-10
CE: C+ 1/3 Si; Weq: W + 2Mo							
Cycle Temperatures (ºC)	min	200	200	200			
	max	**550**	**575**	**600**			
Number of cycles to fracture		**1100**	**25**	**8**			

Table 2.3~~Table 2.3~~ clearly shows that the number of cycles to fracture is highly influenced by the maximum temperature of the thermal cycle. High-speed steel rolls (HSS) (Table 2.3b) are capable of resisting higher temperatures than cast iron shells. This property is taken into consideration in the selection of HSS material for

the manufacture of the shells for the first sets of rolls in the finishing-mills. Nevertheless, an increase on the maximum temperature of the cycle by as little as 25ºC can reduce the life of HSS in one order of magnitude. These results indicate that small increases in the roll surface temperature can drastically increase the formation of fire-cracks and consequent detachment of roll particles, exacerbating the wear.

Wear tests conducted by Lee *et al* (2001) confirmed that the wear resistance is directly related to the matrix hardness. On the other hand, they found that the surface roughness (hence friction coefficient) is reduced with the number of cycles on samples with softer matrix, but increased in the samples with harder martensitic matrix (the matrix was tempered at distinct temperatures to achieve different hardness). SEM observations led them to conclude that the surface condition improves on samples with softer matrix because the finer carbides cannot be retained by the matrix. These fine carbides act as abrasive media, wearing out the coarser carbides on the surface, and reducing the surface roughness.

Although it is well documented that abrasion is accepted to be the main mechanism of roll-wear, in the case of work-rolls in the hot-strip mill, thermo-mechanical cycles play a significant role aggravating the occurrence of wear. Moreover, strip scale and roll material (or roll oxide) are in contact in the roll-bite and heat is transmitted to the roll from the hot strip through the strip-scale. Lee *et al* (1997[b]) demonstrated, as shown in Table 2.3, that small increases in temperature can reduce roll-life significantly; therefore any change in the integrity of the scale, such as fractures or differences in thickness (or even composition), might increase the heat transmission and exacerbate roll wear. It is debatable if the type of oxides formed at different temperatures can affect roll abrasion directly as proposed by Williams (1965) and if other factors can affect the formation and plasticity of the scale. Further insights into oxide morphology and integrity are presented in the following paragraphs.

2.3 Oxide formation, morphology and integrity during hot rolling

2.3.1 Iron oxidation

Iron forms pure oxide compounds in three main forms, wüstite (Fe_xO), magnetite (Fe_3O_4) and haematite (Fe_2O_3), usually non-stoichiometric phases whose exact composition may be temperature dependent, as shown in the Fe-O phase diagram in Figure 2.5.

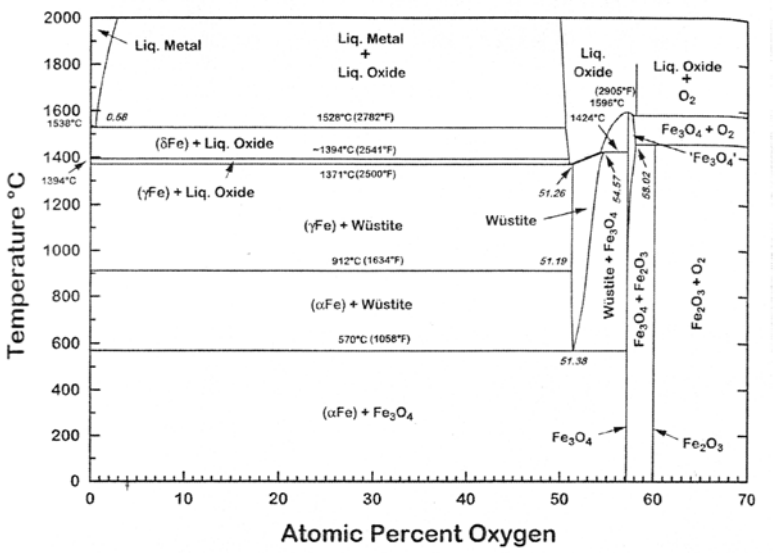

Figure 2.5. The Fe-O equilibrium diagram. After Pelton *et al*, 2000, p. 26.

Wüstite (Fe_xO) is thermodynamically stable above the eutectoid temperature of 570°C and it is a p-type metal deficit semiconductor that can exist over a wide range of stoichiometry e.g. from $Fe_{0.95}O$ to $Fe_{0.88}O$ at 1000ºC (Birks *et al*, 1983). Wüstite has a cubic crystal structure, with anion sites occupied by O^{2-} and most cation sites occupied by divalent Fe^{2+} ions. Some cation sites are occupied by trivalent Fe^{+3} ions, with one half of the cation sites vacant in order to maintain electrical neutrality. Magnetite (Fe_3O_4 or $FeO.Fe_2O_3$) is an inverse spinel structure containing both divalent and trivalent iron ions. It is almost stoichiometric below 1000°C, while at higher temperatures it contains more oxygen in solid solution than the stoichiometric composition. Hematite (Fe_2O_3) is a stoichiometric chemical compound. At temperatures above 570ºC has a rhombohedral structure and shows a disorder in the anion sub-lattice only, behaving as an n-type semiconductor (Birks *et al*, 1983).

The Free Energy of oxide formation under equilibrium conditions is a function of temperature and oxygen partial pressure and these values are typically depicted in an Ellingham diagram as shown in Figure 2.6.

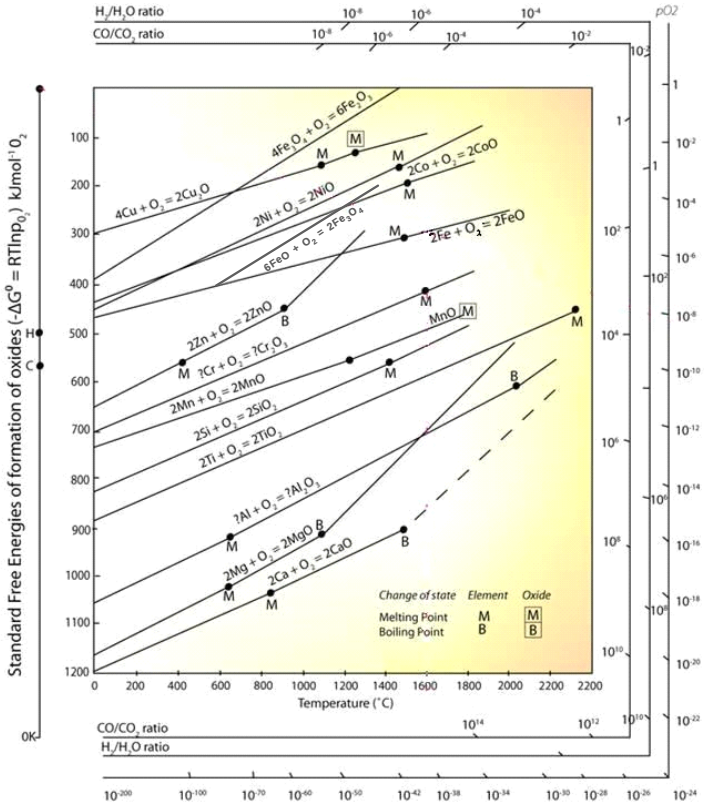

Figure 2.6 Simplified Ellingham diagram for some relevant oxides. After webpage: http://www.doitpoms.ac.uk/tlplib/recycling-metals/ellingham.php

2.3.2 Mechanism of scale formation

The classical theories of oxide thin film formation formulated by Cabrera and Mott (1948-1949) and revised by Fehlner and Mott (1970) explain the formation of thin film at low temperatures. Oxidation starts with the adsorption of gas into the metal surface, driving the electrons from the metal to the surface. The electrons ionise the oxygen molecules that get chemisorbed into the metal by place exchange with an underlying metal atom. The heat of chemisorption aids place exchange, so that additional rearrangements of the surface oxide can take place and multi-layers of oxide form. Figure 2.7 shows the model of the place-exchange process.

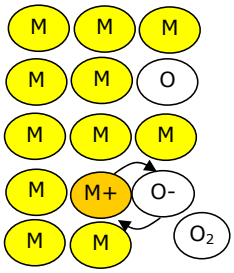

Figure 2.7. Model of the place-exchange process. M: Metal; O: Oxygen. After Fehlner and Mott (1970)

Place exchange becomes more difficult after the formation of a monolayer. A stable film forms and a potential builds up across it. Once the first layers are formed, Fehlner and Mott (1970) demonstrated that ionic movement determine the growth rate, which takes place under a constant electric field. The driving force for ionic drift is provided by oxygen ions located at the oxide surface. These are formed by simultaneous dissociation of oxygen molecules and capture of tunnelling electrons. In an oxide that grows by cation movement, such as wüstite and magnetite, the newly incorporated oxygen ions will remain near the oxide/gas interface. On the other hand, in oxides that grow by anion movement such as haematite, the oxygen ions will move away from the surface to the next interface where full incorporation takes place.

Diffusivity of the species (ions and electrons) dominates the rate of growth after the first monolayer is formed as expressed by the well-known Wagner theory (Wagner, 1933), mathematically formulated in Eq. 2.5.

$$k = \frac{1}{RT}\int_{\mu^I}^{\mu^{II}} D d\mu \qquad \text{Eq. 2.5}$$

where k is the rate of growthof oxide, R is the ideal gas constant, T is the temperature at which the reaction is occurring, D the diffusion coefficient of the species driving the oxidation (cations or anions) and μ is the chemical potential between the oxide-gas interface (II) and the metal-oxide interface (I) as shown in Figure 2.8. The efficiency of the transport of anions or cations depends on the semi-conductivity nature of the oxide formed.

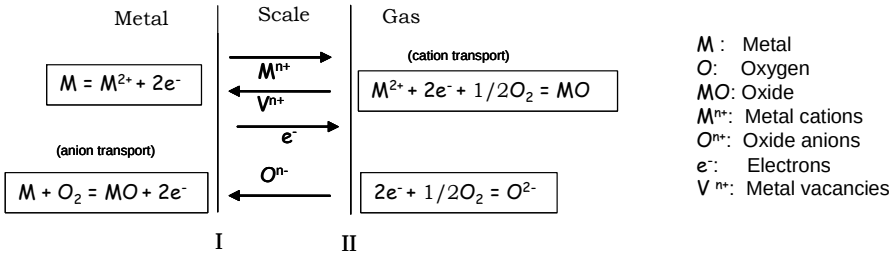

Figure 2.8. Simplified model for diffusion-controlled oxidation. After Birks *et al* (1983, p. 41)

It is now well accepted that diffusion through both the oxide lattice and short circuit diffusion paths contribute to ion transport in oxides. Hart (1957), defined an effective diffusion coefficient (D_{eff}) as the weighted sum of the diffusion coefficients for lattice (D_L) and short circuit diffusion paths (D_B) as shown in Eq. 2.6

$$D_{eff} = (1 - f) D_L + f D_B \qquad \text{Eq. 2.6}$$

where f is the fraction of diffusion sites in the short-circuit paths. Logani *et al* (1971[b]) asserted that some types of oxides formed at high temperature have initially high rates of diffusion through short-circuit diffusion paths. Lattice diffusion becomes the dominant mechanism when the density of the short-circuit diffusion paths is reduced by oxide growth. In Eq. 2.6, the fraction of diffusion sites in the short-circuit paths (f) is variable and tends to zero as the oxide grows in thickness with time.

Formation of layers of oxides cannot be modelled effectively from theories of crystal growth as the reactant species reach the surface from opposite directions (Rapp, 1984) and the vapour phase differs from the solid phase composition. Nevertheless, theories of crystal growth by supersaturated vapour as explained by Ballufi *et al* (2005) might assist in understanding the growth of oxides (Figure 2.9). A crystal grows from its supersaturated vapour phase by the addition of vapour atoms to the free surface of the crystal. The interface moves outward towards the vapour as it acts as a sink for the incoming flux of atoms. Discretely stepped or terraced structures called vicinal surfaces, composed by the surface and ledge vacancies, adatoms and, vacancies and adatom clusters depicted in Figure 2.9, develop as a result of this thermally driven process. Kinks and ledges are the only places on a vicinal surface where an incoming atom form the vapour can become fully

incorporated in the crystal with its full binding energy. The growth of crystals can occur by various mechanisms, direct impingement of an atom from the vapour into the surface, ledge or kink; jumping of an adatom from the surface by surface diffusion into a ledge or kink and its incorporation into the crystal; or jumping of an adatom attached to a ledge into a kink and its incorporation into the crystal.

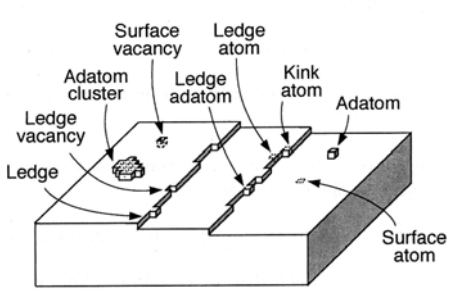

Figure 2.9. Scheme of the various point and line defects on a vicinal crystal/vapour surface. After Balluffi *et al*, 2005, p. 287.

Jungling et al (1984) and Lee et al (1988) observed the growth of wüstite grains *in-situ* by oxidising pure iron samples at 1200ºC and 1050ºC in an environmental scanning electron microscope. At partial pressures of oxygen of 10^{-4}atm, they could observe the growth of wüstite in macro-ledges and the formation of inverse pyramidal pits. Those pits eventually disappear with further oxidation and become ledges again. The authors argue that the formation of pits should be related to the presence of screw dislocations within the newly formed grains of wüstite.

Numerous scale formation experiments on pure iron at long exposure times (~2h), at temperatures above 570ºC, show that scale is composed by approximately 95% wüstite (Fe_xO) in the innermost layer, 4% of magnetite (Fe_3O_4) and 1% of haematite (Fe_2O_3) in the outmost layer (compiled by Chen *et al*, 2002). That particular distribution of iron oxide species can be explained by the relative rates of the diffusion of iron ions through each iron oxide. In Table 2.4, at 1000ºC, the diffusion coefficient of iron in wüstite is much higher than the iron diffusion in magnetite; while the diffusion coefficient of iron in haematite is extremely small.

Table 2.4. Diffusion coefficients of iron through bulk iron and iron oxides at 1000ºC

Fe through:	Diff. coeff at 1000ºC $cm^2 \cdot s^{-1}$	Reference
Iron lattice	1.0×10^{-11}	Nohara *et al* (1977)
Iron grain boundaries	5.0×10^{-7}	Gibbs *et al* (1969)
Wustite (FeO)	9.3×10^{-8}	Kubaschewski & Hopkins (1962)
Magnetite (Fe_3O_4)	1.9×10^{-9}	
Hematite (Fe_2O_3)	2.5×10^{-15}	
Oxygen through hematite	8.6×10^{-14}	

2.3.3 Kinetics of scale formation

Marston *et al* (2004) described the rate of oxide formation as experiencing two stages, a linear growth rate in the early stages of oxidation, followed by a parabolic growth law when a certain thickness of oxide has been achieved. They argued that when hot, scale-free steel is exposed to an oxidizing atmosphere, the metal consumes the oxidizing species in the surrounding atmosphere and the oxygen potential at the gas-scale interface is approximately the same as at the scale-metal interface. Transfer of oxidizing species from the gas to the gas-scale interface therefore controls the rate of reaction. The rate of oxidation at this stage will be linear (k_L) and mostly dependent on the gas flow conditions, the gas composition and the temperature.

$$x = k_L t \qquad \text{Eq. 2.7}$$

where x: scale thickness at constant temperature, t: oxidation time.

As the scale layer thickens, explain Marston *et al* (2004), the rate of further oxidation becomes limited by solid-state diffusion of Fe ions or cation vacancies through the scale. Therefore, the oxygen potential at the gas-scale interface becomes significantly higher than at the scale-metal interface. The concentration gradient of oxygen diminishes as the scale grows and the thickness ratio yields a parabolic rate equation. The parabolic rate constant (k_P) depends on the nature of the scale that forms on the substrate.

$$x^2 = k_P t + x_0 \qquad \text{Eq. 2.8}$$

where x_0: initial scale thickness. Ideally, the growth rate equations should include the influence of all gas species and the activation energy of the substrate components.

The use of a parabolic equation to describe the rate of growth of oxide on a steel surface is widely applied. The parabolic equation is directly derived from Fick's 1st law of diffusion and most authors utilise the empirical values obtained in experiments in long-term exposure experiments to fit a parabolic growth. However, as pointed out by Friedel *et al* (2004), at the relatively short oxidation times experienced in the hot rolling mills, there is a distinct possibility that oxidation may progress at a linear rate. They suggest applying a mixed linear-parabolic equation, such as Eq. 2.9, where j and k are constants related to the rate of growth

Comment [WMC1]: Was this Rapp??

$$x^2 + jx = k\ t \qquad \text{Eq. 2.9}$$

Whether or not a linear rate of oxidation dominates in the early stages of oxidation is a matter of much debate (Marston *et al*, 2004; Friedel *et al*, 2004; Chen *et al*, 2003). Although oxide thicknesses determined experimentally at short exposure times conforms to a linear rate of growth, the experimentally determined thickness values can also be accommodated in a parabolic relation with respect to the oxidation time. Therefore, the mechanism of oxidation cannot be determined by simply comparing the shape of the experimentally determined oxide growth rates. Initially, the rate of oxygen supply to the reaction interface may be rate-limiting and although diffusion might be the governing mechanism after the first monolayer of oxide is formed, the preferable diffusion paths, the nature of the oxide layers formed, the rate of adsorption and desorption, interchange reactions at the different interfaces and indeed the relevant diffusion coefficients may ultimately determine the rate of growth. To the author's knowledge, the relative importance of these various possible rate-determining steps in the very complex iron oxidation scheme have not been uniquely identified.

2.3.4. Scale formation in steels during hot-rolling

Oxidation rates in steel are lower than in pure iron, due to the presence of alloying elements which might reduce the activity of iron in the substrate, the diffusion rates of species through the oxide, and possibly induce the de-cohesion of scale from the substrate. Figure 2.10 illustrates the type of scales formed on the strip while being processed in the hot strip mill. In each descaling box, scale is fractured and removed from the surface. Scale formed on the slab into the furnace during reheating is called primary scale; secondary scale forms during the roughing passes between the descaling boxes and tertiary scale is formed in the finishing mill thereafter. Secondary scale forms in the humid air of the mill, exposed for less than 4 min before reaching descaling box 2. Tertiary scale forms in less than 15 seconds

between descaling box 2 and the last roll of the finishing mill, and continue forming while on the run-out table and on continuous cooling during coiling.

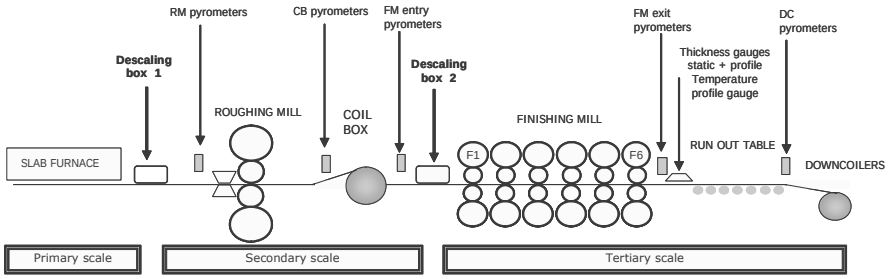

Figure 2.10. Diagram showing location of the descaling boxes 1 and 2 in the hot strip-mill and the types of scales formed during processing

Only a few authors have conducted experiments to determine the kinetics of scale formation at the short times of exposure corresponding to the formation of tertiary scale during finishing rolling (Chen *et al*, 2002-2003; Sun *et al*, 2003-2004 and Boelen *et al*, 2002). Oxidation experiments on low-carbon steel conducted by Chen *et al* (2002) proved that a scale of 30μm in thickness is formed after 12 seconds at 900ºC followed by slow cooling at 0.25 to 1ºC.s^{-1}. The scale structures formed under these conditions have a magnetite:wüstite (M:W) thickness ratio of 1:7, which means that a much thicker magnetite layer forms than on pure iron (1:23). In continuous cooling experiments with no allowance for isothermal oxidation, the ratio M:W was just 1:3. The scale ratio M:W on commercial hot-rolled strip is also 1:3 after coiling, but it should be borne in mind that this ratio includes the effect of the compression exerted on the scale in each roll-bite, deformation of the oxide during rolling, the adhesion of scale to the substrate and the effect of the tight strip wraps when the steel is cooled in the coil. The slow cooling rates used in the experiments of Chen *et al* (2002) and the cooling media should be affecting the proportion of M:W on the samples and this ratio may not necessarily represent the situation of the scale while it is forming in the finishing-mill.

Sun *et al* (2004[b]) conducted experiments at short times of oxidation (less than 160s) showing an approximate linear rate of oxidation of low carbon steels during the first 10 seconds of isothermal exposure to wet-air at 800 to 1000ºC, followed by cooling in a protective atmosphere of nitrogen. Selected results of the experiments of Sun are shown in Figure 2.11. Thickness of the scales formed after 30 secondsof exposure to the oxidising mixture are between 20μm and 55μm and

highly dependent on the temperature of oxidation. Unfortunately, Sun *et al* did not determine the W:M ratios from the samples obtained.

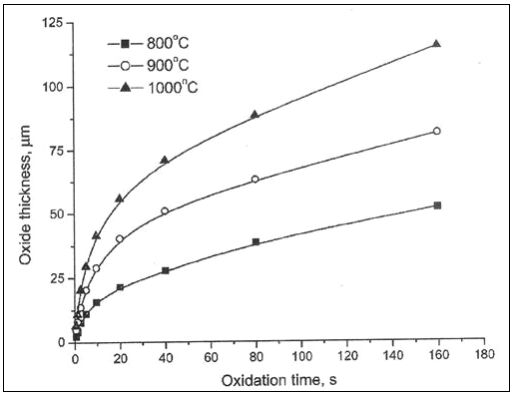

Figure 2.11. Experimental results of oxidation experiments from Sun et al 2004[b]. Conducted on low carbon steels oxidised in atmosphere of 200g.m^{-3} water-air mixture.

2.3.5 Factors influencing formation and adhesion of scales

Blisters

Blisters are zones in where the oxide has separated from the substrate, thereby affecting its adherence. A controversy exists on the mechanism of formation of blisters and a satisfactory explanation of the conditions for the occurrence of blisters has not been found. In the past it was assumed that the formation of carbon monoxide CO or carbon dioxide CO_2 at the scale-steel interface produces accumulation of gases, which cause the separation of the scale (Siebert, 1939; Griffits, 1934). More recent research findings (Matsuno, 1980; Marston *et al*, 2004) indicate that because the formation of scale is accompanied by a volume expansion of 80% (without voids), as the scale thickens, internal stresses can cause the scale to separate from the metal. Moreover, Kizu *et al* (2001) proposed that the presence of crystals of wüstite with orientations {111} and {110} in the {100} matrix deteriorates the adhesion between scale and substrate by increasing the possibility of slip on the oxide grain boundaries. Matsuno (1980) found that the range of temperature where blisters form more rapidly on steels is between 950-1000ºC, while at temperatures above or below that range, the onset time for blistering from the start of oxidation is higher. In continuous cooling experiments, Matsuno (1980) found that the onset of blistering was more rapid at temperatures 100ºC above the ones registered isothermally.

Kizu *et al* (2001) conducted a systematic study of the oxidation of steel of different compositions and found a relationship between steel impurities and alloying elements on the occurrence of blisters. They found that small amounts of Si and P segregate to the interface oxide/metal and the concentration of these impurities at the interface is higher at certain temperatures (950ºC for P, and 1050ºC for Si), approximately coinciding with the shortest onset time for blisters. Their proposal is that the combination of P-Fe-Si-O can form a ternary oxide eutectic compound of FeO, Fe_2SiO_4 and $Fe_3(PO_4)_2$, with a melting point as low as 890ºC; and the presence of this molten zone can affect the adhesion of scale to substrate. They also found that the formation of CO in high carbon steels is a further contributing factor to de-cohesion, while the exclusive presence of fayalite (Fe_2SiO_4) increases the adhesion of the scale. Furthermore, Kizu *et al* found that wüstite formed at 900ºC on steels containing more than 0.25 mass % Mn has higher proportions of {111} and {110} crystallographic orientations (which affect adhesion) than wüstite formed at other temperatures.

Although the results of Matsuno (1980) and Kizu *et al* (2001) are relevant to the understanding on the formation of blisters, some caution has to be exercised in the interpretation of their results as a consequence of the experimentation methods employed. Both of the studies were conducted by determining the blister onset by naked eye observations and therefore, the actual onset of blisters might have occurred prior to the reported temperature-time event because detection of a change in the surface of steel by using this method requires that the blisters reach detectable dimensions. The experiments of Matsuno (1980), relating to the effect of continuous cooling on the onset of the blistering temperature, were conducted by extracting samples from the furnace and allowing oxidation while cooling down to room temperature. The atmospheric control of the furnace was not strictly controlled and scale could have formed on the steel sample prior to extraction of the sample from the furnace. The film of scale is likely to undergo thermal shock on extraction from the high temperature in the furnace to room temperature, affecting the internal stress of further oxides formed. A true comparison cannot be made of these results obtained by continuous cooling, with those obtained when oxidation and cooling where completed in the furnace. Similarly, the experiments conducted by Kizu *et al* (2001) involved injecting air at a low flow rate into a large furnace chamber meaning that, on the early stages of oxidation, the partial pressure of oxygen was not constant. Furthermore, these discussions about blister onset have not considered the effect of the phase transformation of γ–Fe to α–Fe on the stress imposed on the scale. This is specifically interesting because the observed blistering

temperatures are close to the temperature region of the two phase austenite-ferrite region. Moreover, Kizu's reference to the effect of the melting point of the eutectic of Fe-Si-O-P at 890ºC causing de-cohesion of scale is not in agreement with their finding that the shortest blister onset time occurs at 950ºC when the phosphorous content at the interface steel/oxide is higher.

Matsuno (1980) found that scales containing blisters are more easily removed than uniform scales, which is consistent with the uneven morphology of the scale/steel interface observed by Chen *et al* (2003) in the presence of blisters. Moreover, lateral crack formation can occur within the scale when outward movement of the plastically deformed scale above the blisters relieves compressive stresses (Marston, 2004).

Oxidising vapours

Marston *et al* (2004) found that the rate of oxidation is higher on pure oxygen atmospheres, followed by H_2O and CO_2 containing environments. This might be simply attributed to the oxygen activity of the atmospheric mixture. Nevertheless some authors (Baud *et al*, 1975; Sheasby *et al*, 1984; Chen *et al*, 2003) found that the presence of water vapour in air causes the formation of more adherent scales than dry air. Sheasby *et al* (1984) explained that in dry air, pores formed at the interface metal/oxide remain entrapped and coalesce, inducing the separation the scale from the substrate; while vapour phases (H_2O-H_2 or CO_2-CO) assist in the transfer of oxygen and cause the pores to migrate away from the interface forming more adherent oxide layers. Evidently this mechanism explained by Sheasby et al (1984) contradicts the mechanism of blister formation by carbon oxide migration proposed by Kizu *et al* (2001), Griffits (1934) and Siebert (1939).

Alloying elements

Carbon atoms tend to segregate to the steel surface driven by the chemical potential difference caused by the presence of oxygen and decarburisation can occur at the surface when the gases produced (CO_2-CO) are able to escape. Although rapid oxidation might prevent decarburisation by entrapping the gases, it is expected that the surface of the slab entering the hot strip mill already possess a decarburised layer of around 1mm depth formed during the oxidation-controlled reheating process (Birks *et al*, 1983, p. 175). The surface will have lower carbon content than the rest of the slab, displacing the phase transformation temperatures at the surface of the steel to higher values than in the bulk. In terms of oxidation, the diffusion of species will be affected by the presence of ferrite or austenite

phases. Besides, carbon may aid in the formation of blisters in the scale according to the proposals of Griffits (1934) and Siebert (1939).

Chen *et al* (2002) assert that manganese dissolving in wüstite retards iron diffusion, thereby producing relatively thinner wüstite layers. In contrast, Tan *et al* (2001) found that Mn at up to 1.75% promotes scale growth at high temperature. Manganese in the presence of sulphur forms manganese-sulphide (MnS) on the grain boundaries of the metal, which might mask diffusion of iron species through grain boundaries (Kiessling, 1997, p. 9). Aluminium and silicon can form oxides at very low partial pressures, affecting the formation of further iron oxides. A detailed review of the effect of silicon and aluminium on ferrous alloy oxidation is given in the following section.

2.3.6 Oxide formation in silicon containing steels

Oxide formation in steels containing silicon has been the subject of numerous studies, mostly driven by the improvement in room-temperature corrosion-resistance that the addition of silicon imparts on steel. Some other studies have been conducted on high temperature oxidation to determine the origins of a defect called red-scale that is inherent to silicon containing steels (Fukagawa *et al*, 1994; Okada *et al*, 1995). Our interest is to compile studies on high-temperature oxidation of silicon steels to assist in the understanding of the morphology of scale formed in the presence of silicon.

Silicon is added to steel to improve corrosion resistance but also because it imparts certain beneficial electrical properties. Additions of silicon to steel increase electrical resistivity and electrical permeability and decrease hysteresis loss by inducing the rotation of the crystals into certain directions during cold rolling (key-to-steel, webpage). It is well known that fayalite ($2FeO.SiO_2$) is partially liquid above 1177ºC (see Figure 2.12) and the presence of that liquid oxide influences further oxidation and subsequent descaling during rolling (Okada *et al*, 1995; Logani *et al*, 1969). Furthermore, even at temperatures below fayalite melting point, experimental evidence suggests much lower rates of oxide formation in steels containing relative high amounts of silicon compared to other low carbon steels (Marston *et al*, 2004). The exact amount of silicon in the steel is quite important as will be discussed below.

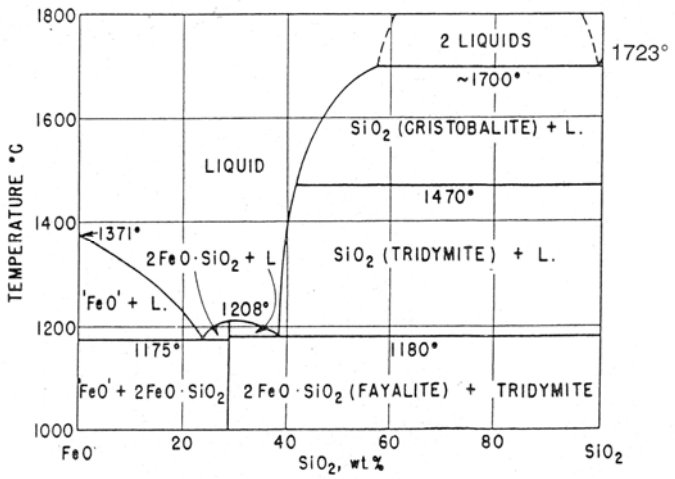

Figure 2.12. Iron oxide – silicon oxide equilibrium phase diagram. After Turkdogan, 1996, p.144.

Logani *et al* (1969) conducted thermo-gravimetric experiments in atmospheres of CO-CO_2 for up to 2 hours and proposed a mechanism for the formation of oxide layers in steel with silicon content up to 2%. The experiments were performed at 890ºC and 1000ºC in a CO_2 atmosphere and they proposed that an inner, intermediate layer of wüstite-fayalite conglomerate formed followed by a top layer of wüstite. The wüstite formed on the scale surface present oxide crystals growing by both lateral and vertical growth of platelets. Furthermore, formation of oxides in Si steels containing 1.5%Si at 1000ºC is described by Logani et al (1971[a]) as initiated by the nucleation of the more stable oxide (in this case SiO_2). TEM analysis performed on their samples indicates the presence of amorphous silica (SiO_2), crystallized silica and fayalite. Precipitates of SiO_2 in the subsurface of the alloy were also observed. They suggested the following mechanism of formation: an amorphous silica film forms on the surface which experience partial crystallisation and those crystals transform to wustite-fayalite nodules. Nodules grow in both vertical and lateral direction within a circular base. Further, nodules containing wüstite and fayalite, located at grain boundaries in the alloy, grew laterally to cover the alloy surface. Concurrent with growth of the oxides externally, oxygen diffuses into the substrate leading to the precipitation of silica. According to Logani *et al* (1971[a]), a completely developed scale is composed of an external wüstite layer and an inner wüstite-fayalite conglomerate layer inter-dispersed with discontinuous fayalite bands.

With respect to the thermodynamics of oxide formation, Atkinson (1982) predicts that at 900ºC, atom fractions of silicon of approximately 0.05 are required to develop and maintain a protective SiO_2 film. Accordingly, alloys containing insufficient bulk Si are expected to be susceptible to internal oxidation at high temperatures. Atkinson (1982) explains that the transport mechanism for the formation of SiO_2 films is thought to be by the inward diffusion of oxygen, while the formation of iron oxides on top of the silica film occurs by Fe transport through the SiO_2 grain boundaries.

Fukagawa *et al* (1994) observed the interface steel-scale on 0.5% Si steel and experimented with combinations of rolling and descaling in laboratory trials. They found that the fayalite melted during reheating (1200ºC) solidifies at the interface steel-scale in zig-zag fashion and also precipitates at the sub-surface of the steel. After descaling the steel, using physical methods, the remaining scale consisted of lumps of wüstite and fayalite, roughly 100µm in size. By comparison, the scale that remained on low carbon steel following similar treatment was only 5µm thick. Besides the apparent strong adherence of fayalite, they also found that fayalite is harder at high temperatures than other iron oxides as it can remain intact after rolling. Fukagawa *et al* (1994) demonstrated that fayalite formed from the melt is adherent and strong, and can, under certain circumstances, remain on the steel surface following descaling.

Based on the information in the literature referred to above, there seems to be general agreement in the that the oxidation products of silicon containing steels consist of an amorphous film of silica, followed by a layer of fayalite or fayalite-wüstite conglomerate and then a wüstite layer. There are however, contradicting arguments, for example, Takeda (2003) and Adachi (1987) proposed that magnetite forms preferentially instead of wüstite. The presence of internal precipitates of silica is well documented (Logani *et al*, 1971a; Takeda, 2003) although the effect of the silicon content of the steel on the formation of internal oxides has not been clarified.

The kinetics of scale formation in steels containing Si has been the subject of a number of studies as the oxidation rates in this type of steels is quite different from those of other low carbon steels. Tan *et al* (2001) found oxide scales of 5µm in thickness formed on steels with 1.9%Si, 0.57%C and 0.79%Mn, while 25µm thick oxide layers formed on mild steel under the same oxidation conditions. Using thermo-gravimetric tests Marston *et al* (2004) determined that the rate of scale

formation on a 0.4%Si steel at 800ºC does not follow a parabolic rate law but is rather sigmoidal (Figure 2.13). A linear oxidation growth rate was observed in the first two minutes of oxidation in silicon steels and the thickness of the layer was 10 times lower than that formed on a low carbon steels (the Si content of this low-carbon was not specified).

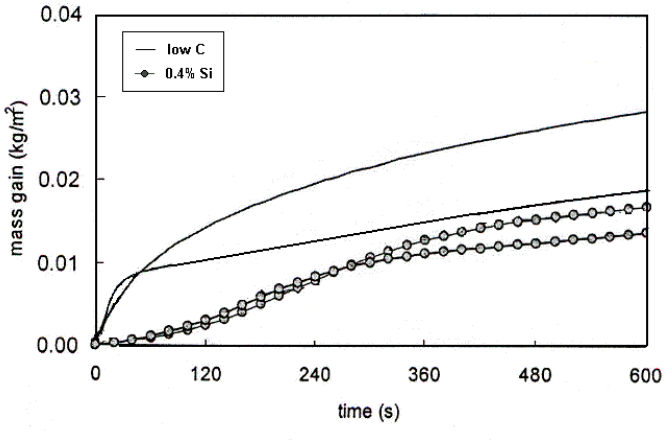

Figure 2.13. Thermo-gravimetric results of oxidation of low-crbon and silicon steels at 800ºC in dry air. Adapted from Marston *et al* (2004)

Logani *et al* (1969) also observed a linear oxidation rate in 2%Si steels oxidized on CO_2 atmospheres for 10 hours at 890 and 1000ºC. They argued that the linear rate of growth is to be associated with the inward migration of oxygen arising from a dissociative reaction of wüstite at its inner interface, resulting in the formation of the wüstite-fayalite conglomerate.

Due to the low rates of oxide formation on steels containing silicon, it is expected that the early stages of oxide growth might be formed by scales with different morphologies than those observed after hours of oxidation. Regretfully, we could not find reports in the open literature of oxidation experiments conducted in the typical oxidation time experienced in the hot-strip finishing mill (<15s).

Alloys of silicon-containing steels explored in this manuscript include small but relevant amounts of Si, Al and Mn (see Table 1.1 in Chapter 1). The effect these minor additions of alloying elements have on the rate and morphology of oxide formation does not seem to have been treated in the literature. It seems that the presence of Mn and Al, besides Si can play an important role in the formation of

oxide layers. Oh *et al* (1986), studied alloys with 6.7%Si - 16.7%Mn and 2.1%Ni and found high concentration of Si occurring near the metal/scale interface after oxidization for 4h at 800ºC. The oxide scales near the gas/scale interface consisted almost entirely of manganese oxide, and virtually no iron or nickel at all could be detected in the scale. Amorphous silica was formed in the first layer, with Mn_2SiO_4 forming the next layer. This finding contradicts the findings of Marston *et al* (2004) from experiments adding Mn to the silicon alloy, which showed that Mn has little effect in the development of oxides layers. Erhart *et al*, (1983) studied the oxidation of alloys containing 30%Mn, 10%Al and 1.25%Si in an environmental scanning-electron microscope and observed the formation of a dense protective scale of Al_2O_3 and the subsequent formation of very scarce and random nuclei of oxides on the top of that scale. The mechanism of formation of these random oxides is not well understood but they argued that it might be that ions of Mn and Fe, which will eventually form the new oxide nuclei, could be transported through point defects existing in the alumina scale.

2.3.7 Experimental techniques to study oxide formation

Traditionally, kinetics of oxide formation has been studied by the use of thermo-gravimetric analytical techniques (TGA), which allow for the calculation of the oxidation rate based on mass changes during oxidation at pre-determined temperatures (e.g. Lee *et al*, 2005; Basabe *et al*, 2004). Thermo-gravimetric methods for the study of oxidation are inherently limited to long-term experiments and it is not possible to observe the progress of the oxidation process. Furthermore, experiments in which oxides are examined after cooling to room temperature cannot reveal oxide formation occurring at high temperature, firstly because the oxide phases can transform on cooling and second because high rates of cooling subject the scale to thermal-shock and the scale may fracture.

Attempts to study oxide formation by *in-situ* observations include the use of scanning electron microscopy (Erhart *et al*, 1983), environmental scanning electron microscopy (Jungling *et al*, 1984 and Schmid *et al*, 2002), high-temperature laser-scanning confocal microscopy (LSCM) (Senk *et al*, 2004; Thorning *et al*, 2005) and high-temperature optical microscopy (Norton *et al*, 1993). The value of SEM and ESEM observations is limited by the oxygen partial pressure that can be introduced into the specimen chamber without unduly affecting the vacuum in the chamber and the effective operation of the electron beam. The main impediment to the use of the laser-scanning confocal microscopy is the limited depth of field resulting from the presence of a confocal pinhole in the laser-optical imaging system.

A technique whereby the dynamics of oxide formation could be studied in-situ and under conditions close to reality would be greatly instructive in order to gain insight into the characteristics of the oxides forming during the short times of finishing rolling.

2.3.8 Scale failure

Hidaka et al (2002) determined experimentally, the plasticity of iron oxides at the high temperatures typically encountered in a hot-strip mill. They found that for strain rates of $2x10^{-4}$ s^{-1}, the ductile-to-brittle transition under tensile testing conditions occurs between a temperature of 600ºC and 700ºC for FeO and between 700ºC to 800ºC for Fe_3O_4 , while Fe_2O_3 appear to fracture in a brittle fashion at temperatures up to 1250ºC (maximum test temperature). In practical terms, scales with high magnetite-to-wustite ratios will be prone to fracture whenever the temperature falls below 800ºC, while hematite will always fracture on the temperature conditions of the finishing-mill.

The deformation applied to a strip during hot-rolling can cause either plastic deformation or fracture of the oxide scale (Stevens *et al*, 1971; Li *et al*, 2001). Fracture of the scale is related to the strain and strain rate applied, rolling temperature, chemistry of the steel and the thickness of the scale. Tan *et al* (2001) asserted that the longitudinal tensile stress at entry into the roll gap may favour the formation of through-thickness cracks in the scale when the rolling temperature is low enough and the oxide scale thickness exceeds a certain limit.

Echsler *et al* (2003) demonstrated by 4-point-bend tests that the fracture strength of the combination of oxides formed on steel substrates, increases with an increase in strain rate and temperature. By distinguishing between the strength of the oxide layer from that of the steel substrate, they determined that at 1000ºC, the strength of the oxide layer is ~25 MPa at a strain rate of 10^{-4} s^{-1} and ~15 MPa at a strain rate of 10^{-5} s^{-1}. Their experiments were conducted on scale layers between 160µm and 900µm thick and therefore, their results cannot be necessarily extrapolated to the likely strength of the very thin tertiary scale layers (10µm to 20µm thick).

Krzyzanowski *et al* (1999) identified two different modes of scale failure based on tensile strength test at high temperature:

Mode I: When oxide is weaker than the interface metal-oxide, failure begins by shear through-scale cracking.

Mode II: When interface is weaker than the oxide, scale slips along the interface oxide-metal without fracturing the oxide.

The scale tensile test developed by Krzyzanowski *et al* (1999) was perfected and described in 2002 as consisting of a cylindrical steel tensile test specimen cut in half along the circumference. The scale is then allowed to form on the surface of the rods, after reaching the testing temperature, while the two parts remain in contact under pressure. After achieving the desired scale thickness, the parts are subjected to a tensile test. The strength thus recorded is very close to that of the scale layer at high temperature.

Krzyzanowski *et al* (2002) also demonstrated that mode II of fracture occurred normally when the steel is at a temperature above 900ºC (0.19%C, 0.18%Si, 0.8%Mn). Mode I failure occurs below 870ºC, while a mixed mode of fracture was observed at temperatures between 870-900ºC. Experiments on scale integrity in silicon-containing steels were also conducted by Tan et al (2001). They found Mode I fracture and also delamination at the interface on scales of Si-Mn steels between 783ºC and 1200ºC. They demonstrated numerically that failure of Si-Mn steels can occur at entry to the roll-bite whenever the entry temperature of the strip is below 1200ºC. Although Krzyzanowski *et al* (2002) and Tan *et al* (2001) successfully demonstrated that scale failure can occur at temperatures typically experienced during hot-rolling, specifically finishing-rolling temperatures, their fracture tests were conducted on scales formed after an exposure to the oxidising atmosphere of more than 800s (13min) compared to the exposure times for the formation of tertiary scale in the finishing-mill (15s). Besides, strain and strain rates used in their experiments are orders of magnitude lower than those experienced under industrial hot-rolling practice.

Das *et al* (2004) and Sun *et al* (2005) found in their experiments evidence of strip material extruding through cracks formed under deformation. Conversely, Li *et al* (2001) argue that under hot-strip mill operating conditions, scale fracture is not normally observed. They assert that strip temperatures are usually higher than the brittle-ductile transition temperature of the oxides and furthermore, the time of contact between the strip and the roll is so short that the heat loss in the roll bite is

minimal. On the other hand, Tang (2006) mathematically simulated deformation of scale under pure ductile conditions (not considering the brittle behaviour of scale below certain temperatures) and assert that in cases where the scale is stronger than the steel, the elongation of scale and steel will not be proportional and scale cracks can occur. Furthermore, Tang (2006) found that if the friction between the roll surface and scale is higher than the friction between scale and steel the formed cracks can heal with further deformation. These arguments are difficult to prove or disprove, as even Li *et al* (2001) admit that the minimum contact times achievable in laboratory trials are still orders of magnitude larger than real contact times in hot-rolling mills. Besides, the scale structures observed after hot-rolling do not necessarily represent the intermediate steps of oxidation and scale compaction occurring between and during rolling passes. There is a possibility that scale can break under load in the roll-bite, and further heal in the time interval between stands or even in the next roll-bite, and therefore not be detectable after coiling.

Kolchenko *et al* (1984) calculated that uniform layers of scale can reduce the heat transmission between strip and roll 10 to 15 times. Conversely, fractured scale might produce an increase in the heat transmission to the rolls of the same magnitude. Leduc (1980), proposed an equation (Eq. 2.10) to calculate the heat flow through the oxide film (q),

$$q = \frac{k_0}{X}(T_m - T_o) \qquad \text{Eq. 2.10}$$

where k_0 is the thermal conductivity of the oxide layer, X is the thickness of the oxide layer, T_m is the temperature at the surface of the strip and T_o at the surface of the oxide.

One of the origins of ridge-buckle defect proposed in the literature is the occurrence of an uneven microstructure on the hot rolled strip (Rocquet *et al*, 1965; Gilbertson, 1965 and Blazevic, 2002). Assuming that grains in a zone of the strip differ in size from the microstructure of the rest of the hot-rolled strip, that zone might experience different deformation during cold-rolling leading to ridge-buckle defect. In the same notion, if any preferential orientation occurs in a zone of the strip during hot-rolling, that zone of the strip would deform differently than the rest during cold rolling. This approach of the microstructural influence on uneven deformation originates from the belief that the sole presence of a 7μm protuberance (or ridge) in the hot-rolled strip is not enough to form a ridge buckle and grain size or crystallographic texture variations should be occurring simultaneously in, and in addition to the zones were ridges occur.

The arguments advanced in this chapter are an attempt at determining if any uneven microstructure or crystallographic texture is developed in the hot rolled strips programmed to be cold rolled. We studied, by grain size analysis and electron back-scattering diffraction patterns (EBSD), hot rolled strips with ridges and strips with good profiles of tinplate and silicon steels. The strips with ridges were selected from a succession of strips in a schedule that were producing ridge-buckle in subsequent operations.

3.1. Experimental methods

Samples of hot-rolled strips of tinplate and silicon steel, the composition shown in Table 3.1, were selected for the microstructural study. Six strips of tinplate (TP) and two strips of silicon steel (LS) were studied. Two tinplate strips presented good profiles without any ridges. The strips of tinplate vary slightly in their carbon content. Ridge height mentioned in Table 3.1 is the maximum deflection in thickness from the ideal parabolic shape of the profile measured on the strips.

Table 3.1 Composition and description of hot-rolled strips of tinplate and silicon steel samples selected for the microstructural studies

Strip name	Strip type	Composition (%, bal. Fe)							Ridge height	Distance from centre
		C	Mn	P	Si	S	Cr	Al	(µm)	(mm)
S1	TP-24	0.045	0.20	0.012	0.005	0.014	0.015	0.03	8	70 O/s
S2									10	70 O/s
S3									10	30 O/s
S4	TP-13	0.07	0.25	0.009	0.01	0.011	0.06	0.03	10	50 O/s
S5									No ridge	
S6	TP-24	0.045	0.20	0.012	0.005	0.014	0.015	0.03	No ridge	
S7	LS-05	0.003	0.4	0.034	0.57	n/a	0.025	0.30	15	80 O/s
S8									16	140 O/s
O/s: Operator side										

Two samples were cut from each of the strips. In the case of strips with ridges (S1 to S4 and S7 to S8) one sample was located centred at the maximum ridge height and the other in a zone away from the ridge as shown in Figure 3.1. Strips without any evident thickness change were also analysed, and although it could not be proved that they would eventually produce ridge-buckle, they served as control specimens in the analysis. From the strips without ridges (S5 and S6), samples were taken from the centre of the strip and 100mm out from the centre.

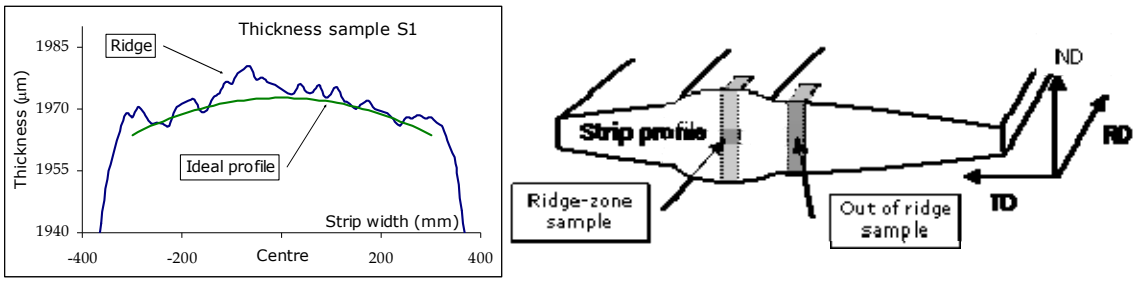

Figure 3.1. An example of the thickness profile of a strip with ridges and the positions from where the samples were cut. TD: Transversal direction, ND: Normal direction and RD: rolling direction

Three specimens were cut from each sample, electro-plated with nickel and mounted in conductive bakelite to display the three planes: ND-TD, TD-RD and RD-ND. Then polished to 1µm in diamond paste and finished with 0.6µm colloidal silica. Samples were etched in Marshall's reagent (Vander, 1986, p.633) for an effective display of ferrite grain boundaries. Images of specimens were taken with a Leica®DMRM optical microscope and grain size distribution determined using video-pro VP-32 software and MS-Excel®. Grain size distribution was determined by line interception method, discarding border grains.

The specimens corresponding to strips S1 to S4, mounted in the ND-TD plane, were selected for electron backscattering characterisation. Further preparation was necessary to eliminate any mechanical distortion. Following recommendations of Katrakova *et al* (2001) for ferrous materials, preparation consisted of repetitive polishing and etching (at least three times). Polishing on 1µm diamond paste and etching in 2.5% Nital (Vander, 1986). The preparation process is finalised with 20min automatic polishing in colloidal silica (0.6µm). Samples were examined in a fully automated electron backscattered diffraction unit (EBSD) with HKL technology® software adapted to a Leica 440 scanning electron microscope.

3.2 Results

3.2.1 Grain Size

An example of the metallography of the specimens studied is shown in Figure 3.2, which displays the three planes corresponding to the tinplate steel sample S2.

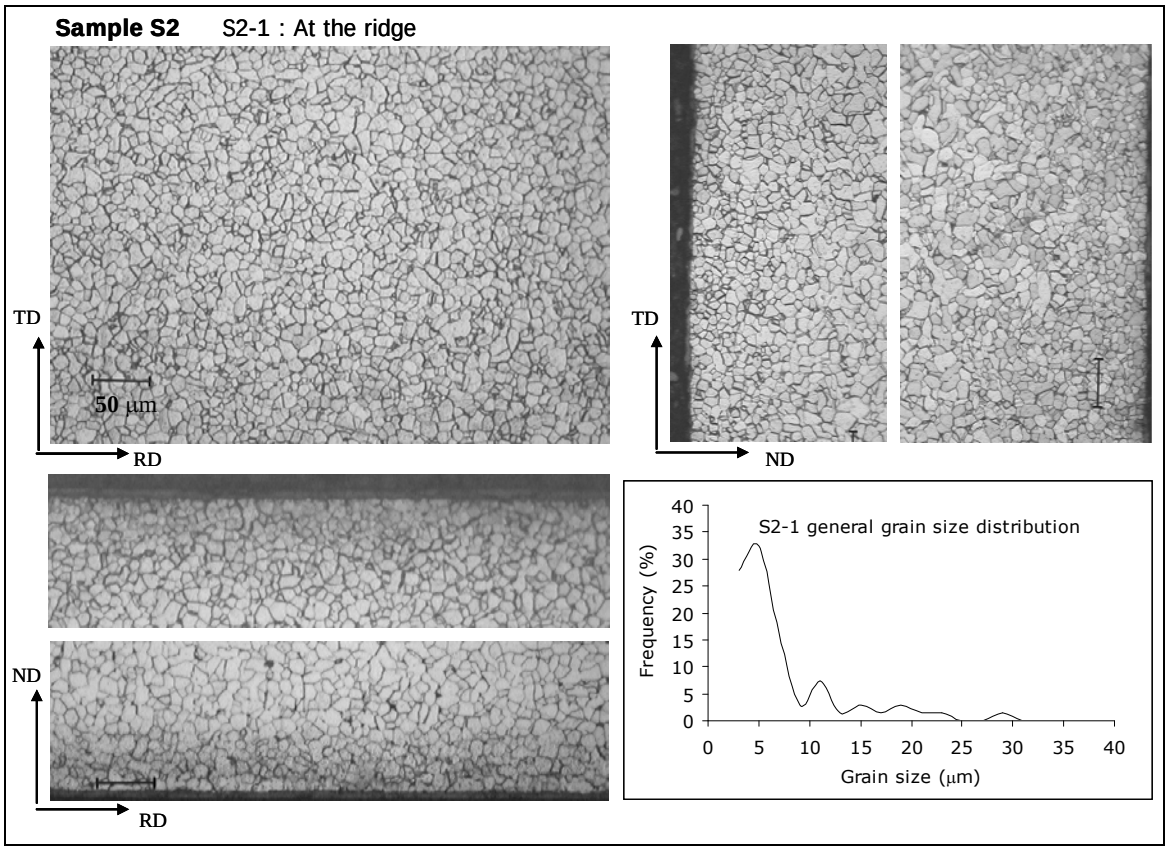

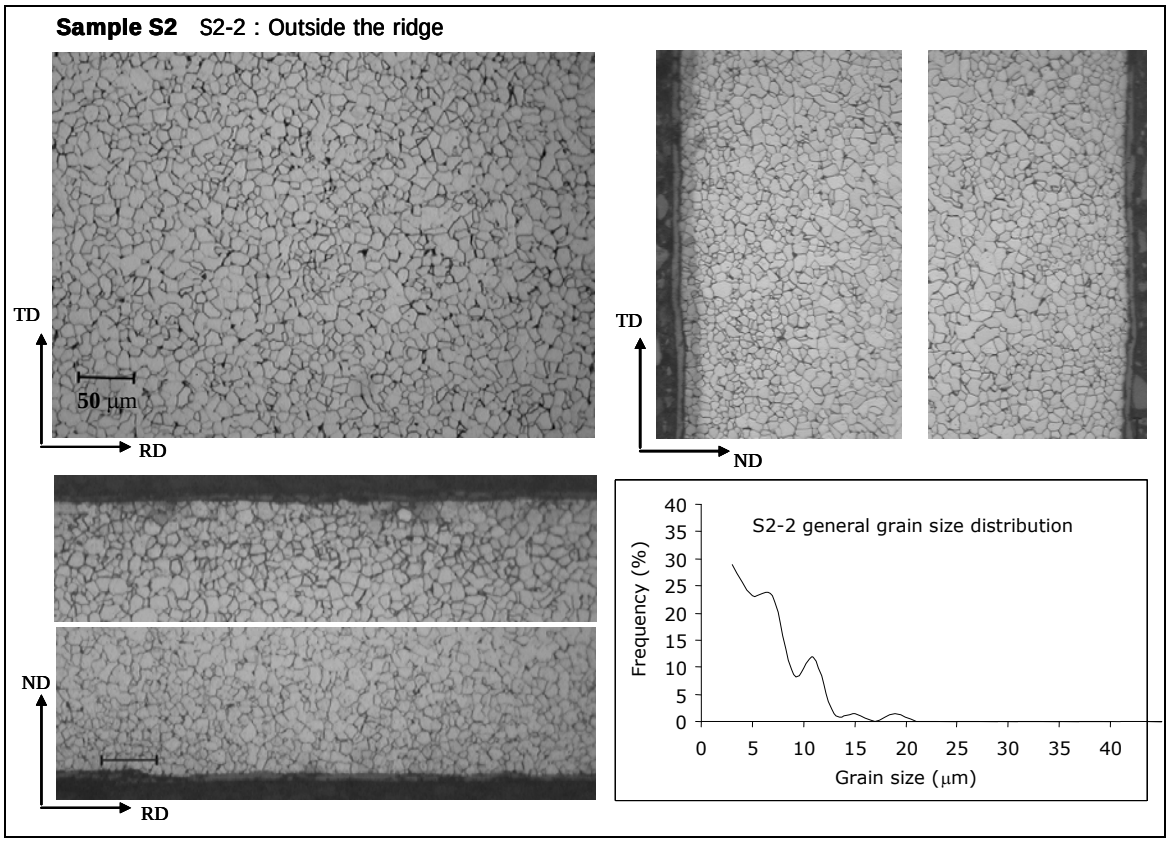

Figure 3.2 Images of the microstructure on sample S2 at the ridge (S2-1) and outside the ridge (S2-2). The general grain size distribution in each case is shown in the graphs. Standard deviation of 3.94 for S2-1 and 4.39 for S2-2. The same magnification has been used for all the images.

All the microstructures display similar grain size and grain size distributions, showing no apparent difference between ridge and non-ridge zones. The grain sizes at the strip surface are smaller that those developed towards its centre. Fully recrystallised grains can be observed in all the tinplate steels (S1 to S6), while partial recrystallisation occurs in silicon steels (S7 and S8) as shown in Figure 3.3. Partial recrystallisation in silicon steels conforms to the design of the rolling process as they are scheduled to be rolled in the dual phase, austenite plus ferrite region.

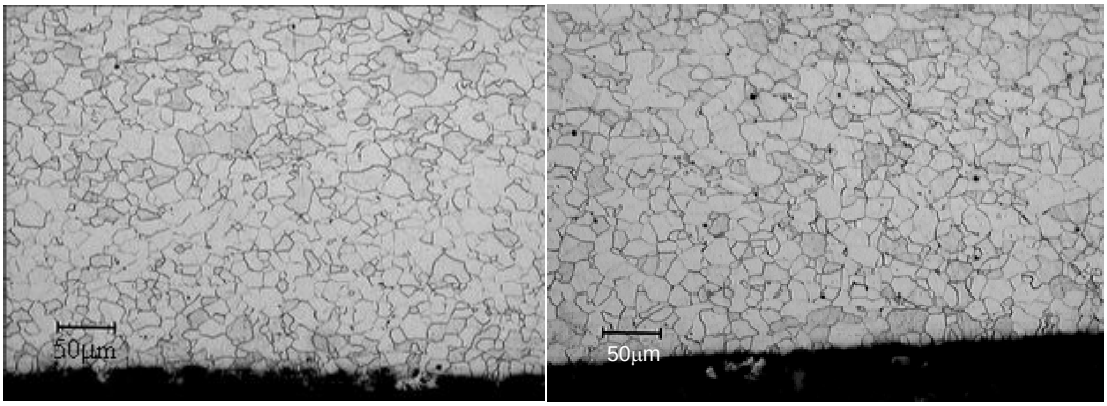

S7-1 At the ridge in plane ND-TD

S7-2 Outside the ridge in plane ND-TD

Figure 3.3. Images showing the microstructure of silicon steel from sample S7. A partially recrystallised structure can be observed in these steels due to the design of the rolling scheme.

Grain size distributions were calculated for the surface and centre of the samples. The surface extended up to 75μm into the bulk sample in both sides, and the centre of the sample includes the entire sample excepting the surface zones. For the sake of comparison, the frequency of occurrence of a chosen grain size in the ridge and non-ridge zones of the samples were subtracted one from the other and these results are represented graphically in Figure 3.4.

The graphs in Figure 3.4 represent the prevalent grain sizes in the ridge zone with respect to the rest of the strip. Comparing the differences in grain size at the surface of the samples, it appears that in the ridge zone for strips of tinplate (type TP13 at the sample surface in Figure 3.4a) there is a higher proportion of small grains, typically 5μm in size, and for strip TP24 there is a higher proportion of these small grains in the non-ridge zone (negative percent in Figure 3.4 c), while for LS05 steels there is no difference in the grain size at the surface between the ridge and non-ridge zones. Similar results were obtained from the analysis of the grain sizes in the centre of the samples, for TP13 there are 10% more grains of 7μm size in the ridge zone, but in TP24 there is just 5% more of 5μm sizes, while in silicon steels there is almost no difference between the grain sizes in the ridge and non-ridge zones. It is not possible to make a connection between the occurrence of ridge and the grain size based on these experimental results because there is not a definitive pattern of preferential grain sizes on the ridge zone compared to the rest of the strip. Samples extracted from the strips with no ridges (S5 and S6) also display no differences in grain sizes between the centre of the strip and an off-centred sample 100mm away.

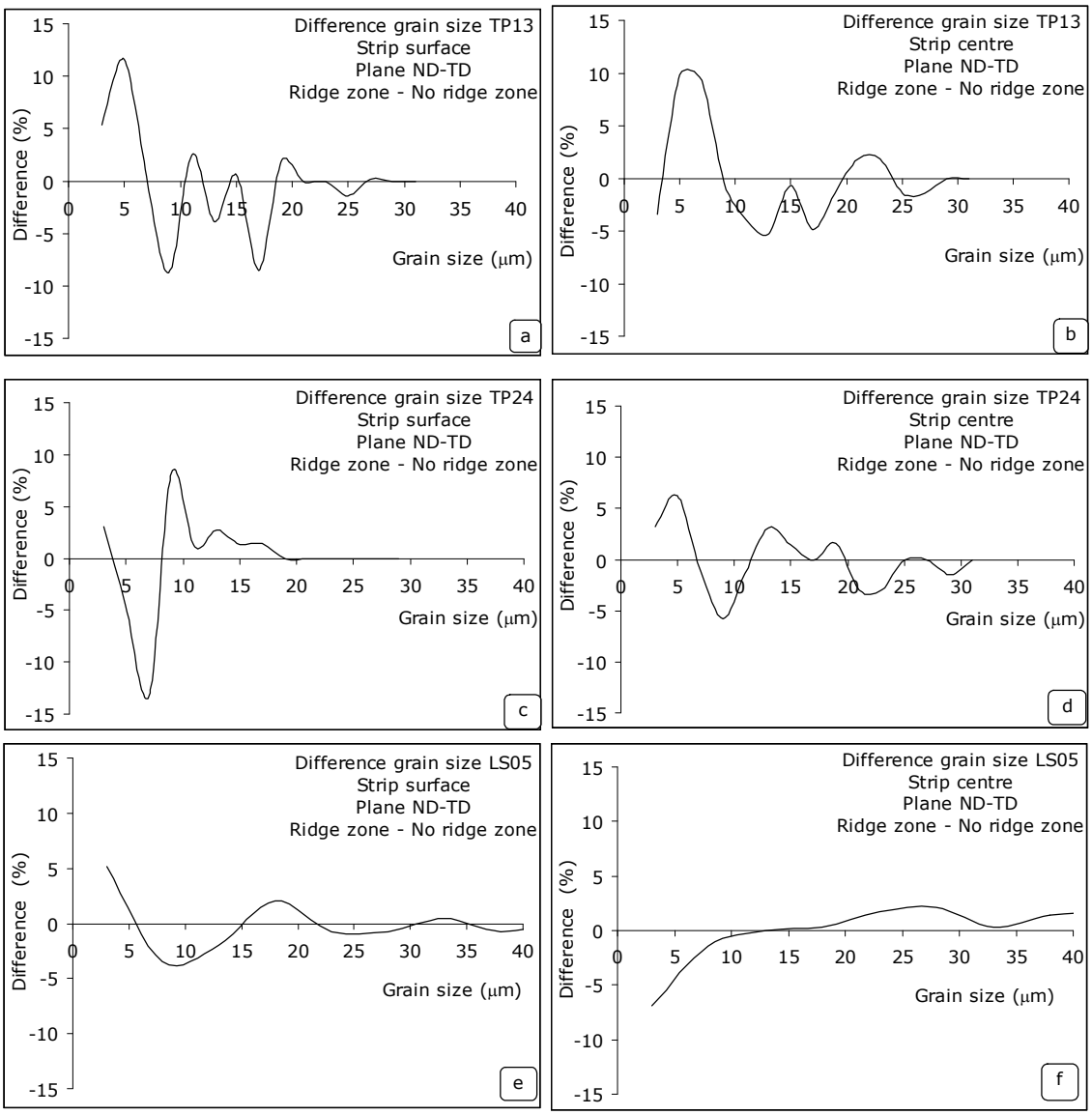

Figure 3.4. Difference in grain size between the ridge and non-ridge zones for the surface and centres of strips: TP13 (S4), TP24 (S2) and LS05 (S7) steels. The standard deviations are 4.93, 4.45, 4.49, 2.93, 2.47 and 2.77 for Figures 3.4 a, b, c, d, e, f respectively.

3.2.2 Crystallographic textures

Crystallographic textures near the surface of the strip were studied by electron back-scattered diffraction patterns analysis (EBSD). Although no differences could be observed in grain size in the optical micrographs, the advantage offered by backscattering pattern is that it displays the orientation of the grains near the surface and any cluster of grains of similar orientation or texture in the material can be detected. Figure 3.5 shows the orientation maps and pole figures corresponding to the specimens from samples S2 and S4.

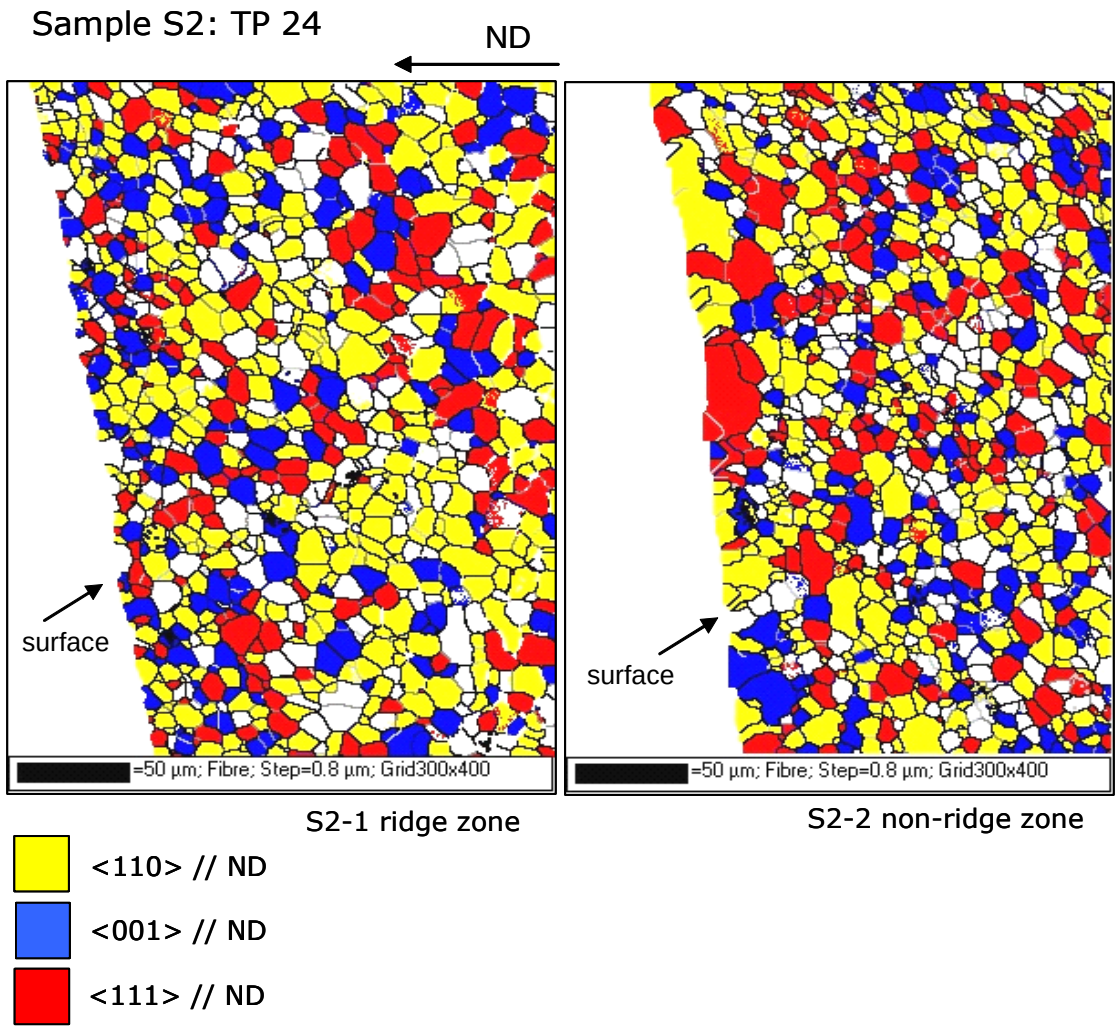

Figure 3.5a. Electron backscattering maps of the surface of the sample S2 of steel TP24, extracted from the ridge and non-ridge zones. Pole figures corresponding to the {100} of ridge and non-ridge zones. Number of grains measured in S2-1: 668 and in S2-2: 553.

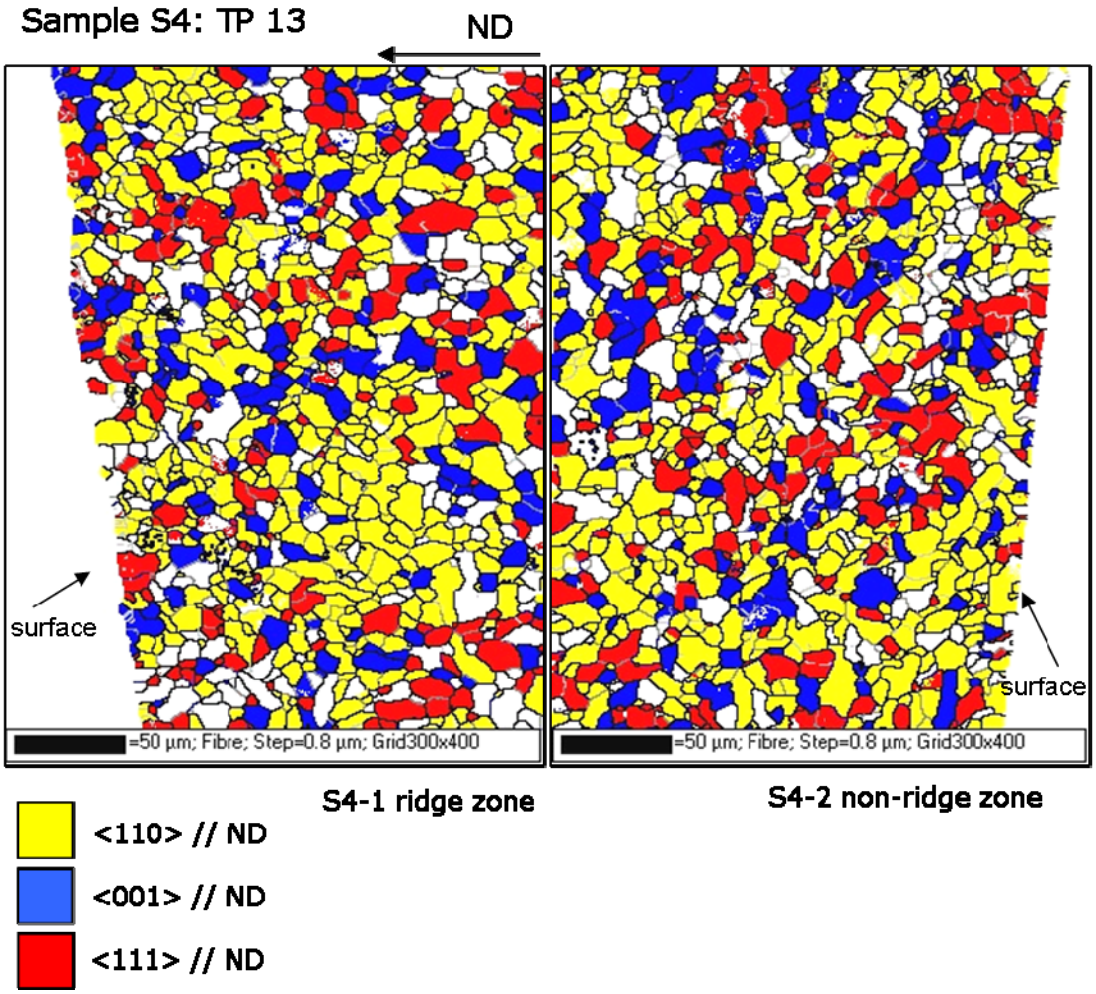

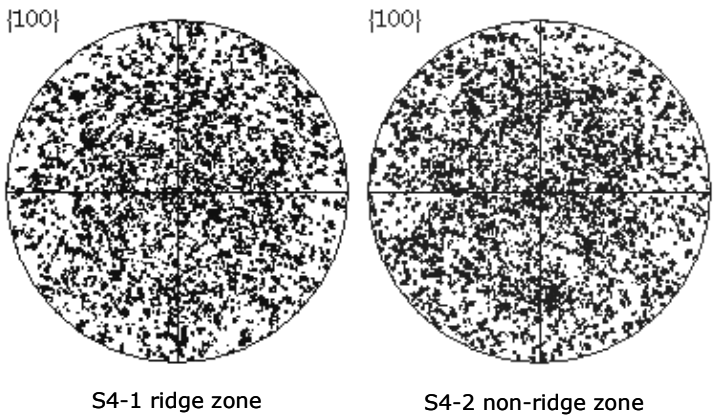

Figure 3.5 b. Electron backscattering maps of the surface of the sample S4 of steel TP13, extracted from the ridge and non-ridge zones. Pole figures corresponding to the {100} of ridge and non-ridge zones. Number of grains measured in S4-1: 602 and in S4-2: 612.

The orientation maps shown in Figure 3.5 a and b display the crystal directions parallel to the normal direction of the strip. Both samples show predominance of <100> but no particular clusters differing from the non-ridge zone. The pole figures in Figure 3.5 and those corresponding to samples S1 and S3 show no particular crystallographic textures in the {100} planes, as expected from the map results. In sample S2 some abnormal grains are observed in the non-ridge zone, but this feature has not been found in other samples. Abnormal grains can be associated with warm rolling, where ferrite grains transformed from prior austenite grains merge with the existing ferrite grains that recrystallize during rolling in dual-phase region.

3.3 Discussion

Microstructure and crystallographic texture in strips that developed ridges during hot rolling, and consequently ridge-buckle during subsequent rolling operations, were analysed. The main aim was to determine if the presence of ridges could be related to the occurrence of specific microstructural features or preferential crystallographic texture in the zone where the ridge is present as compared to the rest of the strip.

No evidence of microstructural differences between ridge and no-ridge zones was found in the strips that were analysed. Rocquet *et al* (1965) and Gilbertson (1965) found some evidence of diverse grain sizes in zones near the surface of the strip which corresponded to positions were ridge-buckle develop in further rolling processes. In our studies we could not detect any evidence of such differences in the microstructure, implying that the occurrence of ridge-buckle is not associated with microstructural variations. Moreover, the occurrence of ridges could not be linked to variations in rolling parameters that could produce different grain sizes in the ridge zones compared to the rest of the strip. Gilbertson (1965), found evidence of excessive cooling acting in two zones along the width of the strip while it was being hot-rolled and consequently found microstructural differences along the width of the hot rolled strip. We have not found evident occurrence of excessive cooling or lack of cooling along the length of the strip and hence, the ridges we observed cannot be explained by Gilbertson's observations. Furthermore, through our crystallographic texture analysis, we were unable to detect clusters of preferred orientation in the strips.

The experimental findings presented in this chapter provide convincing evidence that the formation of ridge in hot-rolled strips is not necessarily related to microstructural differences. Although the strip might be subjected to changes in temperature along its width and hence both static and dynamic recrystallisation may occur in the course of the rolling process, these changes do not seem to lead to variations in microstructure or crystallographic texture along the width of the hot-rolled coil. The sole occurrence of a ridge in the strip seems to be enough to produce ridge-buckle. In the next chapter, models of recrystallisation are utilised in an attempt to predict the effect of variations of temperature in the microstructural development of the strip.

Chapter 4
Influence of temperature variations on grain size development in hot-rolled strips

Significant variations on grain sizes in the ferritic structure of the hot rolled strip at room temperature were not found, as demonstrated in the later chapter. Nevertheless, the grain size on the strip after cooling does not necessarily reflect the evolution of microstructure in the different rolling passes during finishing-rolling. Minor temperature variations along the strip-width in the order of 20-30ºC are commonly observed at the exit of the finishing-mill. It is debatable as to whether these variations play a role on ridge formation, in part because of the slight changes in temperature and in part because in the past, these temperature fluctuations could not, be associated with the position of the ridge on the strip. The effect of these minor variations on the onset of recrystallization under practical rolling conditions has to the author's knowledge, not yet been determined and for that reason, an attempt was made to make an assessment of the possibility that such temperature variations might influence the mechanical properties of the material to the extent that it could lead to different mechanical behaviour in different parts of the strip. The objective is to simulate the hypothetical situation where a band of the strip enters the finishing-mill at a different temperature than the rest of the strip and to determine the microstructural development (and hence, mechanical property variations) under these circumstances.

In this chapter, a preliminary assessment of such a possibility is made. An attempt was made to use existing recrystallization models in order to determine to what extent temperature variations in the strip could lead to different degrees of recrystallization and hence, to variations in the microstructure attained at the end of the hot-rolling operation. However, imposing temperature variations within the strip along its width increases the complexity of the analysis to such an extent that a more simplified approach was taken as described below.

The main objective of the prediction of micro-structural development in cases where temperature variations are present along the width of the strip, is to determine the austenite grain size at various stages within the finishing mill and the final ferrite grain size following cooling on the run-out table. However, the three

dimensional effects of heat transfer within the transfer bar and strip are extremely complex and as a first and simplifying step, microstructural development was assessed by simply studying variations in the entry temperatures of the transfer bar and the strip as a whole. Briefly, the temperature of the strip going into the hot-strip mill was changed in discreet steps and the ensuing recrystallization studied.

4.1 Modelling recrystallization changes due to temperature variations in the strip

Strip temperature in the finishing-mill is measured by two pyrometers located before the descaling box and after the last set of rolls (F6) respectively, as illustrated in Figure 4.1. These infrared pyrometers detect the temperature at the centre width of the strip in a circular area of about 100mm diameter. The temperature measured by the pyrometer located at the exit of F6 is used as a boundary condition in a temperature model, which will activate inter-stand-cooling water sprays (located after F1, F2, F3 and F4) to lower the strip temperature when required.

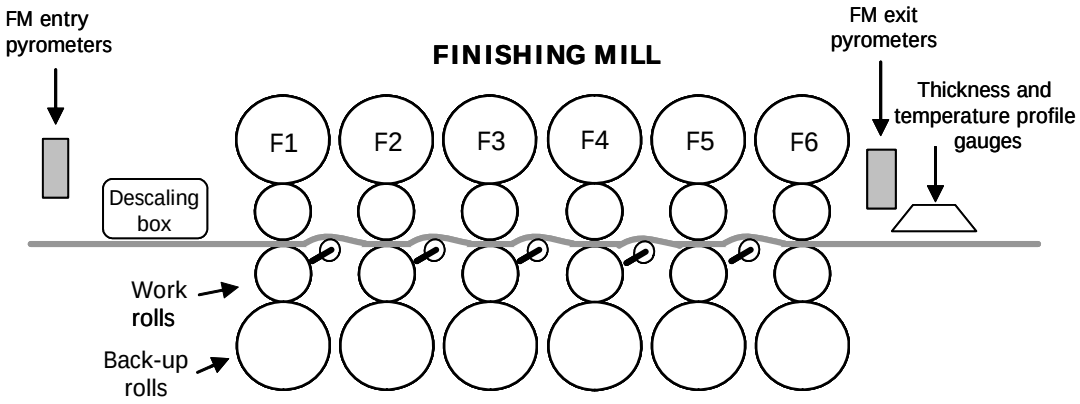

Figure 4.1 Schematic of the finishing-mill studied in this project showing the position of the pyrometers and Landscan temperature profile gauge.

Additionally, the temperature of the whole strip is measured by a linear infrared system (Landscan) located at the exit of F6, which reads on-line, the temperature along the strip width while the strip passes underneath the sensing device. Landscan provides the strip-width profile of temperature at any point along its length, as shown in Figure 4.2. The figure shows that at a position 100mm from the centre of the strip, the temperature is ~16ºC below the temperature recorded at

the edges of the strip, and in general, the temperature in the centre of the strip is lower than at the edges.

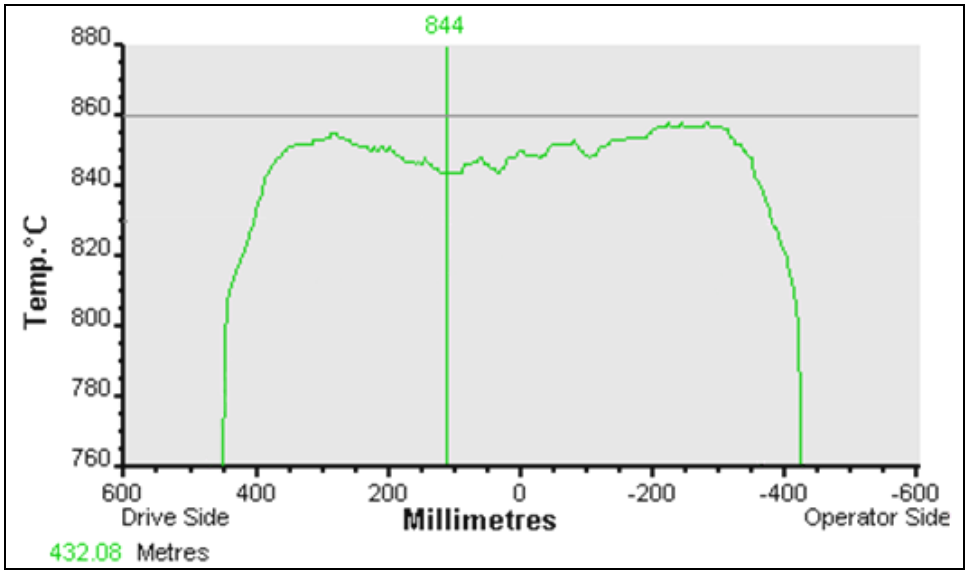

Figure 4.2 Typical Landscan profile of the temperature in a central position through the length of the strip.

From a practical point of view, the main questions to be answered about microstructural development are:

- whether the observed variations in temperature are sufficient to have a significant influence on the microstructural development of the strip during hot-rolling and
- whether the differences (if any) in final ferrite grain size that result from differences in microstructural development during hot-rolling, will be large enough to render significant differences in the mechanical properties between areas of the strip.

The premise is that if a band of material in the strip had different mechanical properties than the rest, that zone will deform differently during cold-rolling and may in this way lead to the formation of ridge-buckle defect.

We calculated grain size variations occurring in the finishing-mill when minor entry temperature variations occur by using the three empirical recrystallization models compiled in Table 2.1. These equations are presented in the forms proposed by the authors, Devadas *et al*, 1991c; Siciliano *et al*, 2000 and Stumpf, 2003 respectively so that they can be applied to the analysis of plain low-carbon steel devoid of alloying elements additions. By applying the equations we were able to predict the influence of minor temperature variations on the austenite grain size formed in

between the six rolling stands of the finishing-mill and the ferrite grain size formed after cooling.

In an operational hot-strip mill, there are many ways in which the strip is cooled, water from the descaling action, quenching by contact with the colder rolls, inter-stand cooling sprays and sweepers. The sweepers are a low pressure spray of water applied in the opposite direction to the travelling strip, located before entering the roll-bite and used to displace excess water accumulated on the top surface of the strip. All of the sources of cooling are approximately applied uniformly to the surface, so that the temperature in the bulk of the strip will quickly be equalised. The total variation of temperature in the bulk of the strip along the finishing mill is about 200ºC (from entry into the descaler to the exit at F6); and the descaler action alone can contribute to a reduction of about 70ºC of the entry temperature of the strip (Devadas *et al*, 1986). On the other hand, irregular cooling or heating patterns can develop on occasions when normally well-controlled mill operating conditions fail, for example when roll cooling water comes in direct contact with the strip, when nozzles fail in the descaler or in the cooling system of the rolls.

In order to evaluate the significance and meaning of strip temperatures measured by the Landscan instrument, at the exit of the finishing-mill, it is important to determine whether or not the bulk temperature or merely the surface temperature of the strip is measured. Devadas *et al* (1986) used finite element analysis to calculate the rate of heat transfer into the strip following cooling of the surface. They demonstrated that when the strip makes contact with a work-roll in the finishing-mill, the strip surface temperature will be reduced by up to 400ºC, this temperature drop penetrating no more than $1/10^{th}$ of the strip thickness. On exiting the roll-bite, the temperature of the strip surface is recovered almost instantaneously to only 20ºC or 30ºC below the bulk strip temperature. After a few milliseconds the surface and bulk reach the same average temperature as the centre-strip temperature, while most of the heat loss occurs in the roll bite. According to these calculations, the temperature detected by Landscan few meters after exiting F6 should be an indication of the bulk temperature of the strip and not solely the surface temperature

4.1.1 Boundary Conditions

- The recrystallization models shown in Table 2.1 were used to analyse recrystallization behaviour of a strip of tinplate in a six-stand finishing mill, using data from a typical tinplate hot-rolling schedule as shown below. The equilibrium

transformation temperature of austenite to the two-phase region (A_3) is ~887ºC for the steel used in this study, the composition of which is shown in Table 4.1.

- The six 4-high stands of the finishing mill are referred to as F1 to F6 from entry to exit.
- The rolling conditions used in the following analysis were selected from plant data pertaining to the rolling of a tinplate strip and are shown in Table 4.2. The interstand time under the F6 column corresponds to the time it takes to the strip to travel 6 meters from the last stand.

Table 4.1 Composition of the tinplate steel used in the analysis

% by mass	C	Mn	Si	Mo	Cr	Cu	N	Ni	P	Fe
Tinplate steel	0.046	0.26	0.005	0.002	0.065	0.007	0.004	0.024	0.01	bal

Table 4.2. Rolling conditions selected from plant data for the rolling of tinplate strip

Input		unit	F1	F2	F3	F4	F5	F6
Entry thickness	h_f	mm	32.99	15.82	8.63	5.12	3.26	2.44
Exit thickness	h_0	mm	15.82	8.63	5.12	3.26	2.44	2.11
Temperature	T	ºC	982	974	953	932	911	890
Roll radius	r	mm	306.62	349.29	332.75	313.50	342.12	349.70
Interstand time	t_{ip}	s	5.24	3.16	1.96	1.19	0.82	0.68
Rolling force	P	MN	16.159	16.530	14.595	13.507	12.167	10.907
Strain	ε		0.85	0.70	0.60	0.52	0.34	0.16
Strain rate	$\dot{\varepsilon}$	s^{-1}	12.28	24.29	49.56	99.40	134.24	135.76

The following assumptions were made:

- In an attempt to simplify the calculations, the temperature losses between stands are not taking into account and heat transfer is assumed to occur solely in the roll bite. Hence, the strip temperatures displayed in Table 4.2 remain constant in the roll bite and in the inter-stand space until the strip contacts the following roll.
- The temperature in each stand was calculated by relating the exit temperature of the strip and the thickness in each stand using the same models that are used in the industrial hot-strip mill. For the strip thickness range under discussion, the difference between enter and exit temperatures in F1 is 7.6ºC, and the difference in the other stands is 21ºC.
- The grain size of the transfer bar entering F1 is taken as 60μm.

- The cooling rate on the run-out table is 20ºC.sec^{-1}, and the coiling temperature used in the calculations is 600ºC
- Because the model of Devadas *et al* does not allow the calculation of the ferrite grain size after transformation, the equations of Siciliano *et al* (originally proposed by Sellars *et al*, 1979) have been used for this purpose.
- Reference to grain size is to austenite grain size unless otherwise stated, although rolling may be occurring in the two-phase region.

4.1.2 Model calculations

In order to simulate the effect of temperature changes in the hot-strip mill, the following methodology was employed:

The strip temperature at entry (F1) was changed in steps of 50ºC from 900ºC to 1150ºC and the respective temperatures in stands F2 to F6 estimated by linear interpolation. These new temperatures were then used in the recrystallization equations from Table 2.1, keeping the remaining parameters constant as indicated in Table 4.2. Using the three different models shown in Table 2.1, the austenite grain sizes were calculated after grain growth has occurred, following rolling in a specific stand (and before entering the next stand). The final austenite grain size at a distance of 6m from the exit of stand F6 was also determined. The results of the calculations for each model are shown in Figure 4.3.

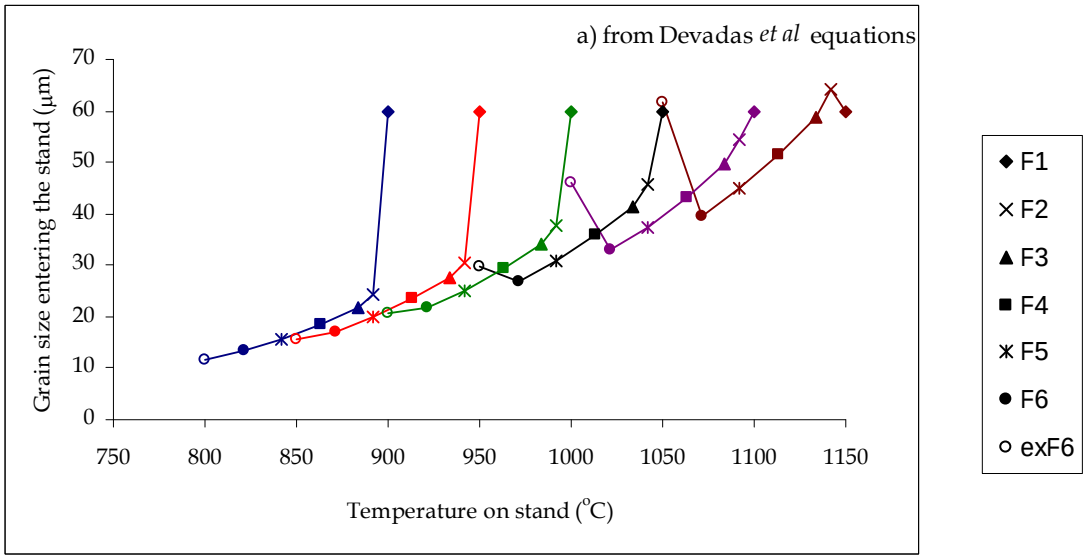

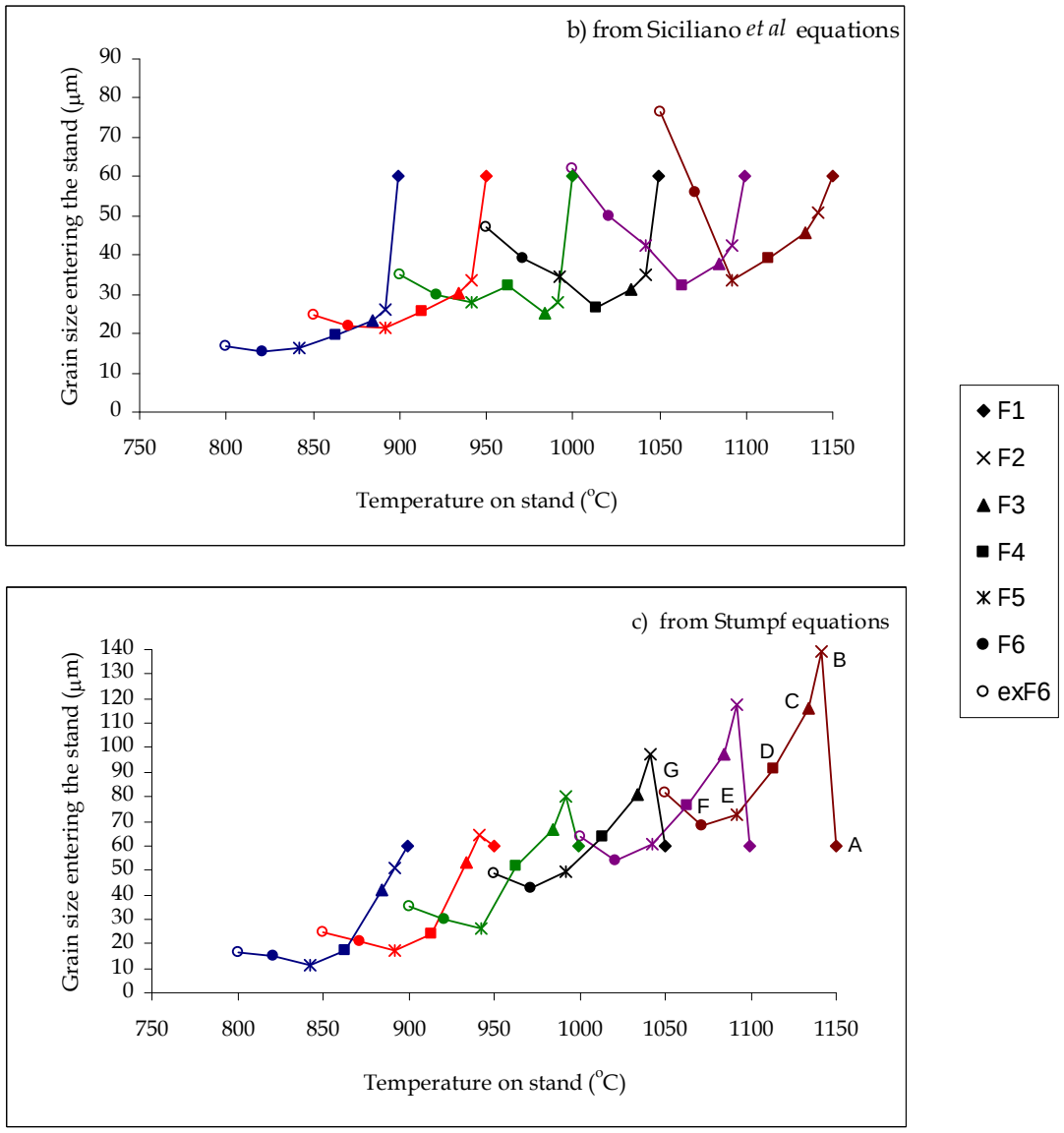

Figure 4.3 Grain size formed after recrystallization and growth in each stand at the specified temperatures. Grain sizes at exF6 correspond to the values developed at a distance of 6 meters from the last stand. Calculated by using the equations compiled from a) Devadas *et al* b) Siciliano *et al* and c) Stumpf.

The construction of the curves in Figure 4.3 is explained by following the line marked with letters in Figure 4.3c. Entering F1 in point A, the strip has a selected temperature of 1150ºC and an austenite grain size of 60μm. The strain applied in F1 is high enough to exceed the critical strain of the material calculated according to the temperature and strain rate applied therefore, the recrystallization will occur during deformation (DRX). After grain growth, occurring in the 5.24s between F1 and F2, the grain entering F2 (point B) has reached 140μm in size. With the new value of grain size, temperature and strain rate at F2, the critical strain is calculated again, compared to the applied strain in F2 and it was determined that DRX is also occurring in F2. The appropriate equations (in this case corresponding

to Stumpf work) should be used according to the dominant mechanism of recrystallization and the interstand time. The grain size entering F3 (point C) after grain growth is 110μm. Following the same method it is determined that recrystallization is dynamic also in F3 and F4, but SRX occurs in F5 and F6. In point G (exF6) is represented the grain size of austenite that will develop after grain growth for the time it take to the strip to travel 6 meters from the last stand (0.68s). The change from dynamic recrystallization (DRX) to static recrystallization (SRX) can be identified in Figure 4.3 as a sharp increase in the grain size in the same curve. To read the recrystallization mechanism it should be considered that the grain size represented is an illustration of the mechanism occurring in the previous stand, for example, points F and G denote that SRX occurred in stands F5 and F6 respectively. In the same fashion, on the blue curve of Figure 4.3c, corresponding to entry temperature of 900ºC, DRX occurs in F1 and F2, while SRX is occurring on F3 to F6.

It is important to note that it has not been the objective of the present study to assess the accuracy of the different models. The models were merely used to predict changes in microstructural development as a function of changes in the entry temperature of the strip. In general, an increase in temperature increases the grain size following recrystallization and grain growth although the different models render different predictions of the actual grain size and onset of dynamic recrystallization. The Stumpf model (Figure 4.3c) predicts that dynamic recrystallization will occur in the first 4 stands when the entry temperature of the strip is higher than 1050ºC, whereas at lower temperatures DRX occurs in the first 2 to 3 stands only. In similar vein, Siciliano *et al* predict that DRX will occur in the first 4 stands at high temperatures and SRX in all stands at low entry temperatures. The lower the temperature, the higher the possibility of having static recrystallization and hence larger grain sizes. On the other hand, the equations of Devadas *et al* predict that DRX will occur in the first 5 stands irrespective of the entry temperature. Static recrystallization leads to a larger austenite grain size than DRX, and SRX occurring in the last stand can develop austenite grain sizes as large as the grains formed after the first stand.

In terms of grain dimensions, the Stumpf model predicts that austenite grain sizes between 10μm and 140μm can form during rolling, while the Devadas and Siciliano models predict austenite grain sizes ranging between ~10μm and 80μm. Nevertheless, all the models calculate that the austenite grain size at a distance 6m from the last stand will vary between 10μm and 80μm. Although the different models predict the development of different austenite grain sizes within the

process, all three models predict that the final ferrite grain size will vary by less than 10μm between the two extreme temperatures studied, as depicted Table 4.3.

Table 4.3 Calculated ferrite grain sizes entering the coiler based on the austenite grain sizes calculated by the recrystallization models

		Calculated grain sizes (μm)	
		Austenite exiting F6	Ferrite entering coilers
Devadas *et al* (1991[c])	max	62	14
	min	12	5
Siciliano *et al* (2000)	max	77	18
	min	17	7
Stumpf (2003)	max	82	21
	min	17	11

4.2 Strength of the strip

In order to determine the strength of the strip deformed during recrystallization, the equations of mean flow stress proposed by Misaka (1967) and Stumpf (2003) and presented in Table 2.2 can be used according to the occurring recrystallization mechanism (SRX or DRX). The results of the strength calculations as a function of temperature in a specific stand are presented in Figure 4.4.

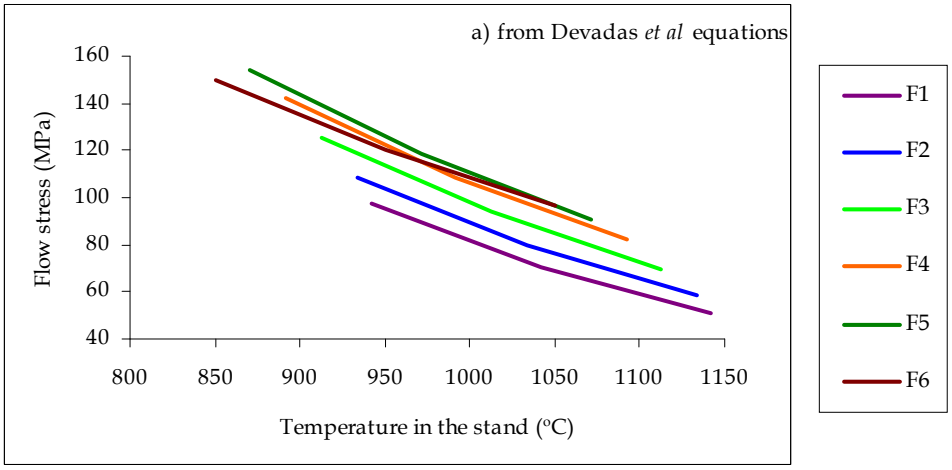

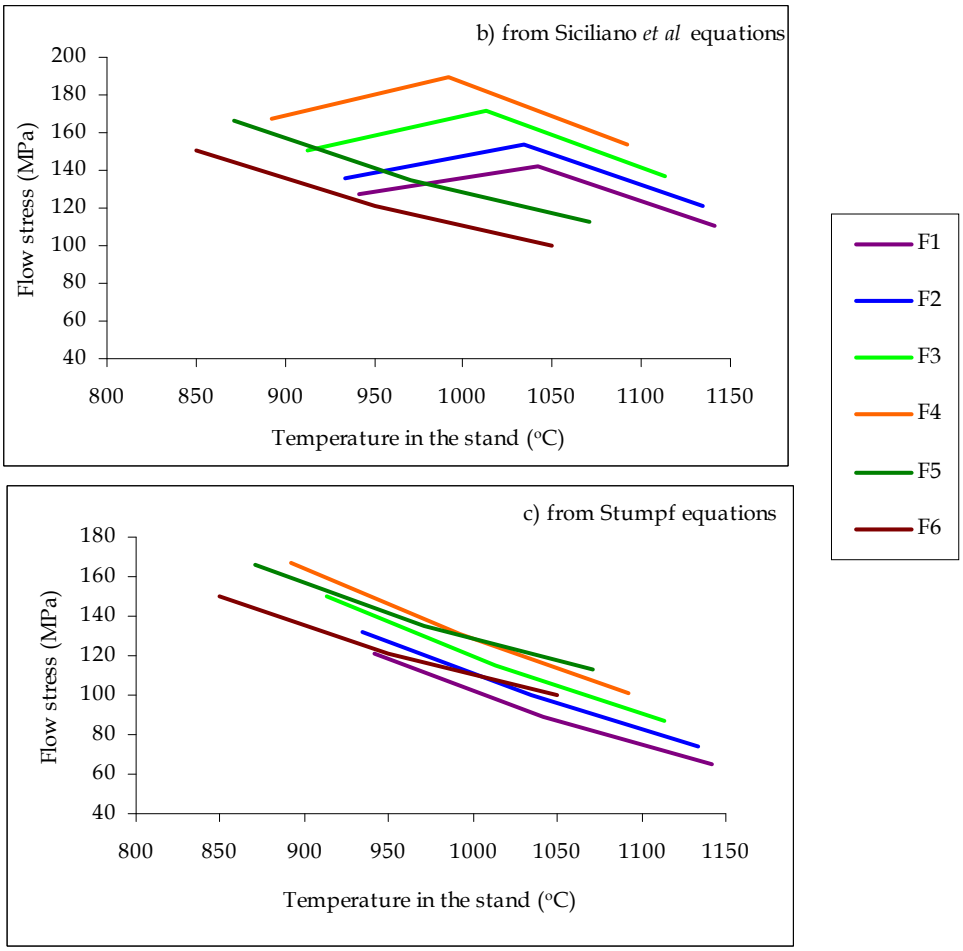

Figure 4.4 Effect of temperature on the flow stress. Assuming the control values of strain and strain rates from Table 4.2 are applied to the strip.

The curves in Figure 4.4 are constructed by using the results of the recrystallization models. After elucidating the recrystallization mechanism that is occurring in each stand at a determined temperature, then the corresponding equation from Table 2.2 is selected and the flow stress calculated. Similarly to Figure 4.3, a sharp change in the slope of the curve represents the change in the mechanism of recrystallization affected by rolling temperature. Figure 4.4 shows that there are significant differences in the strength calculated by the different models. Nevertheless, it seems reasonable to conclude that a 200ºC temperature variation will cause a maximum strength change of 50MPa during hot rolling.

The Modified Hall-Petch equation (Eq. 2.5) was used to calculate the effect of ferrite grain size at room temperature on the strength of the strip. The results compared with the grain sizes obtained in the three models are depicted in Figure 4.5.

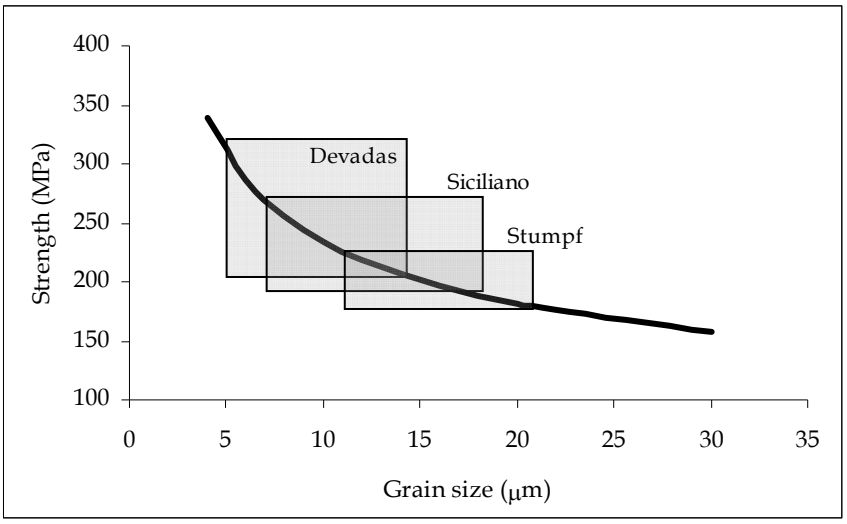

Figure 4.5 Influence of ferrite grain size on the strength of the material at room temperature.

It is evident in Figure 4.5 that the strength of the strip at room temperature is strongly influenced by ferrite grain sizes smaller than 20μm. The prediction of strength depends on the ferrite grain size calculated in every model. The biggest strength change is predicted by Devadas *et al* equations in where a temperature variation of 200ºC during hot rolling, would change the strength of the cold strip by 130MPa. In the predictions, using the equations of Stumpf, the grain sizes obtained were much larger than those predicted by the other models and the strength variation due to the same 200ºC temperature change, is of only 48MPa. The experimentally determining ferrite grain size in this type of steel (See Chapter 3) varied between 5 to 8μm, meaning that the predictions using the Devadas *et al* (1991[c]) model seem to more closely resemble reality.

4.3 Discussion

Recrystallization and strength models (See Chapter 2, sessions 2.2.1 and 2.1.2 respectively) were used to predict variations in grain size and strength of hot rolled steel strips. Temperature variations of the order of 200ºC were imposed as boundary conditions in the three popular recrystallization models referred to above. Using these models, austenite grain size deviations induced by the imposed changes in temperature were predicted for the steel strip entering each one of the six stands of the finishing mill. These same models were used to also predict the ferrite grain size as a function of the calculated austenite grain size variations in the coil of hot rolled strip following cooling on the run-out table. The likely strength variations that the strip will undergo as a result of the recrystallization that occurs

in each stand during hot rolling were calculated and finally, the strength of the strip that is to be cold-rolled was calculated as a function of the final ferrite grain size.

The model predictions have shown that variations in temperature of the order of 200ºC may lead to significant variations in the grain size of austenite in the first four stands of the mill, but very little variations occurred in the last stands or when the strip exits the mill while still in the austenite phase. At constant strain and strain rate, a decrease in temperature will result in more stands being subject to static recrystallization only. On the other hand, relatively large temperature variations within the hot-strip rolling mill can be accommodated without unduly affecting the final ferrite grain size.

The recrystallization models used in conjunction with strength models (Chapter 2 sessions 2.1.1 and 2.1.2 respectively), predict an increase in strength of 50MPa if the temperature of the transfer-bar entering the hot-strip mill is lowered by 200ºC. This change in strength is significant enough to cause differences in mechanical behaviour in the roll-bite, should temperature variations of this magnitude be present along the width of the strip. However, experimentally, the maximum temperature variation along the strip at the exit of the finishing mill that has been recorded, assuming that the austenite to ferrite transformation has not yet occurred, was 30ºC. Such a variation in the worst scenario, can lead to changes in strength in the order of 9MPa, which is unlikely to be of great significance.

The final strength of the hot-rolled coil at room temperature is governed by the ferrite grain size and the composition of the strip. Following the same argument explained before, in where the maximum temperature variation recorded is of about 30ºC; the worst scenario in terms of strength (as shown in Figure 4.5) will be a variation between the smallest calculated ferrite grain size (5.07μm) and the grain size developed at a temperature 30ºC hotter (5.57μm). These result in a variation of strength of 12MPa. It is therefore highly unlikely that local variations in temperature across the width of the strip can lead to significantly different microstructures and hence, mechanical properties in the final product.

To finalise this chapter, some further observations regarding the temperature measurements with landscan should be emphasised. The temperature system is based on comparison of infrared emission from the top surface of the strip and it can accurately measure variations of temperature within ±5ºC. The fact that the temperature is measured by infrared emission from the surface means that scale

formed on the strip may play an important role in the accuracy of measurements. Das *et al* (2004) demonstrated that the scale thickness has a linear inversely-proportional influence in the heat transfer from strip to roll (e.g. for scale 26μm thick, the convection heat transfer coefficient, h = 170 $kW.m^{-2}.K^{-1}$; for scale 100μm thick, h = 30 $kW.m^{-2}.K^{-1}$). Furthermore, numerous heat transfer models (Devadas *et al*, 1986 and Colas *et al*, 1998) demonstrated that the strip regains a uniform temperature in a very short time. It is therefore possible that the strip temperature variations depicted by Landscan when the strip exits the mill, are likely to be a reflection of the state of the scale on the strip rather than the temperature on the strip itself.

The minor changes in temperature observed in Landscan might be causing variations during hot rolling, but produce little variation on the final ferrite grain size. These findings confirm the results presented in chapter 3, in where no significant variations in grain size or crystallographic textures were found on strips at room temperature. It is unlikely that those variations in ferrite grain size can produce further uneven rolling loads. Further exploration on the plant conditions were done to discard or validate the possibility that the shape of the roll might be influencing the formation of ridges in the hot rolled strips, and are presented in the following chapter.

Chapter 5
Plant data analysis

The findings described in the previous two chapters led to seriously question some of the proposed causes for the origins of ridge-buckle defect. A thorough experimental investigation, described in Chapter 3, failed to establish appreciable differences in microstructure across the width of hot-rolled strips and it seems unlikely that ridge-buckle defect can be attributed to microstructural differences in hot-rolled strip. Attempts were made, and described in Chapter 4, to assess the possibility that temperature variations across the width of the strip could lead to significant differences in mechanical properties in bands of the hot-rolled strip, thereby leading to ridge-buckle defect. By using recrystallization and strength models, our calculations have shown that the variations in mechanical properties of either the strip within the rolling mill, or the final product are insufficient to cause significant variations in mechanical properties across the width of the strip to be able to account for ridge-buckle defect. The next approach in our quest to establish the root cause of ridge-buckle defect was to attempt to link ridge formation during finishing-mill rolling with the integrity of the work-rolls in contact with the hot strip while it is being rolled.

Effectively, work-rolls wear during rolling and it is this phenomenon that delimits the schedules. A schedule consists of a number of slabs being rolled between work-roll changes and the material of the slabs in each schedule is of similar composition. Models of roll-wear under normal conditions are used to design the schedule and predict the life of the rolls. Once the rolls are extracted from the mill after each schedule, they are processed in the roll-shop and ground to new dimensions in order to eliminate the worn zone and to re-introduce the required crown. It is possible that roll shape can play a role in the formation of ridges in the hot-rolled strip, especially if any unusual or uneven wear occurs while the schedule is being rolled. The main purpose of the in-plant investigation, described in this chapter was to establish if uneven roll-wear could be correlated with the appearance of ridge in the hot-rolled strip. Data on the characteristics of roll wear and the strip profiles were collected after rolling for 40 consecutive schedules and are presented and discussed in this chapter.

5.1 Description of the work-rolls

The six pairs of work-rolls used in Port Kembla Steel-works (see Figure 4.1) are of two types, high-speed steel (HSS) and indefinite-chilled double-poured cast iron (ICDP). HSS coated rolls are used in the first three stands while the rolls in the last three stands are coated with ICDP. The selection is dictated by the strain and speed of rolling. The microstructure of both types of roll shell is basically a combination of carbides embedded in a martensite matrix. The typical composition and properties of the work-rolls are shown in Tables 5.1 and 5.2.

Table 5.1.Typical composition of the finishing-mill work-roll shells at Port Kembla BSL plant. Content of the additives V, W, Co and Ti are common values in these types of steel because exact compositions are not available. After Kubota and Nippon steel technical specifications and Sano *et al* (1992)

Coating type	**Chemical composition (mass %)**											
	C	Ni	Mn	Cr	Mo	V	W	Co	Ti	Si	P	S
HSS for stands F1 to F3	2.07	0.11	0.53	3.99	5.01	3 - 10	2 - 10	<5	-	0.6	0.028	0.019
ICDP for stands F4 to F6	3.4	4.3	0.7	1.8	0.35	0	0	0	<0.03	0.64	0.038	0.008

Table 5.2. Typical properties of the finishing-mill work-roll shells at Port Kembla BSL plant. After Kubota corp., work-roll specifications.

	Shell metal structure			**Bulk properties**					
	Graphite	Carbides	Matrix	Tensile strength $(MPa)_1$	Hardness (HV)	Thermal Diffusivity (m^2/s)	Young modulus (GPa)	Thermal conductivity (W/m*K)	Friction coef.
HSS	No	MC, M_2C, M_6C	Martensite	780-850	777-809	$5.6x10^{-6}$	218	25.5	0.34
ICDP	Involved	M_3C	Bainite, Martensite	400-500	746-774	$4.3x10^{-6}$	170	23.5	0.3

In HSS rolls, thermal treatments after casting transform the retained austenite to stable martensite matrix and promote the precipitation of secondary carbides (Sano *et al*, 1992). The stoichiometry of the carbides varies depending on the added elements as shown in Table 5.3. The high-carbon iron cast by the ICDP process consists of a martensitic matrix with dispersed graphite particles and seams of iron carbide at the grain boundaries.

Table 5.3. Carbides and carbide forming elements in HSS steels. From Ohata, 2002.

Carbide Type	Main carbide-forming elements	Hardness (HV)	Shape of carbide
M_3C	Fe	1100-1300	Eutectic
M_7C_3	Cr	1400-1800	Eutectic
MC	V	2800-3000	Particle
M_2C	Mo, W, Cr, Fe, V	1600-2000	Eutectic
M_6C	W, Mo, Fe, Cr	1200-1800	Eutectic

One feature of the operational practice employed at the finishing-mill that is of significance, is the practice of side-shifting of the rolls. In order to assure uniform wear of the roll surface, the top and bottom rolls from F2 to F6 can be displaced 20mm parallel to their axis in opposite directions before each strip enters the mill, for a maximum distance of ±140mm from the central position. The displacement of the rolls is controlled according to the design of the schedule and the rolling parameters in the roll-stand.

5.2 Data collection method

Data were collected from 40 hot-strip mill schedules on Port Kembla Steel-works included in schedules numbers 576 to 621 year 2004.

- Graphics of the profiles of the 12 work-rolls used on each schedule were extracted from the database of roll shop grinders 1 and 2 between 17 April 2004 and 8 May 2004.
- Centre ridges in the strips rolled in those same schedules were determined by analysing each strip profile in a program designed for the detection of ridges

5.2.1 Roll wear analysis

- The objective is to discriminate rolls that display uneven wear from rolls that have worn in a normal fashion. Uneven wear is defined as any deviation in the diameter of the roll more than 20μm from the normal wear shape. An example of two types of roll profile and uneven roll wear are shown in Figure 5.1. Continuous variable crown (CVC) roll profiles are used in stands F2 and F3, which have an S-type shape allowing a continuously adjustable roll-gap contour (shown in Figure 5.1) (Lu *et al*, 2002).

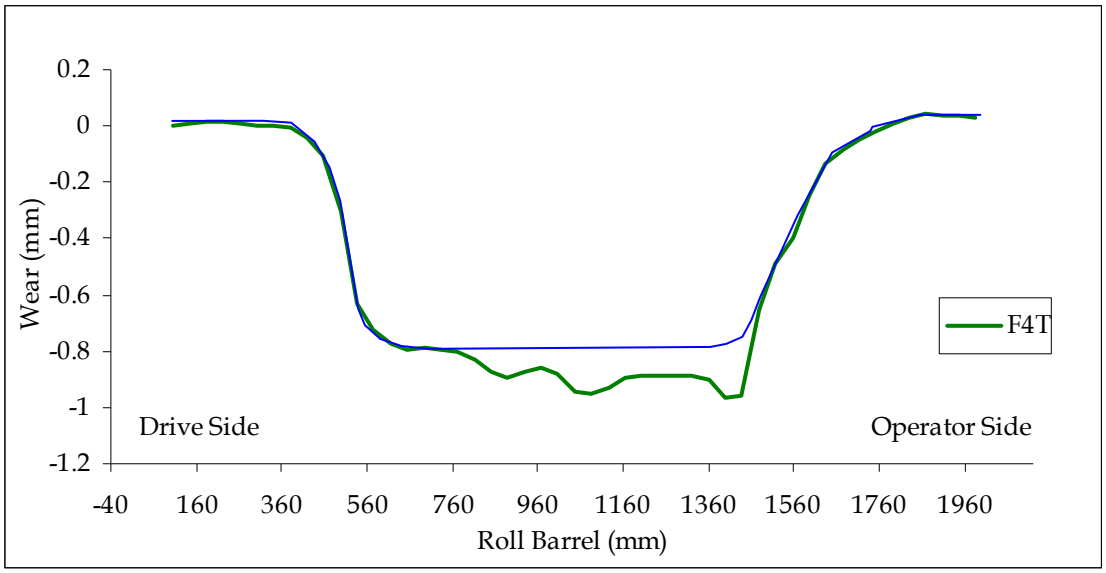

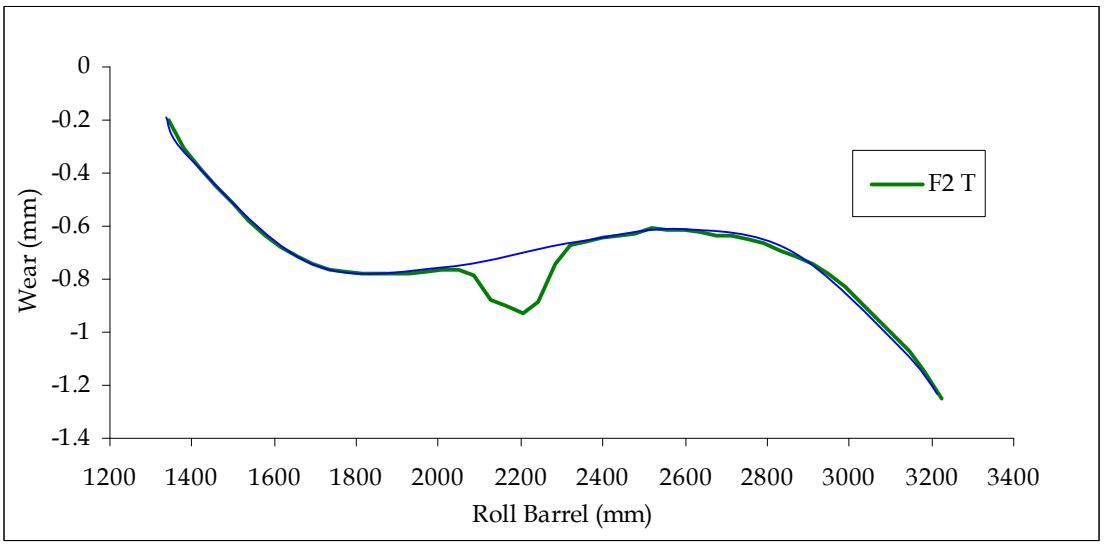

Figure 5.1. Example of uneven roll-wear in the profile of rolls corresponding to F4 and F2 top work-rolls. F4 rolls are ground to a cylindrical shape , while F2 rolls are ground with CVC shape. Blue lines represent the normal wear profiles

For the rolls that showed uneven-wear, the position, width and thickness deviation from the ideal profile of each groove was recorded. These measurements were made manually by making measurements from the prints provided by the roll-grinders of the profiles of 480 rolls. The roll-profiles so determined were then compared with the profiles expected when a roll wear in a normal way, as shown in Figure 5.1.

a) Three positions of uneven wear were recorded:

- *Edge left*: grooves in the roll that are positioned at the left edge of the worn zone. In case of F1, F2 and F3 rolls, in which the total wear is minor and the shape can be CVC, the position is compared with the width of the last strip to determine if it is edge wear.

- *Edge right*: At the right edge of the worn zone
- *Centre*: Any groove not touching the edges. Only centre grooves of less than 400 mm were considered.

b) The width and depth of any groove with a difference of more than 20μm in height with respect to normal roll wear was considered to be caused by uneven roll wear and recorded. The severity of roll wear was classified as follows:
   - Severe groove > 51μm
   - Mild groove 26 μm to 50μm
   - Soft groove <25μm

5.2.2 Strip analysis

Centre ridges are detected between −350 mm to +350 mm from the centre of the strip. Each strip profile that was measured by the thickness profile-meter located at the exit of the mill was compared with its ideal parabolic shape. In order to calculate the parabolic shape it is required to use the real profile measurements of the strip and accommodate it to the closest parabola, as the dimensions in each strip can be different and a common parabolic shape cannot be used. A fitting program had therefore to be developed to detect the occurrence of centre ridges on the strips rolled during the selected period. The fitting program for the parabolas was constructed in MS Excel software and it is shown and explained in more detail in Appendix A. By using the fitting program for the parabolas and comparing it with the real data made it possible to extract ridge occurrences in widths between 30 and 300mm and heights above 6μm.

In the production line, four types of schedules are run. Strips with similar end use are rolled together, schedules of tinplate (TP) group all strips to be cold rolled, tempered and metal-coated; schedules called CR arrange steels that are going to be cold rolled for the manufacture of corrugated material and also include silicon containing steels; PL schedules consist of material to thicknesses greater than 5mm, mainly for pipeline use. Any other steel that remain in the hot-rolled condition for different uses are grouped in the HR schedules.

5.3 Results

5.3.1 Roll wear analysis

Uneven roll wear occurred on at least one roll in 98% (39 out of 40) of the schedules studied. Although in some instances more than one roll in the same schedule was affected. From the 480 rolls used in the schedules studied, 163 (34%) were affected by uneven roll-wear. The distribution of uneven wear per work-roll in the finishing mill in the period studied is shown in Figure 5.2.

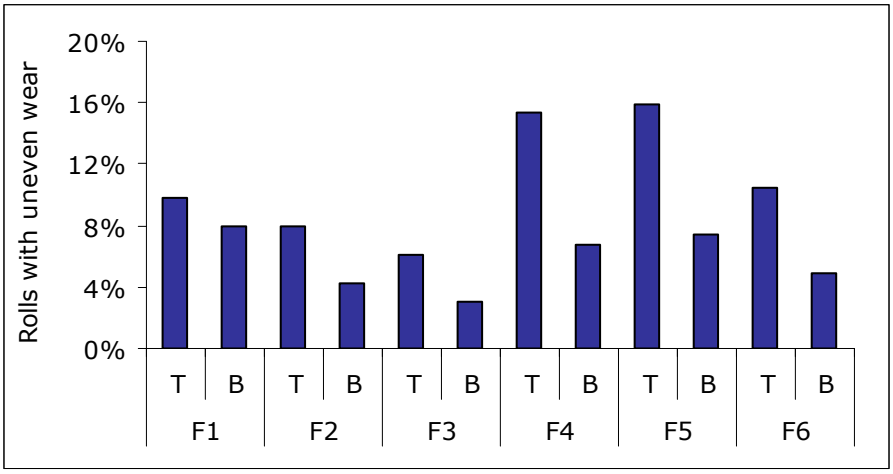

Figure 5.2. Frequency of uneven roll wear occurrence in the finishing mill. T: Top rolls, B: Bottom rolls

As shown in Figure 5.2, uneven-wear might occur in any roll, being more common in F4 and F5 top rolls. The F3 rolls are the least likely to be affected by roll wear with just 3% of all bottom rolls used presenting uneven roll-wear. From the total number of rolls affected, 66% were top rolls, which is consistent with the fact that top rolls wear more under normal circumstances. The position of the grooves on the roll is depicted in Figure 5.3.

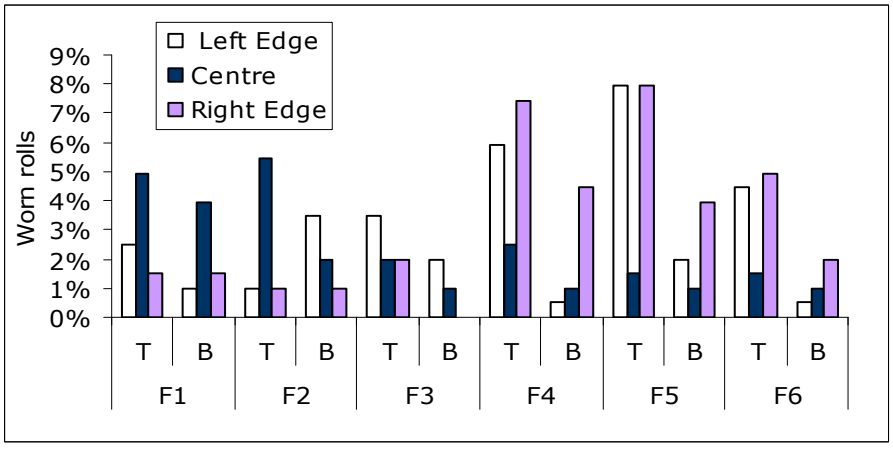

Figure 5.3. Uneven wear frequency in each work-roll according to the position on the rolls

It follows from Figure 5.3 that rolls from stands F1 and F2 have the highest incidence of centre wear while the wear on F4 and F5 is mainly occurring at the edges of the worn zone. The uneven centre-wear of rolls is the main interest of our study because it might lead to centre ridge on the strip; while edge wear will produce another defect known as edge ridge. Nevertheless, sometimes uneven wear on the edges of the wear zone of the roll can overlap near the centre and possibly be contributing to –centre-ridge formation.

The severity of the grooves formed on the rolls is represented in Figure 5.4. It is shown that medium-size centre grooves are most common in the rolls of the F1 and F2 stands, while soft wear occurs more frequently in the last 4 sets of rolls.

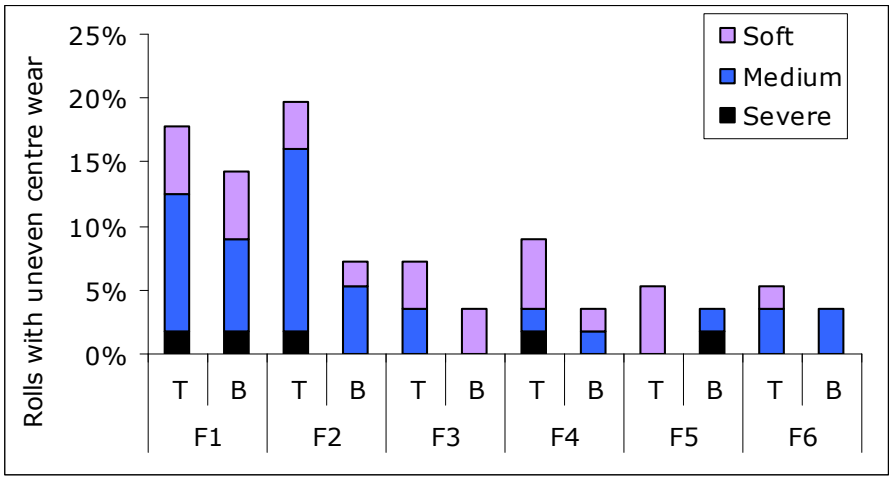

Figure 5.4. Representation of the frequency of uneven wear in the centre of rolls with respect to the severity of the groove. Severe groove > 51μm; mild groove 26 μm to 50μm and soft groove <25μm

The type of schedule rolled affects the occurrence of roll-wear. It is observed in Figure 5.5 that the two schedules of pipeline (PL) rolled during the period were not affected by uneven centre roll-wear. The schedules of tinplate (TP) are less affected than hot rolled or cold rolled schedules while centre wear is higher in rolls F1, F2 and F4 in tinplate schedules.

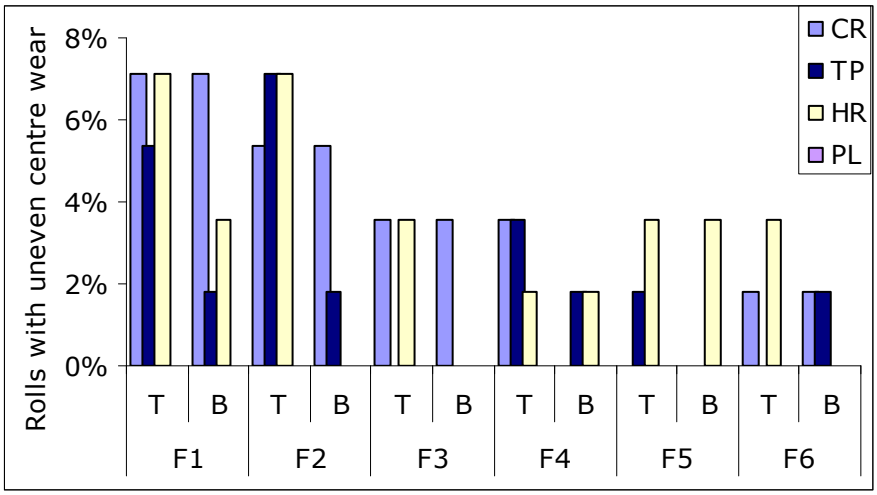

Figure 5.5. Uneven centre-wear occurrence by type of schedule. CR: strips to be cold rolled, TP: strips to be used in tinplate fabrication; HR strips that remain in the hot rolling sizes, PL : strips used for pipeline products.

Figure 5.6 represents uneven roll-wear occurring in the centre of the roll in the sequence of 40 schedules studied. The data represented in this figure is used to make a comparison so as to determine whether uneven centre-wear is repetitive under some circumstances. For example, few rolls are affected in the first 3 consecutive schedules, in further schedules none are affected and then they start to be affected again by uneven centre-wear for two consecutive schedules, and so on. Some schedules can have as much as five rolls affected while others might not have rolls affected with uneven centre-wear at all. Figure 5.6 also show that top and bottom-rolls can wear independently in a given schedule, and there were only three schedules in which a bottom-roll wore exclusively.

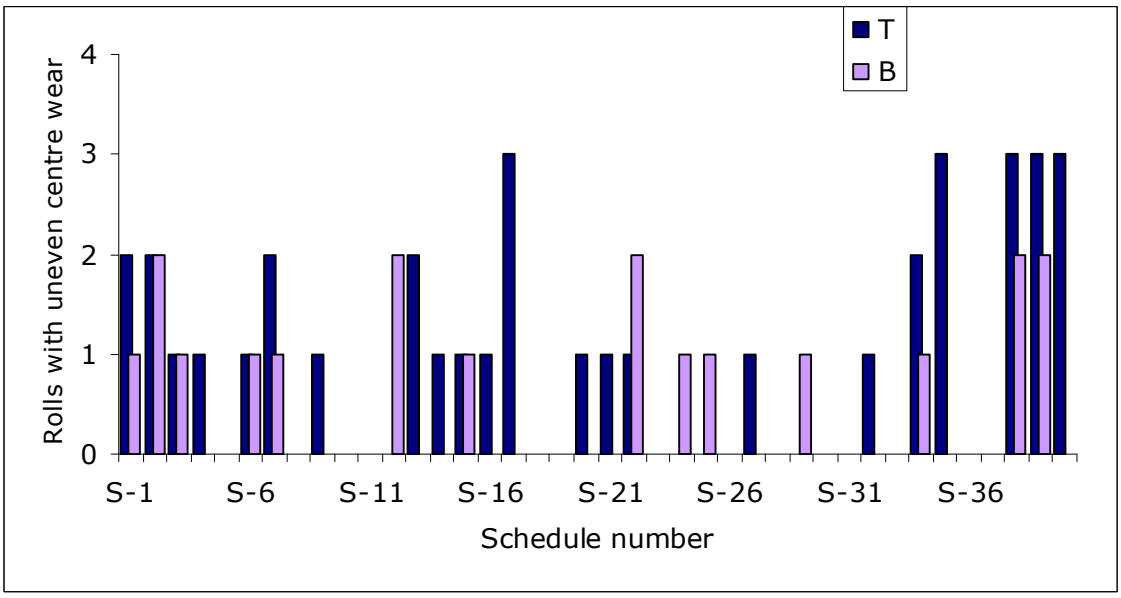

Figure 5.6. Representation of the number of rolls with uneven centre wear occurring in each schedule, separated by top and bottom rolls. S: schedule number.

To better illustrate the effect of the worn rolls in each schedule, the distribution of the rolls affected with uneven centre-wear according to the type of schedule and the stand affected is presented in Figure 5.7.

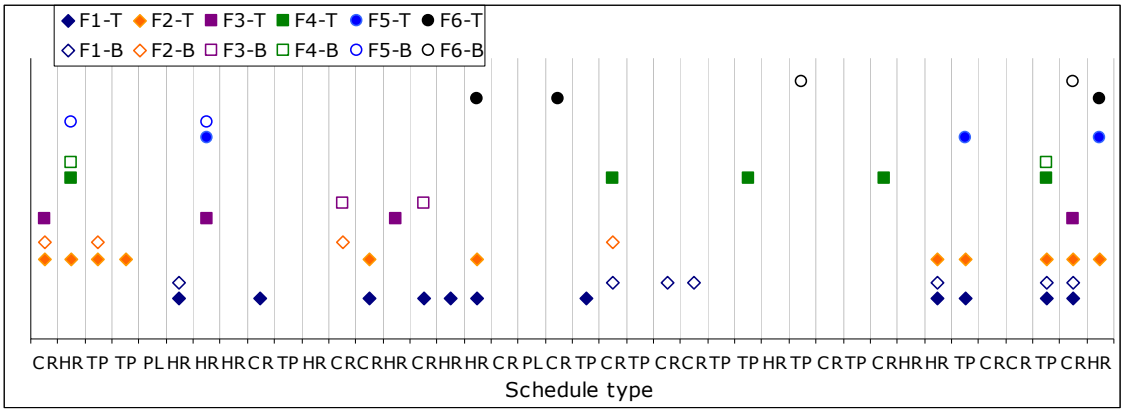

Figure 5.7. Distribution of rolls with centre uneven wear in each schedule analysed, including the type of schedule

In Figure 5.7, the rows show the position of the roll with respect to the stand number and whether it is located on the top or bottom of the stand; the columns are the consecutive schedules specified according to the type of schedule rolled as explained in session 5.2.2. Every mark in Figure 5.7 denotes that the roll experienced uneven centre wear. It can be read for example that the first schedule was of cold rolled products (CR) and the rolls positioned in F2 top and bottom and F3 top presented uneven centre wear. On the next schedule (with new set of rolls), the product rolled was to remain hot rolled (HR) and the rolls affected with centre wear were in this case F2 top, F4 top and bottom, and F5 bottom.

Analysing Figure 5.7 it can be found that uneven wear on roll occurs sporadically. The wear is sometimes repeated in the top and bottom rolls of the same stand, but it is not a restrictive condition. In some instances, the wear of one roll in a set is repeated in the following schedules irrespective of the type of material rolled. It should be emphasized that the rolls used in one schedule are not reused in the next schedule. Sometimes rolls of HSS from F1 to F3 can be reused when passing a visual test of quality. Nevertheless this process requires the rolls to be extracted, transported to the roll-shop, checked and then placed in queue to be reused, meaning that the same roll type without being grinded is only reused after at least two schedules have been rolled since the roll was extracted from the mill.

As it is shown in Figure 5.7, the wear of the roll positioned in a set can be repeated for three or four consecutive schedules and then stop occurring in the following schedule. See for example the first schedules in where F2 top roll present uneven centre-wear repeatedly for four consecutive schedules, but cease to occur in the next 8 schedules and reappear again in the 9th schedule, and so on. This pattern of repetition and cease of uneven centre-wear might be related to changes in the mill conditions which are not necessarily evident or are checked in the common practice. Profiles of the rolls that can serve as evidence of uneven roll-wear are usually collected hours after the schedule occurred, therefore a follow-up on possible changes that could have occurred in the mill while the roll was in operation is quite difficult. Moreover, minor changes in the mill conditions are not systematically reported, therefore variations in the parameters of rolling like strip temperature along the width, number of interstand coolers activated or simple maintenance routines can modify some conditions in the mill leading to correct the uneven roll-wear without knowing exactly the factors that originate it in the first place.

5.3.2 Strips analysis

Ridges occurred in all of the schedules analysed, with at least six strips of the schedule affected. Tinplate schedules displayed the lowest ridge occurrence, while pipeline has the highest ridge incidence as shown in Table 5.4.

Table 5.4. Frequency of ridges in each steel type

	Coils to be cold rolled	Tinplate	Hot rolled coil	Pipeline	Total
# Strips	1902	772	904	136	**3714**
# Strips with ridges	989	298	591	121	1999
Percentage containing ridge	52%	39%	65%	89%	**54%**

Ridge size is a function of the thickness of the strip being rolled. In Figure 5.8 the ridge height is depicted as function of final thickness (or gauge) of the strip rolled. Strips with ridges below 5μm in height are grouped in the 0μm size; measurable ridge sizes varied between 6μm and 16μm. The solid line represents the calculated average ridge size.

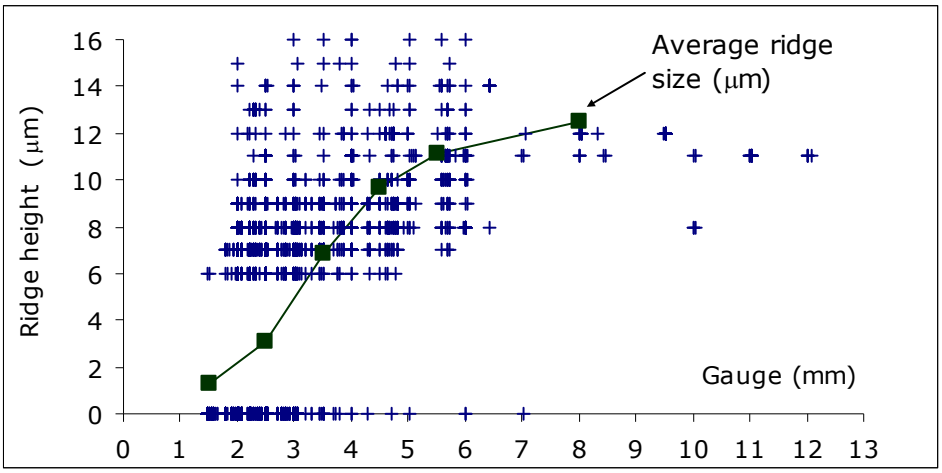

Figure 5.8. Influence of strip gauge on the height of ridge. The solid line represents the calculated average of ridge size.

It follows from Figure 5.8 that ridge size increases as the gauge of the rolled sheet is increased. These results are consistent with the high occurrence of ridges in pipeline products (see Table 5.1) that are rolled to a final thickness of 5mm or more. In the interpretation of these results it is important to take account of the fact that the accuracy of the thickness determination by the X-ray device decreases with strip thickness. Moreover, the background noise of the signal is increased because thicker strips are shorter and fewer measurements are used in calculating the average thickness of the strip. It has not been possible as yet to determine the absolute accuracy of the ridge height measurement but the trends are clear.

In an attempt to interpret the data it is pertinent to note that in practice, in a given schedule, thicker gauges are rolled first, while the thinnest gauge strips are rolled last. The percentage of ridges occurring as a function of the number of strips rolled in a schedule is displayed in Figure 5.9 (top curve). Also shown in the figure (lower curve) is the average gauge as a function of the number of strips rolled in a schedule.

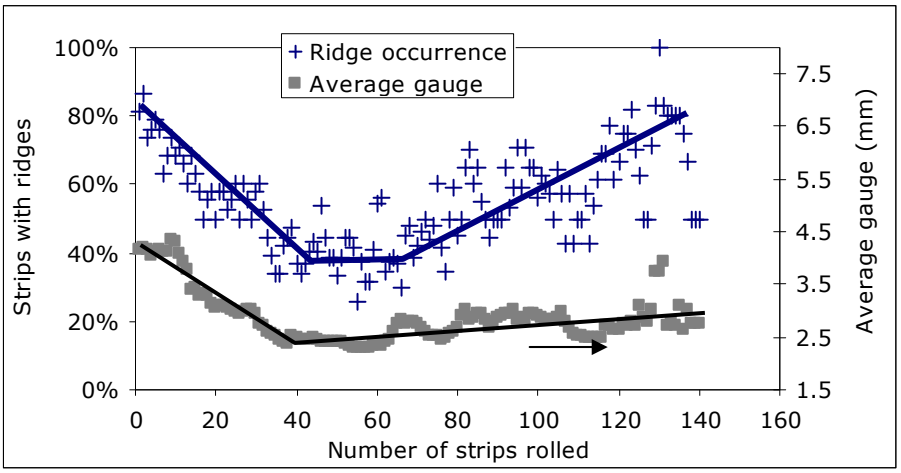

Figure 5.9. Frequency of ridge occurrence as a function of the number of strips rolled. Also shown is the final strip thickness

It follows from Figure 5.9 that of the first 40 strips rolled in a given schedule, the percentage of strips containing ridge decreases as the gauge is reduced, a finding that is consistent with the results shown in Figure 5.8. On the other hand, ridge occurrence increases as more strips are rolled in the same schedule at the same gauge. This is a most significant finding and it appears that there is an approximately linear increase in ridge occurrence with the number of strips rolled in the same schedule to similar gauge. The significance of Figure 5.9 can be summarised by asserting that the occurrence of ridge in hot-rolled strip is more prevalent when the rolled gauge is above 3mm and whenever more than 65 strips are rolled in the same schedule.

It should be pointed out that the presence of ridges in strips rolled to gauges above 3mm does not mean that the product have defects. The ridges are detected when the protuberance on the strip measures above 6μm and are not usually thicker than 12μm above the ideal strip profile. This slight variation on thickness is not relevant on the hot rolled product, unless it is scheduled to be cold rolled, annealed and tempered to very thin specifications, in where the variation in thickness can be the origin of ridge-buckle defect.

The next figure (Figure 5.10) shows the frequency of ridge occurrence according to its position on the strip in a range of ±350mm from the strip centre. Centre position corresponds to ±100mm from the strip centre. There is a slight preference for ridges to occur in the drive side of the mill, but it is not significant compared to the operator side, although it is evident that ridges do not occur as frequently in the exact central region of the strip

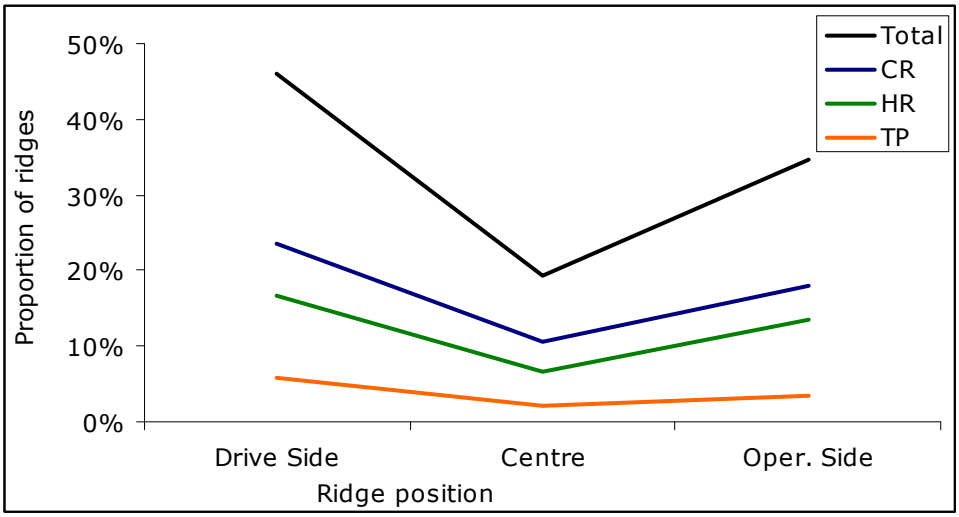

Figure 5.10. Representation of the proportion of centre ridges as a function of the position in the strip.

In an attempt to elucidate possible causes of ridge formation, temperature measured by the centre pyrometers at the entrance of the mill (before descaling) and at the mill exit (after last set of rolls) as well as the roll force applied in each stand for each of the rolled strips were collected and compared with the height of the ridges observed in the corresponding strip.

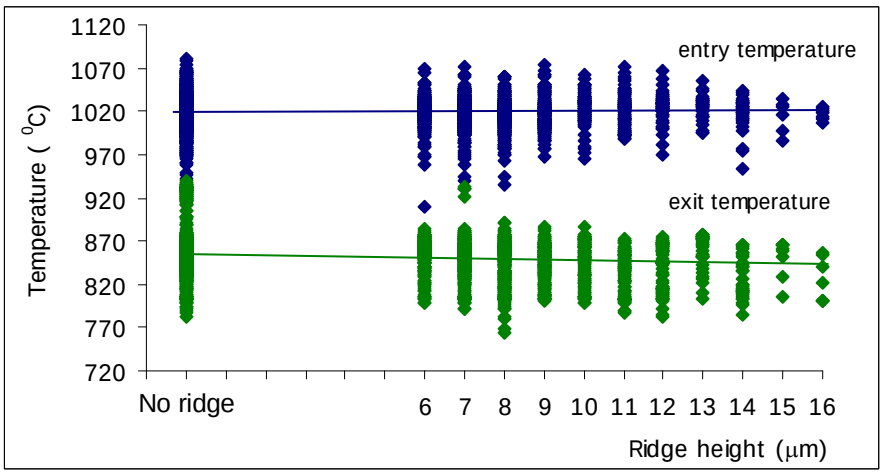

Figure 5.11. Comparison of ridge height and entry or exit temperature of the strip

In Figure 5.11, the blue dots represent the entry temperature of each strip, compared with the size of the ridge occurring; the green dots are the corresponding exit temperature for the same strips. Although the entry and exit temperatures are highly variable on the strips analysed, Figure 5.11 shows that there is not evident correlation between the measured temperature and the prevalence of ridges. Neither exit nor entry temperatures are specifically higher or lower when the ridge

height is higher or simply when ridges occur, compared with strips with no ridges. The bulk temperature of the strip does not seem to influence ridge formation, nonetheless, it is pertinent to point out that the measured temperature does not take into account any variations in temperature that may be present along the width or thickness of the strip as the temperature is measured as the average of the infrared emissions of the strip surface in a single position.

The roll force applied on each stand also shows no clear-cut correlation to the prevalence of ridges. The total roll-pressures are too high (in the order of 10^6 N) to be able to detect small changes in roll pressure that may result from ridges in the strip or grooves in the rolls, which are only a few microns in thickness or depth respectively. As it was demonstrated in Chapter 4, the small changes on temperature that are possibly occurring could lead to variations on strip strength of just 9MPa, which are far too small to be detectable as a change in the total roll-force.

Further information about the temperature distribution in the strip was extracted from the temperature maps developed by the temperature-profile meter at the exit of the mill, but again no correlation could be found between temperature variations and ridge occurrence. Currently, it is not possible to measure experimentally the changes in temperature along the strip width in the roll-bite while rolling is taking place. Some attempts have been made by plant operators in measuring the temperature of the rolls after extraction from the mill, but clearly that attempt will not give any indication of the instantaneous temperature variations occurring on the surface of the roll during rolling.

5.3.3. Comparison of uneven roll wear and the occurrence of strip ridges

Roll wear can only be measured at the end of a schedule and if a relationship is to be found between roll-wear and ridge incidence, it is important to compare the roll profile with the profile of the last few strips rolled in a given schedule. Such a comparison of roll-wear with the profile of the last four strips in a schedule revealed the following:

- In 58% of the schedules where rolls contained centre grooves, ridge occurred in the last 4 strips
- In 18% of the schedules, the rolls did not contain centre-grooves and ridges did not occur in the last four strips.

- In 24% of the schedules the rolls contained grooves but there were no ridges in the strips or alternatively there were ridges in the strips but no grooves in the rolls.

The behaviour of pipeline steel was especially interesting as all the strips rolled were thicker than 5mm and 89% of them developed irregular profiles, which can be classified as multiple ridge occurrence, but the rolls corresponding to those schedules did not present uneven centre wear. This shows that the multiple ridges observed cannot be necessarily classified as centre ridges. For this reason, it is likely that the profiles thicker than 4 mm shown in Figure 5.8 might be associated with inaccuracies on the profile measurement.

5.4 Discussion

Uneven centre-wear on finishing-mill work-rolls and ridge formation on hot-rolled strip are a common occurrence. Most steels rolled in the hot-strip mill will develop ridges irrespective of composition and rolling temperature. Ridges occur more frequently in strips thicker than 4mm and the incidence of ridges increases linearly and independent of the strip gauge after more than 65 strips have been rolled. The top rolls are more likely to be subjected to uneven wear than bottom rolls and centre grooves are more common in the first two stands and in F4. Ridge formation does not seem to be related to the type of steel being rolled. It is customary on the plant to control the rolling practice of tinplate or silicon steels more carefully because of the risk of forming ridge-buckle defects following further processing. However, hot-rolled strip ridges are not exclusively found in these steel types. Actually, tinplate schedules experience less ridge occurrence than the rest of the materials and this is basically because only short schedules (approximately 70 strips) are rolled of this material. Operators ensure that they do not exceed the inflection point of the curve in Figure 5.9. Also the mill conditions are carefully checked before tinplate products are rolled, reducing the risk of having irregular cooling patterns on the rolls and descaler. Although the material of the strip does not seem to influence ridge occurrence, certain steel types like silicon steel (0.5 to 1%Si) develop more pronounced ridges in fewer consecutive strips rolled than any other product.

It has not as yet been possible to establish why the top rolls wear so much more (Figure 5.2) than bottom rolls. It may be because heat losses are higher on the top of the strip as it is more extensively exposed to the atmosphere than the bottom-

side. A higher cooling rate at the top surface of the strip lowers the surface temperature of the strip, thereby increasing the possibility of scale fracture. Also it is worth to mention that the cooling system of the rolls is in a fixed position, meaning that when the roll diameter is reduced due to normal wear, the gap between rolls is corrected by moving the top roll only, thereby increasing the distance between the top roll surface and the roll-cooling nozzles. Reduced cooling of the top roll increases the overall roll temperature, thereby increasing its thermal wear. Furthermore, our analysis reveals that centre grooves are more likely to occur in the first two sets of rolls, which might also be related to the higher temperature of the strip when it enters the finishing mill (the entry temperature is approximately 200ºC higher than the exit temperature).

Our analysis has established a significant correlation between roll wear and ridge occurrence. There is a 76% probability that roll wear is the principal cause of ridges. However, the finding that in 24% of the schedules, ridge in the strip and grooves in the roll could not be related point to the fact that there might be another operational variables that cause ridge-buckle defects to form. It is pertinent to point out that in the 40 schedules studied, the practice of side-shifting of the work rolls has been adopted. The implication of this practice is that a ridge that has developed when the grooves in rolls of different stands coincide in the same position along the width of the strip may be masked when, by side-shifting, the grooves cease to coincide. Ideally the correlation between grooves formed in the work rolls and the formation of ridges needs to be done when no side-shifting is practiced.

An important finding that confirms the influence of roll wear on ridge occurrence is that ridge incidence increases proportionally to the number of strips rolled in a given schedule at constant gauge as shown in Figure 5.9. The number of cycles reduces the life of the roll surface exposed to thermo-mechanical loads and increases the temperature to which a roll is exposed. Although the rolls are constantly being worn and fresh surfaces exposed, the penetration of the heat in each cycle will reduce the life of the newly exposed material. Any uneven change in the roll or strip temperature might facilitate selective detachment of particles from the roll surface as the life of the roll surface material has already been affected and the roll surface has deteriorated.

Rolls are expected to wear as a result of a combination of abrasion, adhesion of oxides and thermo-mechanical effects. Uneven roll wear might be initiated by local

changes in the rolling conditions, specifically occurring in certain zones on the roll surface. Temperature plays a major role in wear, for example, an increase in temperature can reduce the thermal fatigue life of the roll material; a decrease in temperature beneath the plastic-brittle temperature transition of the oxide may cause the strip scale to fail in the roll-bite; very high cooling rates can cause the strip scale to fail by thermal shock; at higher strip temperatures rougher scale is formed; and the morphology of the oxides formed at the roll surface are significantly altered by the temperature at which they form.

The fact that silicon steels develop ridges more quickly than tinplate products shifts the attention to the important role that the scale, formed on the strip, may play in roll wear. The scale formed on the strip is in contact with the roll surface, acting either as lubricant or abrasive media when the work-roll, oxide layers and steel strip are compressed into the roll-bite. Besides, any variation in the scale thickness or integrity of the oxide layer can cause an increase in the heat transfer to the rolls, thereby decreasing the thermal fatigue life of the roll material. In the next chapter, the nature and morphology of the scale formed under operating plant conditions in the finishing-mill is studied and analysed as an approach to contribute to a better understanding of the origins of uneven roll-wear.

Chapter 6
In-situ oxidation studies

The integrity of oxide layers that form on steel strip during hot rolling play a significant role on the uniform wear of the work-rolls. It has been proposed by Das *et al* (2004) that if the scale failed in, or before the strip enters the roll-bite, the steel of the strip can extrude through cracks in the oxide layer, thereby increasing the heat transfer rate from the strip to the roll surface. Furthermore, Lee S. *et al* (1997[b]) demonstrated that an increase in temperature of the surface of the rolls can lead to a significant reduction of the roll material life due to fail by thermal-fatigue. Therefore it can be argued that a loss of integrity of the oxide layer in the roll-bite, may lead to an increase in heat transmission to the rolls or to variations in friction, which can produce uneven roll wear.

Since uneven roll-wear was observed in the work-rolls of the finishing mill and it was related, in the majority of the cases, with the occurrence of ridge in the hot rolled strips, the investigation described in this chapter is aimed at understanding the conditions of formation of the tertiary scale on the steel strip. Strip samples of tinplate and silicon steels were selected for this study because they are the two types of steels rolled to thin gauges (<0.4mm) and therefore predisposed to be affected by ridge-buckle defect. Furthermore, our investigation revealed that strips made of silicon steel were the most susceptible to ridge formation during hot-rolling. Tertiary scale forms within about 15 seconds between the exit of the descaler and the exit of the last stand of the finishing mill, assuming a complete scale extraction in the descaling box 2 (see Figure 2.11). The inter-stand and accumulated times of exposure to air calculated for a strip of low-carbon steel that is being reduced in thickness from 34 to 2mm, are shown in Table 6.1 (the time spent in the roll-bite is included).

Table 6.1 Inter-stand times from descaler 2 to exit of F6 in the finishing mill on BlueScope Steel Port Kembla Steel works for a typical rolling of tinplate product, including the contact times in the roll-bite

	Desc - F1	**F1- F2**	**F2- F3**	**F3- F4**	**F4- F5**	**F5- F6**
Time inter-stand (s)	2.64	4.91	3.05	1.89	1.20	0.82
Accumulated time (s)	2.70	7.64	10.71	12.60	13.81	**14.62**

Study of the scale in such short periods of oxidation is a complex matter, mainly because it is of interest to observe the changes occurring on the steel surface during its exposure to air. In practice, the steel strip is exposed to a mixture of air and water. However, for the purpose of this study, only the interaction between the steel strip and oxygen in the air was considered. This approach was taken firstly to simplify the experiments, but secondly and most importantly, to isolate the effect of air in an attempt to better understand the fundamental mechanisms of tertiary scale formation in the hot-strip mill. Numerous experiments have been conducted and theories developed of early-stage scale formation on steels and although a number of viable mechanisms have been proposed, credible validation of most of the proposed mechanisms is still lacking.

This chapter deals with a study of the scale formation during the early stages of oxidation of two commercial steels. A high-temperature microscope was used to observe scale formation *in-situ*, to monitor the initiation of oxidation and to study the kinetics of the early stages of oxide formation. We also studied the morphology of the scales formed by using a variety of microscopy techniques and we determined the nature of the oxides phases. The main objective of this part of the study is to evaluate the differences in scale formation between plain carbon steels and silicon steels with emphasis on scale formation within the first 30 seconds of oxidation. In the course of the experimentation, we came across interesting findings that, we believe, contribute to a better understanding of the mechanisms of oxide formation and the occurrence of scale separation or 'spalling' during oxidation.

6.1 Experimental methods

6.1.1 High temperature microscopy

We have studied, for the first time as far as we can determine, the oxidation of the steels of interest (low-carbon and silicon steels) under simulated conditions of temperature, exposure time and oxygen partial pressure that pertain to the industrial practice of the hot rolling of steel strip.

In our experiments, oxidation occurring on the surface of a steel sample, placed within a high-temperature microscope (HTM) chamber, is observed *in-situ* while the temperature is recorded, allowing for a study on the dynamics of the early stage oxidation of steels. In the furnace used, a sample is placed in a crucible suspended in a gold plated ellipsoidal infrared heating furnace as shown in Figure 6.1 while an

inert atmosphere is maintained. In our experiments high purity argon (<2 ppm impurities) was used for this purpose. A 1.5 kW-halogen lamp located at one focal point of the ellipsoidal cavity, heats by radiation the specimen located at the other focal point. Images from the heated sample are captured by a CCD camera at a rate of 24 frames per second. The HTM is normally used as a laser-scanning confocal microscope (LSCM) (Phelan *et al*, 2005) where a laser beam scans the surface of the specimen, but we found that the CCD camera provides far better resolution in the case of oxidation experiments due to its ability to compensate for differences in light emission and the greater depth of field. The temperature, measured by a thermocouple incorporated into the crucible holder as shown in Figure 6.1, is displayed on a monitor while the digital image is simultaneously recorded directly into a computer.

Once the sample has reached the desired temperature under the inert atmosphere, and following a pre-selected annealing program, air is inserted into the microscope chamber and the oxidation of the steel is observed in-situ and recorded.

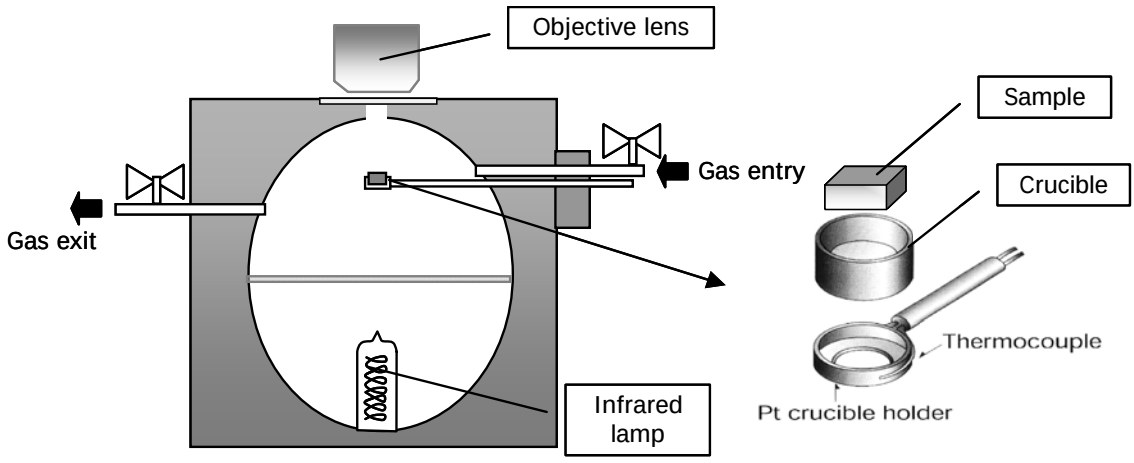

Figure 6.1. Transverse section through the high-temperature microscope furnace chamber, which includes a closer perspective of the sample holding system.

The oxidation of a low-carbon and a silicon steel was studied by this in-situ experimental observation technique. The compositions of the steels studied are shown in Table 6.2.

Table 6.2. Composition of the steels used in the oxidation studies

	Composition (%mass, bal.Fe)						
	C	Mn	P	Si	S	Cr	Al
Low-carbon	0.045	0.21	0.012	<0.005	0.014	0.015	0.03
Silicon steels	0.003	0.4	0.034	0.57	n/a	0.025	0.30

Samples are cut into squares 2.8mm side length from a hot rolled strip of tinplate of 2mm thickness and of silicon steel of 2.2mm. Then the sample surface to be observed was carefully polished up to 0.6μm with colloidal silica. The polished sample is placed in a 4.3mm external diameter alumina crucible and levelled with the crucible border to ensure repeatability. In the HTM, except when air is deliberately introduced, all the heating and cooling is conducted in inert atmosphere of high purity argon (<2ppm impurities).

Two alternative methods were used for the introduction of oxidising gas into the chamber:

Method 1

Compressed air of industrial grade is introduced to replace the inert gas through the main gas valve; see Figure 6.1, allowing progressive increase of the partial pressure of oxygen into the furnace chamber. The flow of gas was varied between $6x10^{-6}$ and $5x10^{-5}$ $m^3.s^{-1}$.

As the air is progressively injected into the HTM chamber, it is of interest to determine the time it takes for a total replacement of argon by air. In order to do so, we adapted a mass spectrometer to the exit gas of the chamber. The capillary tube of a quadruple mass-spectrometer was connected near and before the exit gas valve to record the intensity variations of the Ar signal from the time the air valve is opened until the intensity of the Ar-signal reaches a minimum plateau. Figure 6.2 shows the decay of the Ar-signal when air is introduced instead of argon at the maximum air flow used of $5x10^{-5}m^3.s^{-1}$.

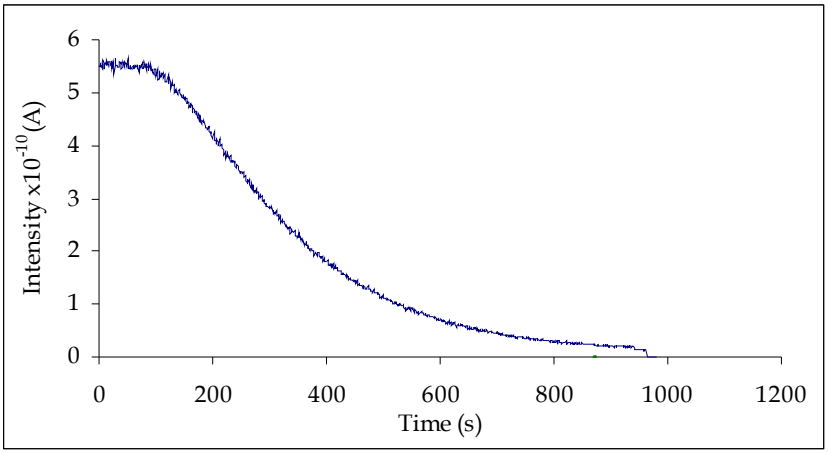

Figure 6.2. Variation in the intensity of argon inside the HTM chamber from the moment the air valve is opened, using Method 1 of air insertion. Intensities are measured with a mass spectrometer connected before the exit valve of the chamber.

Figure 6.2 shows that the mass spectrometer only detects a change in the intensity of the argon measurement after about 100 seconds from the moment the exchange valve from argon to air is opened; it also shows that the argon is completely replaced by air after 800 seconds. However, the mass-spectrometer was not calibrated to determine the exact changes in concentration as a function of time because that information was not of the essence. What is important in the present context is that the argon gas is not instantaneously replaced by oxygen and for this reason Method 2 of air insertion was implemented.

Method 2

A stainless steel tube (2 mm, inner diameter) was positioned close to the sample holder as shown in Figure 6.3. Accordingly, the oxidizing gas is inserted through the tube and propelled directly onto the polished sample surface. Also in this case, compressed air (industrial grade) is used as oxidising gas. The flow of air was kept constant at 3.1×10^{-5} $m^3.s^{-1}$, which results in a speed of air exiting the tube of 12 $m.s^{-1}$.

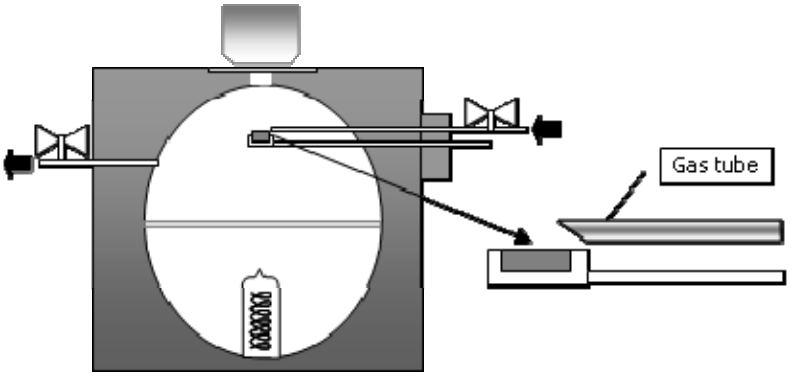

Figure 6.3. Transverse cut showing the HTM furnace with detail of the sample and the gas tube adapted for the experiments.

The heating-cooling cycles used in the experiments were:

For silicon steels

Method 1

- Heat to 900 or 950ºC and soak for 5min.
- Introduce air at flow rates of $6x10^{-6}$, $3x10^{-5}$ or $5x10^{-5} m^3.s^{-1}$ until oxidation was completed.
- Close the valve to stop oxidation by supplanting the air with argon.
- Cool in argon at $1.7ºC.s^{-1}$ to room temperature.

Method 2

- Heat to 950ºC and soak for 5min.
- Introduce air at a flow rate of $3.1x10^{-5} m^3.s^{-1}$ with variable times of 0, 1, 3, 5, 10, 20 or 30 seconds while the steel specimen is maintained at constant temperature.
- Cool rapidly at 23 $ºC.s^{-1}$ to 700ºC, closing air entry when the temperature reaches 700ºC.
- Further cooling in argon to room temperature at a rate of $1.7ºC.s^{-1}$.

For carbon steels

Method 1

- Anneal at 1300ºC for 5min.
- Cool to the experimental temperature (temperature at which the oxidation is to be observed) of 1050ºC at a rate of $1.7ºC.s^{-1}$ and soak for 5min.
- At isothermal conditions, introduce air at flows of $6x10^{-6}$, $3x10^{-5}$ or $5x10^{-5} m^3.s^{-1}$ respectively until oxidation is completed.
- Close the valve to stop oxidation by supplanting the air with argon.
- Further cool in argon to room temperature at a rate of $1.7ºC.s^{-1}$.

Method 2

- Anneal at 1300, 1200 or 1100ºC for 5min, to allow for a study of the oxidation at different austenite grain sizes.
- Cool to the experimental temperature (temperature at which the oxidation is to be observed) of 1000, 950, 915 or 880ºC at a rate of 1.7ºC.s^{-1} and soak for 5min
- Introduce air or oxygen at $3.1x10^{-5}$ $m^3.s^{-1}$ with variable times of 0, 1, 3, 5, 10, 20 or 30 seconds while the specimen is maintained at constant temperature
- Cool rapidly at 23ºC.s^{-1} to 700ºC, closing the air entry when a temperature of 700ºC is reached.
- Further cool in argon to room temperature at a rate of 1.7ºC.s^{-1}.

6.1.2 Sample analysis

Samples of oxidised silicon steel obtained by applying method 1 of oxidation were analysed in a Dual-beam SEM-FIB facility FEI-XP200. The Dual-beam permitted the extraction of thin-foils from pre-selected areas of the oxidised samples. Thin-foil samples were mounted on 200 mesh carbon-coated copper grids and observed in a transmission electron microscope JOEL® JEM-2010, 200keV. The TEM is equipped with an EDAX® electron dispersive X-ray spectroscope.

Selected samples obtained from method 2 of air insertion were mounted in vacuum impregnated resin with the experimentally formed oxide layer perpendicular to the surface mould of the resin. They were then carefully polished, starting with silicon carbide paper 15.3µm particle size (P1200) and finishing with colloidal silica (0.6µm particle size). The thickness of the oxide layers was determined by direct measurement, following calibration, in the scanning electron microscope Leica 440 with backscattering detection, after gold coating the resin-mounted samples.

Some of the oxidised samples were selected for powder X-ray diffraction analysis. The steel scale was extracted from the sample at room temperature by lateral pressure, then ground and placed in a glass. Analysis was conducted in a Phillips PW 1730 powder X-ray diffractometer. In addition, electron-probe micro-analysis (EPMA) was performed on transverse sections of oxidised samples of low-carbon steels. A Cameca® Camebax-SX50 EPMA was used for this purpose.

6.2 Results

6.2.1 High temperature oxidation of silicon steel

The silicon steels rolled at the Port Kembla works of BlueScope Steel are of non-oriented type, it contains not just silicon (0.5-1%) but also Al (0.3%) and Mn (0.4%). It is pertinent to briefly refer to the use of this type of steel and the function of the different alloying elements: silicon steels of the non-oriented type are used extensively in electric rotating equipment where a low-cost soft magnetic material is required. Addition of silicon to iron increases resistivity, decreases hysteresis loss, increases permeability, and virtually eliminates aging. Impurities in the silicon steel that can affect magnetism and other electrical properties are controlled by restricting the carbon content (<0.005%) and by adding Mn and Al; the first to alloy with the sulphur present inhibiting grain growth, and the second to increase resistivity and lower the temperature of primary recrystallization (key-to-steel webpage). The phase transformation map constructed by MTData for this type of steels is presented in Figure 6.4. MTData is a software package for the calculation of phase equilibria in multi-component multiphase systems using, as a basis, critically assessed thermodynamic data. Addition of silicon stabilises the ferrite phase and the transformation temperatures for the silicon steel composition studied (see Table 6.2) are A_1: 902ºC and A_3: 997ºC

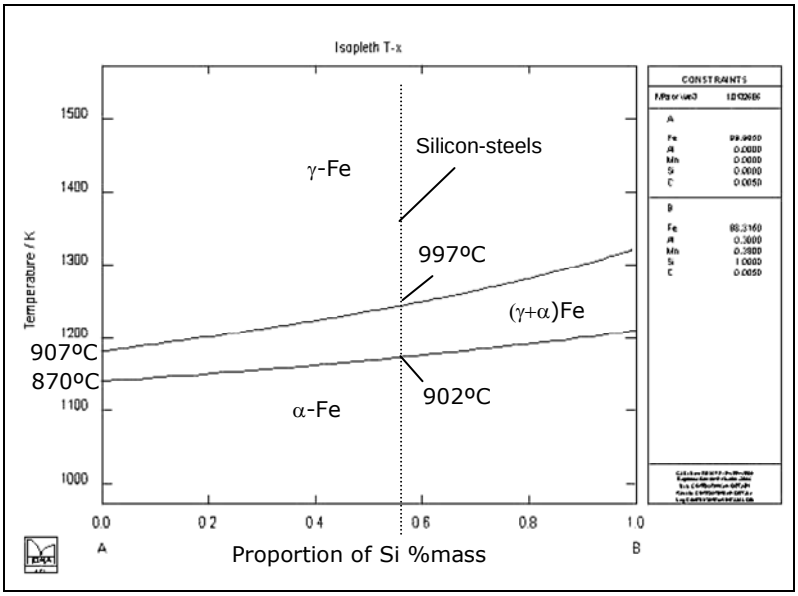

Figure 6.4. Phase diagram for the silicon steel used. The diagram was constructed by using MTData software using the composition shown in Table 6.2 and varying the concentration of Si.

In situ-observations

In the first instance, samples of silicon steels were oxidised using Method 1 of slow air insertion into the chamber. It is possible to observe the formation of oxide nuclei and its lateral growth as shown on the sequence of events depicted in Figure 6.5.

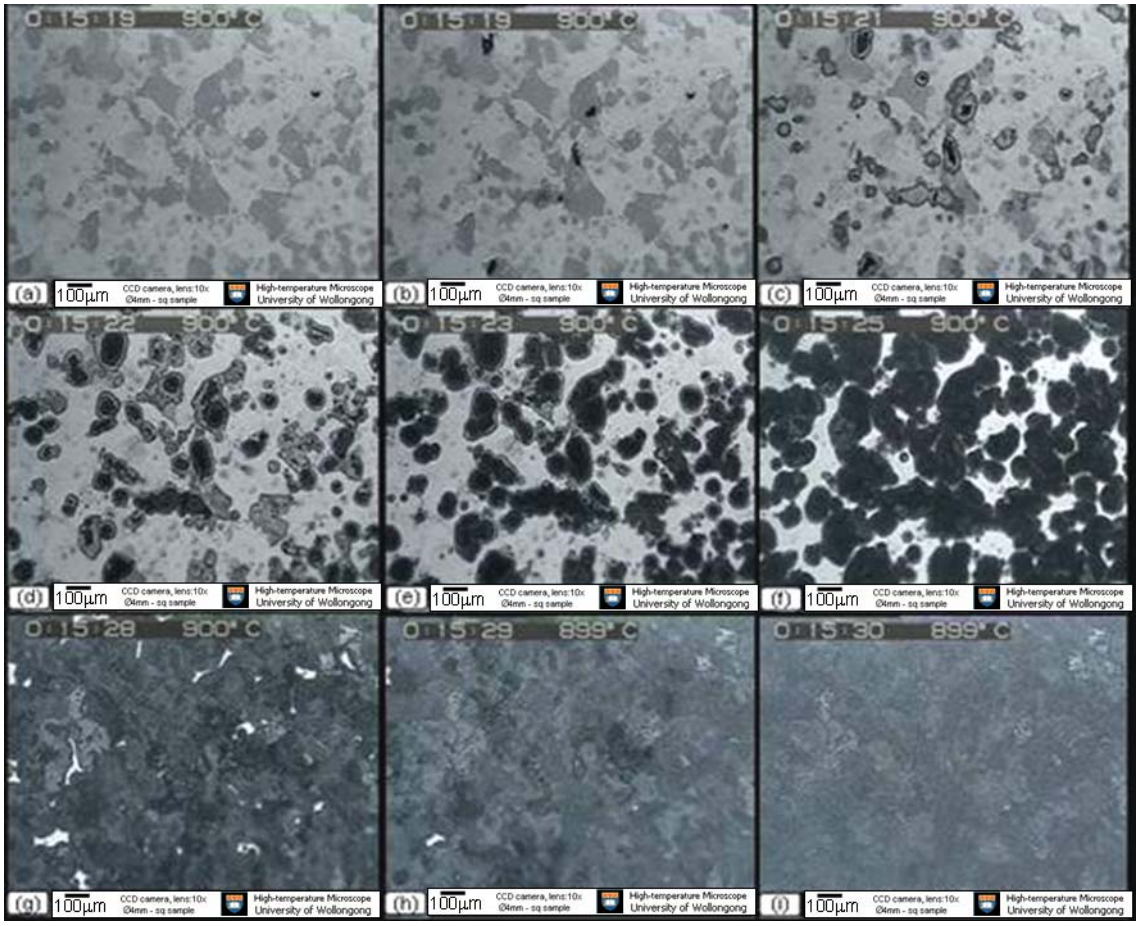

Figure 6.5. Sequential pictures of oxide formation in silicon steels. Frames are extracted from the digital video images taken by the camera. Sample was oxidised at 900ºC using method 1 of air insertion with an air flow rate of 1.55×10^{-5} $m^3.s^{-1}$. The video corresponding to this oxidation is available in the annexed CD.

In the sequence shown in Figure 6.5 the following events can be identified:

Frame (a) Even before the air valve is opened, there are already some signs of oxidation as there is a distinct difference in appearance of some grains. Because this particular steel (see Table 6.2) has relatively high concentrations of aluminium, this very early indication of oxidation is presumably related to the formation of aluminium oxides, the formation of which is thermodynamically possible even at the low oxygen partial pressure in the chamber before the oxidizing gas is introduced ($<10^{-20}$ atm).

Frame (b) Following the introduction of air to replace the argon, a few discrete dark oxide nuclei appear on the surface, seemingly to start preferentially on the former darker grains

Frames (c), (d) and (e) The nuclei formed seem to grow concentrically in what appears to have five different layers. These features are better depicted in Figure 6.6 in which a magnified version of one of the nuclei in Frame (c) is shown. In Figure 6.6, Zone (1) indicates the first oxide that formed, perhaps an interface reaction between the substrate and the layer of oxide in Zone (2). Zone (3) is another rim that resembles again an interface, this time formed between oxides in Zone (2) and Zone (4) and finally the central area, marked as Zone (5), is clearly another layer of oxide.

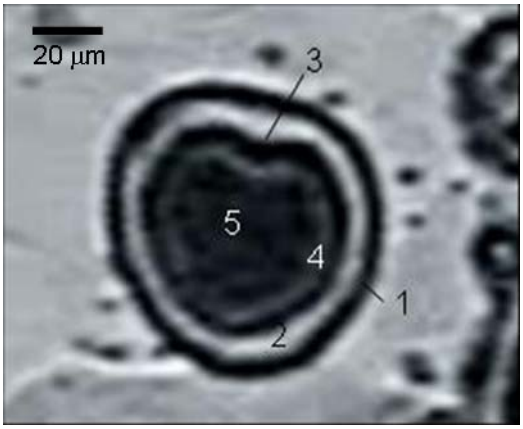

Figure 6.6. Detail of one of the oxide nuclei formed during oxidation of silicon steels

It seems evident that the newly formed oxides show in Frame (e) cover firstly the substrate grains that already appeared darker even before the introduction of air into the chamber (Frame (a)).

Frame (f) It looks like oxides in Zone (4) and Zone (5) are growing faster than those in Zone (1) and Zone (2) and hence, the firsts are overgrowing the later. At this stage, the newly formed oxide begins to grow laterally covering the whole surface of the substrate.

Frame (g) The growing oxides still present different tonalities of grey meaning that the surface is still not uniformly covered by the same oxide morphology.

Frame (h) A new 'grey phase' nucleates in multiple points on the surface and expands laterally over the surface, covering all the former oxide.

Frame (i) From this stage onward, no further changes occur in the appearance of the oxide layer.

Morphology of oxide nuclei formed in silicon steels

The morphology of the first nuclei was studied by closing the air valve immediately upon its formation, in order to prevent further oxidation. Few of the newly growing oxide crystals could be isolated and the morphology developed in the early stages of growth is clearly depicted in the SEM photo shown in Figure 6.7. The nucleus in Figure 6.7 show approximately the same five oxidation stages identified during the in-situ experiments (see Figure 6.6). An interesting feature is the 'melted-like' oxide (4) in between the crystals (5) and the dark circumference (2).

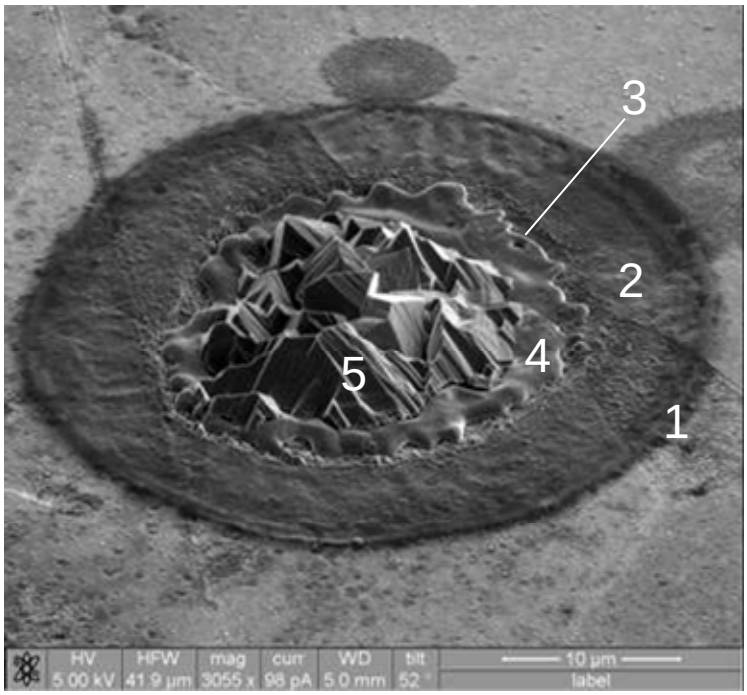

Figure 6.7. SEM tilted image of a developed nucleus of oxide on the surface of silicon steel. The zones observed during in-situ oxidation are clearly visible in this nucleus.

In order to elucidate the nature of these oxides, maps of the electron dispersive X-ray (EDS) corresponding to each element of interest were constructed from the top of the sample and are shown in Figure 6.8.

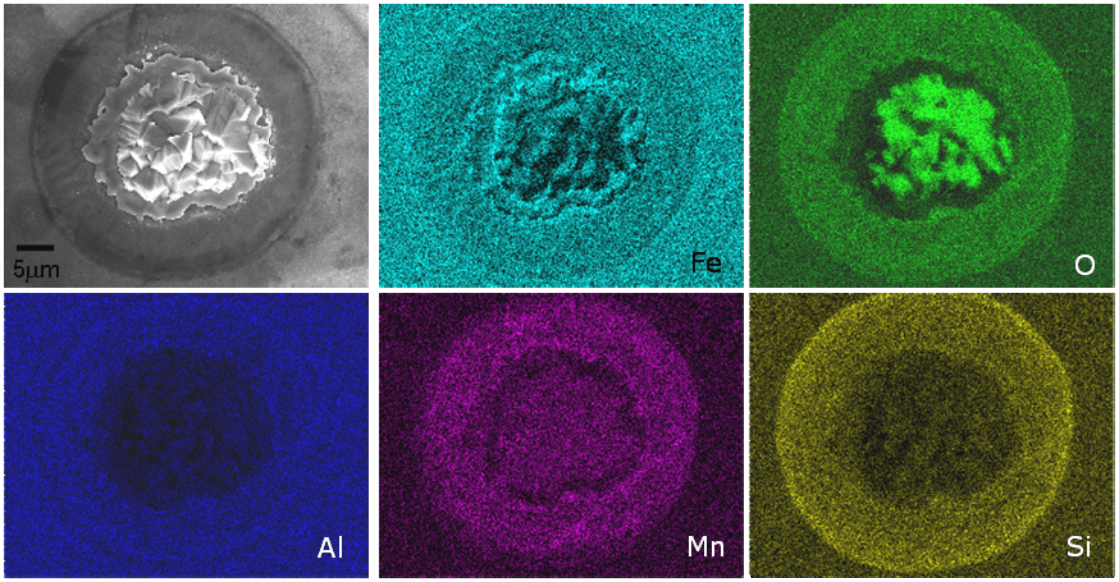

Figure 6.8. EDS map of the surface elements contained in the nucleus of Figure 6.7

The EDS maps in Figure 6.9 assist to elucidate some of the oxide features,

- The surface surrounding the nucleus seems to be exclusively aluminium oxide. As was pointed out before, Al_2O_3 might be forming even at the low partial pressures of oxygen in the chamber before the introduction of air.
- The first rim (Zone(1)) is formed exclusively by silicon, while the circumference (2) seems to be a complex oxide formed by Al, Mn, Si and O but it does not seem to contain any iron. It should be pointed out that the EDS analysis inevitably detects X-rays generated from the subsurface; therefore, iron will always be detected. Nevertheless it is evident that the iron concentration is reduced in the area corresponding to Zone (2).
- Zone (3) seems to be formed by higher concentrations of Mn and O, which is vaguely visible in the corresponding maps.
- Zone (4) corresponds to the 'melted-like' feature and it is clearly shown by EDS that is it formed exclusively by Fe.
- Zone (5) consists of crystals of Fe and Mn oxides, the details of which will be discussed below

In order to further analyse the sample, a thin-foil was extracted from the same nucleus by using the dual focussed ion-beam microscope. The sequence of steps taken to extract a sample is illustrated in Figure 6.9.

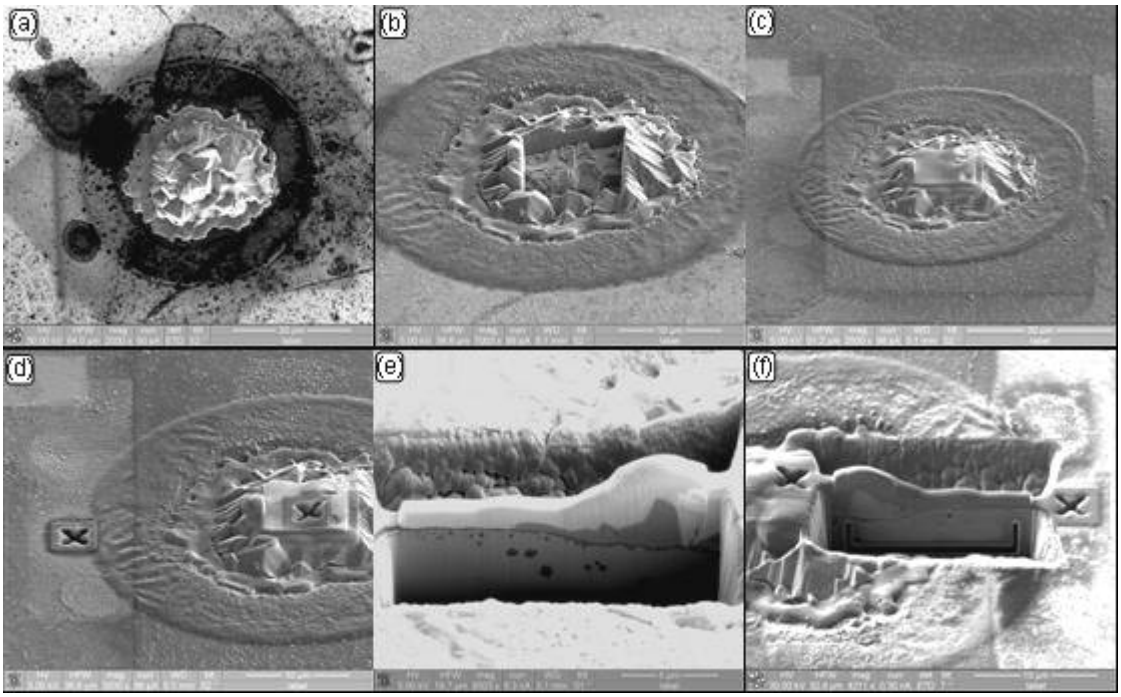

Figure 6.9 Sequence of thin-foil extraction from a nucleus formed in silicon steels. Alternative images form FIB and SEM are used to illustrate the process.

In Figure 6.9 the following sequence is performed:

Frame (a) Nucleus from Figure 6.7 in an image generated by low-current ions from the focused ion-beam (FIB). Observe the non-coherent layer corresponding to Zone 2.

Frame (b), (c) and (d) A cavity is progressively carved in the centre of the nucleus by using the FIB high-current ion-beam. The hole is filled with Pt and the cross-marks are placed as reference points on the surface. This procedure was used to ensure that a sample is extracted from the exact area of interest part of the nucleus, including all five zones of oxides.

Frame (e) After covering with Pt a band between the two cross-marks, sections of ~5μm depth on both sides of the band of interest are removed from the sample, by bombarding it with controlled Ga-ions.

Frame (f) Finally the thin-foil is prepared by thinning the piece to approximately 80nm, cut it from the rest of the sample, extract and mount it on a carbon-coated copper grid.

Further analysis of the oxide nucleus is performed in a transmission electron microscope, and the results are shown in Figure 6.10. In this figure, the dual-beam as well as the TEM images are shown of the two zones of interest. The left-side TEM

image shows the edge of Zone (4) and Zone (2). The right-side TEM-image shows details of Zone (2).

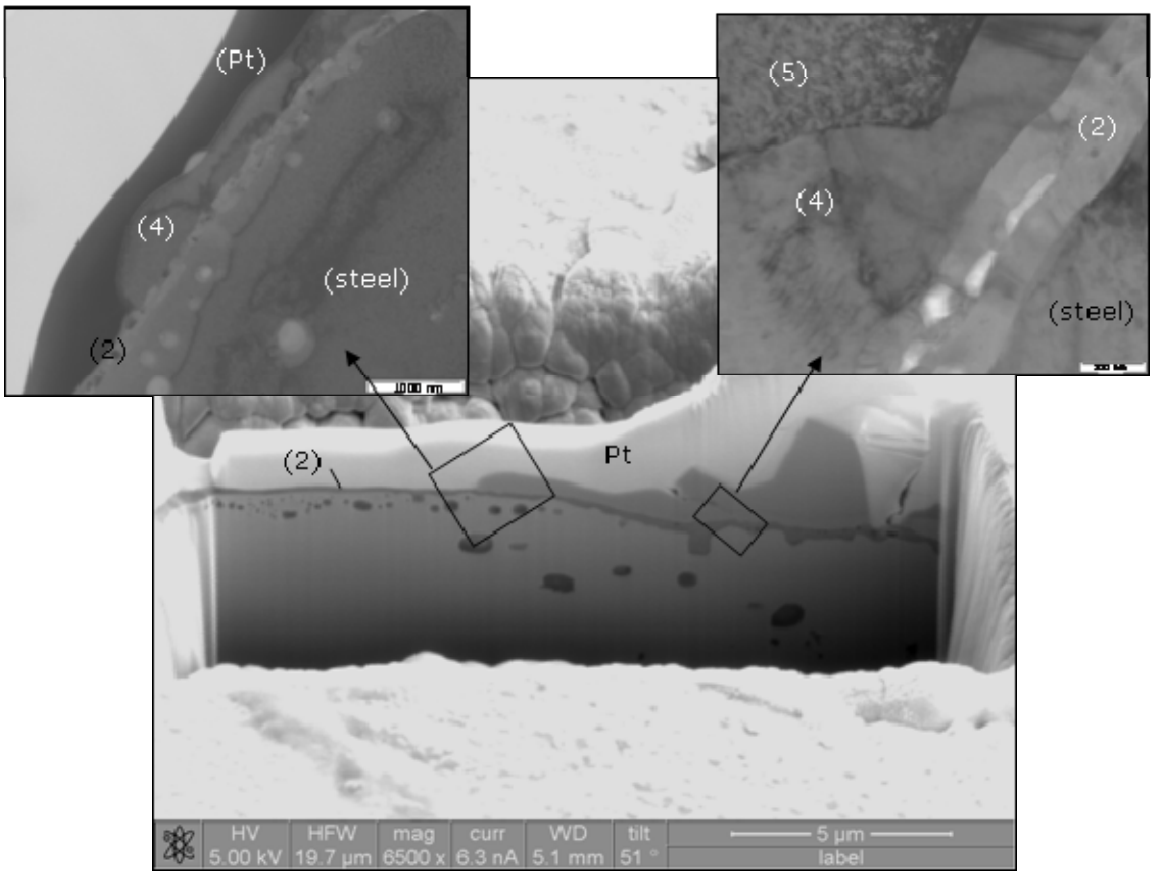

Figure 6.10. Combined images from dual-beam and TEM showing the zones of interest.

An additional feature that was observed in all of the transverse cuts obtained from oxidised silicon steel samples is the presence of 'black' precipitates in the subsurface of the steel. Figure 6.10 clearly shows that small precipitates concentrate on the side where only Zone (2) has formed. The same kind of precipitates, but bigger, are present below the Zones (4) and (5). These precipitates can be observed to distances up to 3µm into the surface. Focussed EDS analysis in the TEM provided convincing evidence that the precipitates contain silicon and oxygen, meaning that they are most likely SiO_2.

The EDS map in Figure 6.8 indicates that Zone 2 contain Mn, Al and Si oxides. Comparing this information with the TEM image in Figure 6.11 provides strong evidence that the interface is formed by three layers (marked by black lines in Figure 6.11, and referred to as 2.a, 2.b and 2.c).

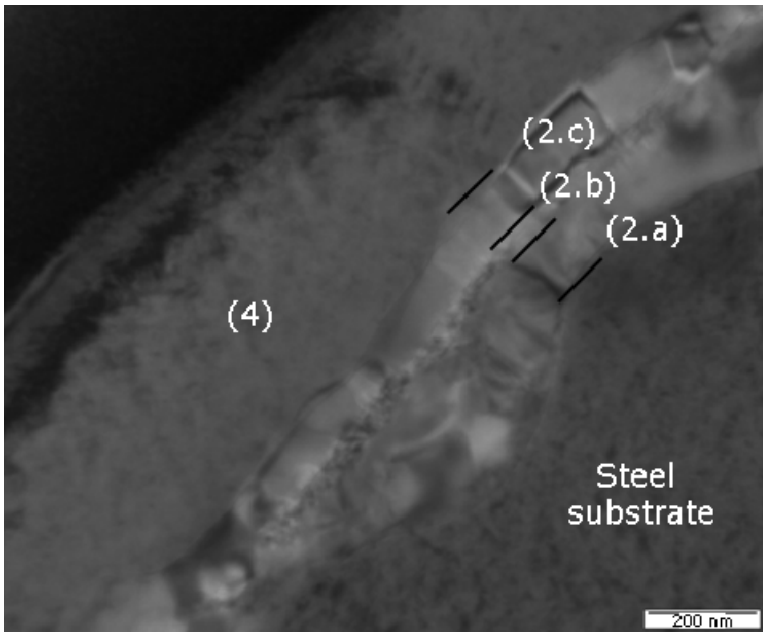

Figure 6.11. TEM image showing details of the features occurring at the interface previously identified as Zone (2)

Using an aperture of 70μm, each of these layers was subjected to point EDS analysis and the corresponding distribution of the elements, calculated from the X-ray intensities are shown in Table 6.4. As the X-ray intensities are extracted from a thin-foil it is not necessary to correct for fluorescence and absorption and it is possible to quantify the approximate proportions of elements using the well-known Zaluzec (1979) method of standard-less calculations. The method permits the determination of the proportions of Fe, Mn, Si, Al and P but not of any element with atomic number lower than 10. To predict the proportions of oxygen (Z=8), the counts corresponding to the silica particles containing solely Si and O were used as quasi-standards in order to determine the conversion of oxygen peak intensity into proportions. Peak intensities were all taken exclusively from the Kα peak of the elements.

Table 6.3. Results form quantitative point EDS analysis in each of the oxide layers depicted in Figure 6.11

	Approximate mass %				
Layers	O	Fe	Al	Si	Mn
2a	39	27	0	15	19
2b	45	26	16	4	9
2c	43	27	11	7	12
Steel base	0	100	0	0	0
Silica precipitate	53	0	0	47	0

The quantitative analysis shows that the interface layer closest to the steel substrate (2a) is mainly formed by Si and Mn oxides. Aluminium is not present in that first layer (2a) but it is found in the other two layers. There are not significant differences between layers 2b and 2c but a slight increase in the Fe and Mn content at the expense of Si and Al.

The crystals formed in the nucleus of Zone (5) can be better analysed by using electron diffraction analysis and an example is shown in Figure 6.12.

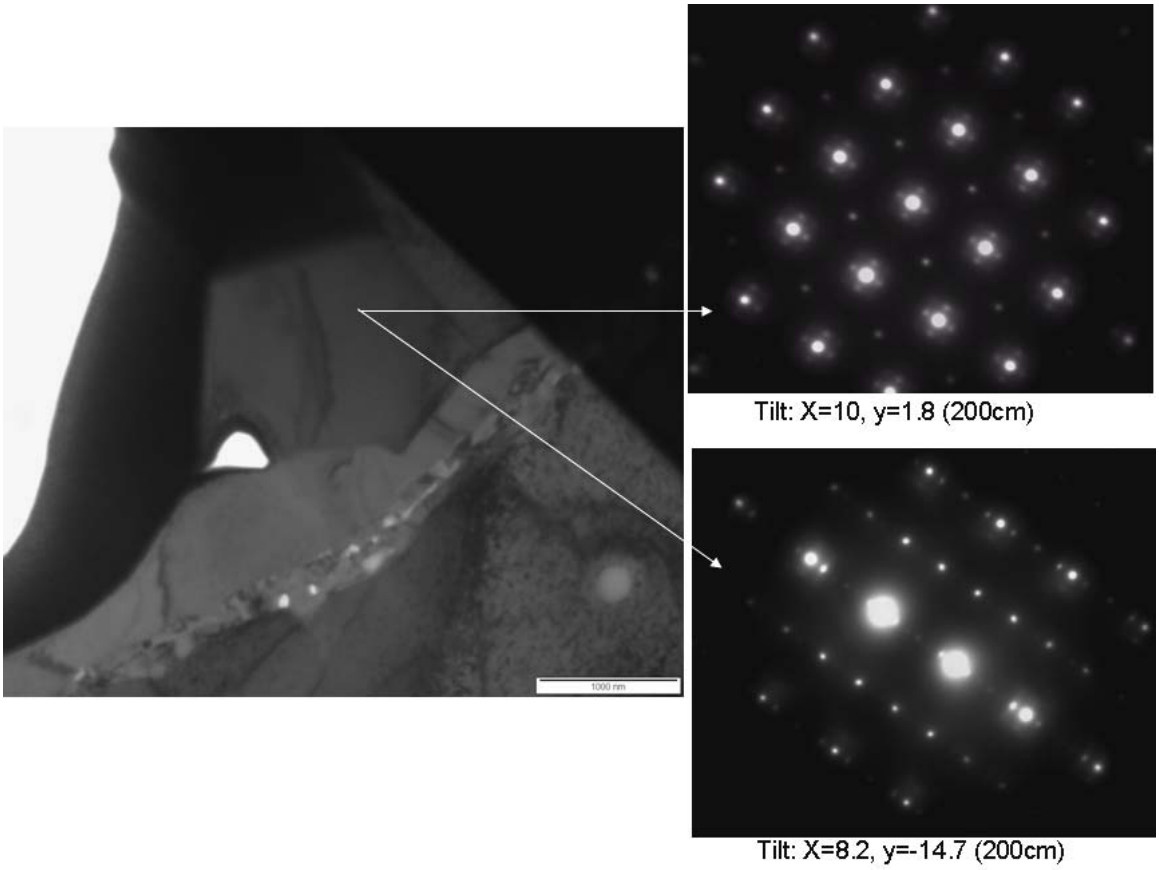

Figure 6.12. Diffraction patterns from the crystal formed on top of the nucleus corresponding to zone (5) of the growing oxides.

From three diffraction patterns as the ones shown in Figure 6.12, interplanar spacings of the main Bragg peak positions were measured. The interplanar distance corresponds to wüstite (Fe_xO) d[200]=2.15Å, d[220]=1.52 Å, d[331]=0.983Å and d[311]=1.29Å. The satellite patterns surrounding the main peaks have been extensively analysed by Welberry *et al* (1997) demonstrating that they are product of the metal-defect structure of the wüstite, formed by Fe^{+3} interstitials and Fe^{+2} vacancies forming clusters in the structure, in what they referred to paracrystal-like distribution of defects. Those clusters lie at the vertices of a highly distorted simple

cubic lattice, with spacing $2.7a_o$ where a_o is the basic average rocksalt (wüstite) lattice repeat.

Morphology of the interface formed at constant oxygen partial pressure

The morphological analysis presented before corresponds to the oxidation occurring with slow insertion of air (method 1), which is equivalent to a slow increase on the oxygen partial pressure. In order to better simulate the oxide formation under industrial conditions, Method 2 of air insertion (by propelling air directly onto the sample surface) was implemented to reduce the influence of variable oxygen partial pressures in the kinetics of oxidation. It can be assumed that by using this method, a constant partial pressure of oxygen equal to the oxygen content (activity) in air (0.21atm) should be acting on the sample surface. The morphology of the interface formed on silicon steels by using Method 2 to induce oxidation at 950ºC for 30 seconds is depicted in Figure 6.13. The figure shows transversal cuts of the oxide with the steel mounted in resin and polished by traditional methods. An SEM image is shown in the left-hand side of the figure while the right-hand side is an optical image.

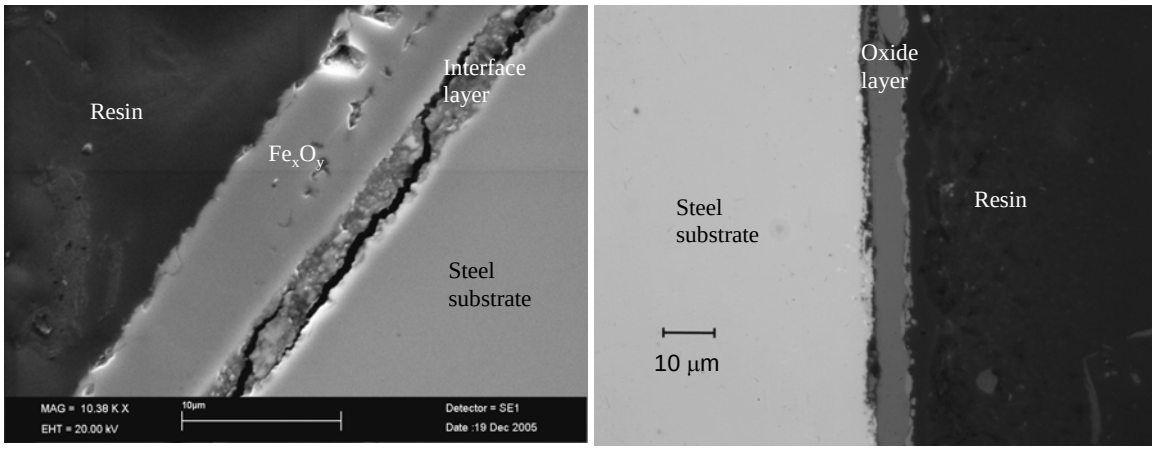

Figure 6.13. Transverse section of the oxide formed in silicon steels when oxidised by method 2 at 950ºC for 30s. Left-hand side shows the SEM image and right-hand side the optical image.

The transverse section of the oxide formed on silicon steel observed in the SEM and shown at the left-hand side of Figure 6.13 shows that the layer of oxide formed at constant partial pressures consists exclusively of an iron oxide layer and a thick interface layer. Experiments were also conducted under the same conditions at shorter times of oxidation and the ratio of the interface thickness to the iron oxide thickness remains constant. On the optical image, at the right-hand side of the figure, it appears that a second layer of iron-oxide might have formed on the outer oxide surface but, unfortunately the resolution in the optical microscope was

insufficient to resolve the constituents of the scale. Our experience with the analysis of iron oxides in low-carbon steel (see section 6.2.3) indicates that we can discriminate between wüstite and magnetite by using the backscattered detection mode in the SEM but the contrast is not enough to uniquely identify hematite. In order to determine the composition of the oxide layer on the silicon steel surface, samples of the oxides were extracted form the samples oxidised for 30 seconds, ground to powder and analysed with a powder X-ray diffractometer. The results of the X-ray analysis are depicted in Figure 6.14,

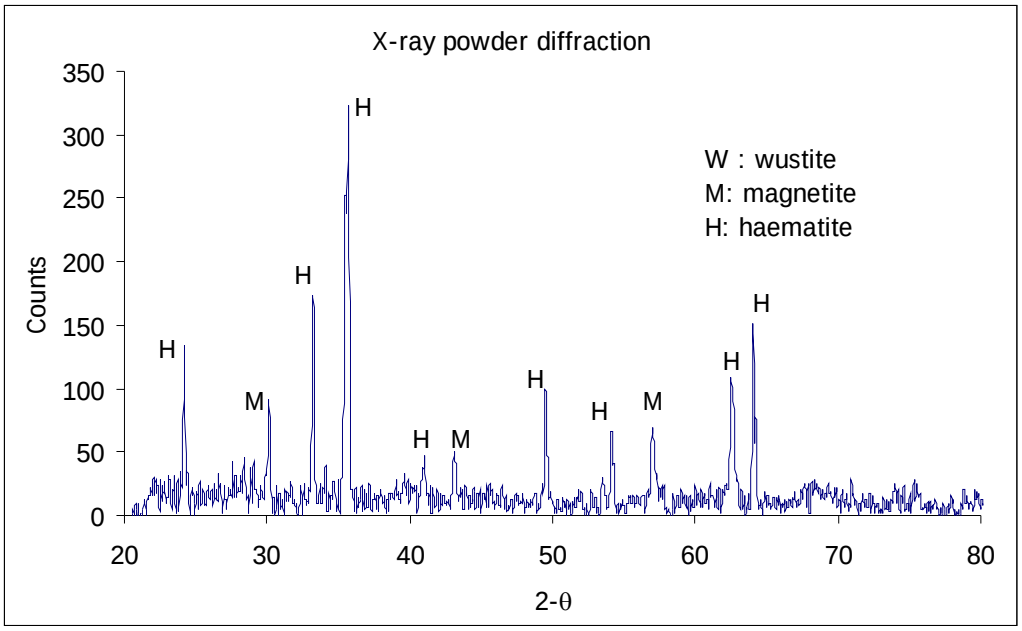

Figure 6.14. X-ray diffraction spectrum of the oxide formed in the surface of silicon steel. Oxidation conducted by Method 2, exposed for 30s at 950ºC.

Figure 6.14 show the composition of the oxides formed when silicon steel is oxidised for 30 sec. Hematite and magnetite are clearly present. Wustite is not present under these conditions of oxidation. Although an interface it is visible in Figure 6.13, no other compounds can be detected by X-ray analysis. We might argue that the interface formed is retarding the flow of iron ions to the surface and the higher iron oxides form preferentially. A more detailed study of the interface characteristics is presented below.

The analysis of the single nucleus, shown in Figures 6.8 to 6.13, strongly suggested that an interface layer forms on the steel surface before the formation of bulk iron oxides. This interface layer seems to be a complex mixture of aluminium, silicon and manganese oxides. This phenomenon was further investigated and a thin-foil sample, extracted from the interface layer formed after 30 seconds of oxidation is

shown in Figure 6.15. The top iron oxides were removed and the thin foil is just composed of the steel substrate and the interface layer topped with the platinum layer deposited by the dual-beam.

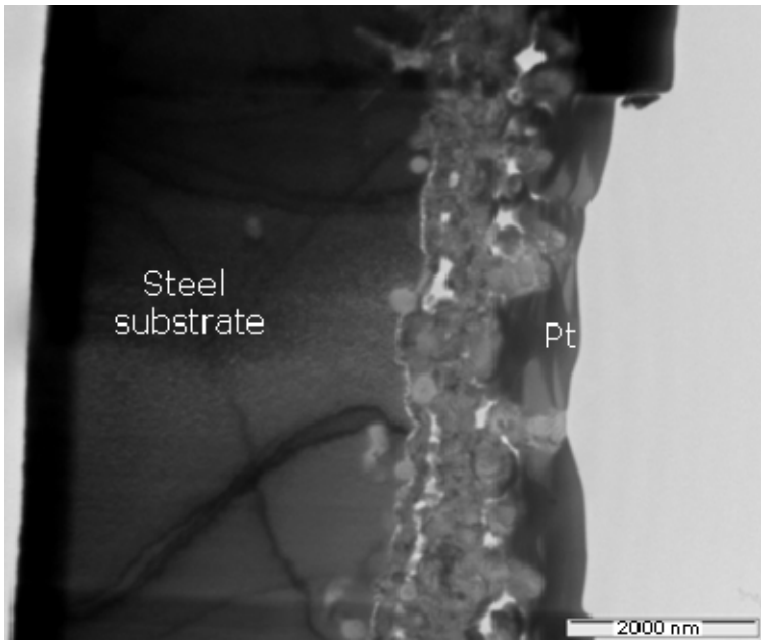

Figure 6.15. TEM image of the interface layer formed on silicon steel by Method 2 of gas insertion at 950ºC for 30s. The top iron oxides were removed and the thin foil is just composed by the steel substrate and the interface layer.

As shown in Figure 6.15, the interface is not coherent and seems to be formed by a collection of particles, this feature being better presented in the TEM micrograph shown in Figure 6.16

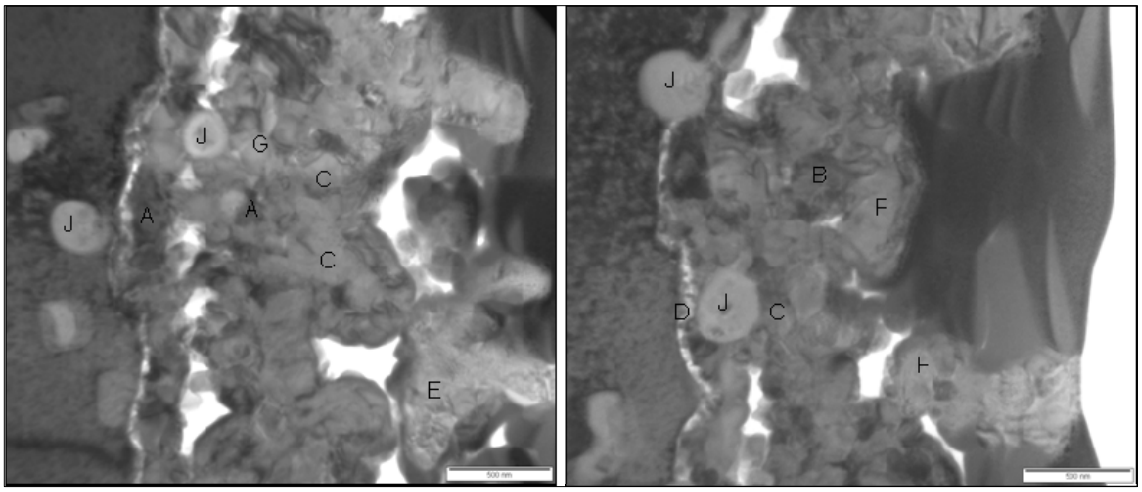

Figure 6.16. Detail of the oxide-interface morphology formed on silicon steels oxidised at 950ºC for 30s, using Method 2 of air insertion. The two images were taken from different positions on the same sample and features with similar appearance are indicated by letters

By using point EDS analysis in some of the particles that presented diverse morphology it was possible to obtain their constituent elements. Applying Zaluzec's (1979) method of standard-less calculations combined with a pseudo-standard from a pure oxide (in this case FeO), it was possible to obtain the approximate compositions of the particles (Table 6.4).

Table 6.4. EDS analysis of the features presented in Figure 6.15. Calculated by Zaluzec (1979) standard-less method.

	Approximate mass%					
Feature	O	Fe	Al	Si	Mn	P
A	22	78	0	0	0	0
B	24	71	0	5	0	0
C	16	59	0	21	0	4
D	20	19	8	53	0	0
E	19	37	10	30	0	4
F	18	55	11	16	0	0
G	17	83	0	0	0	0
J	22	13	40	17	10	0
Steel	0	100	0	0	0	0

From the results on Table 6.4, the composition of the particles can be estimated. Particles marked as A can be assumed as some form of iron oxide (FeO, Fe_3O_4 or Fe_2O_3). We assumed wustite to start with, and then compared it with calculations assuming magnetite or hematite. The results of the possible compounds formed in the other particles did not vary extensively, therefore we are presenting in table 6.4 the weight percents corresponding to the calculations assuming particle A as FeO. Particle A was used as a reference for the calculation of oxygen contents. Particle B is formed by Fe, Si and O and is presumably Fayalite, ($2FeO.SiO_2$) combined with an excess of iron oxide. The interface detected in point D contains Fe, Si, and Al so that it is most likely mullite ($3Al_2O_3.2SiO_2$) and fayalite; but even with this assumption, a high proportion of Si remains free. Another possible combination (due to the lack of oxygen) is the formation of inter-metallics such as $FeSi_x$ or $FeAl_x$. The likely formation of inter-metallics is also evident in particles F, C and J where the percent of oxygen is very low. Particle G is very high in iron and it is perhaps a mixture of wüstite and pure iron. Pure iron as well as intermetallics could be the result of the reduction of oxides, caused either when the air source is cut or by the reduction effect from other more stable oxide-forming elements.

It was not possible to deduce an exact composition of the particles from the EDS X-ray intensities of single elements. Moreover, when powder X-ray diffraction was applied as shown in Figure 6.14, we were also not successful in our attempts to detect any compounds formed in the interface layer.

6.2.2 High temperature oxidation of low-carbon steels

The low-carbon steel analysed in this study is typically employed in the manufacture of tinplate products. It contains basically C and Mn as shown in Table 6.2. The corresponding phase transformation diagram is shown in Figure 6.17 constructed with the software for phase equilibria calculations MTData.

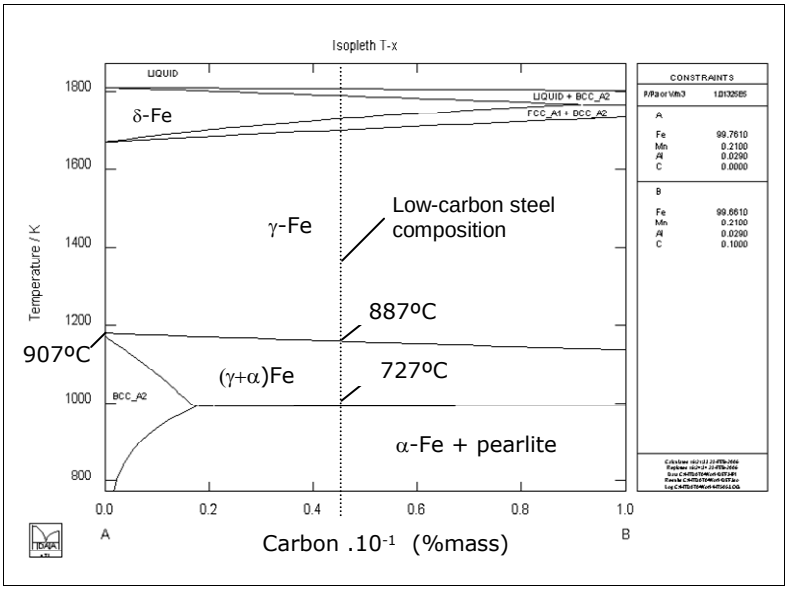

Figure 6.17. Phase diagram showing equilibrium transformation temperatures of the low carbon steel composition used in this study. Constructed with the MTData software

During the oxidation of low-carbon steels, the growth of a first layer of oxide and the subsequent formation of two other oxides has been observed in all of the experiments. The sequence of events shown in Figure 6.18 depicts the evolution of an oxide layer and the subsequent changes when, ostensibly, a new layer of oxide sweeps over the surface, the original oxide regains its original structure and then another oxide seems to sweep over the surface. This sequence of events, which will be discussed in more detail below, was obtained on the surface of a low-carbon steel sample oxidised by Method 1.

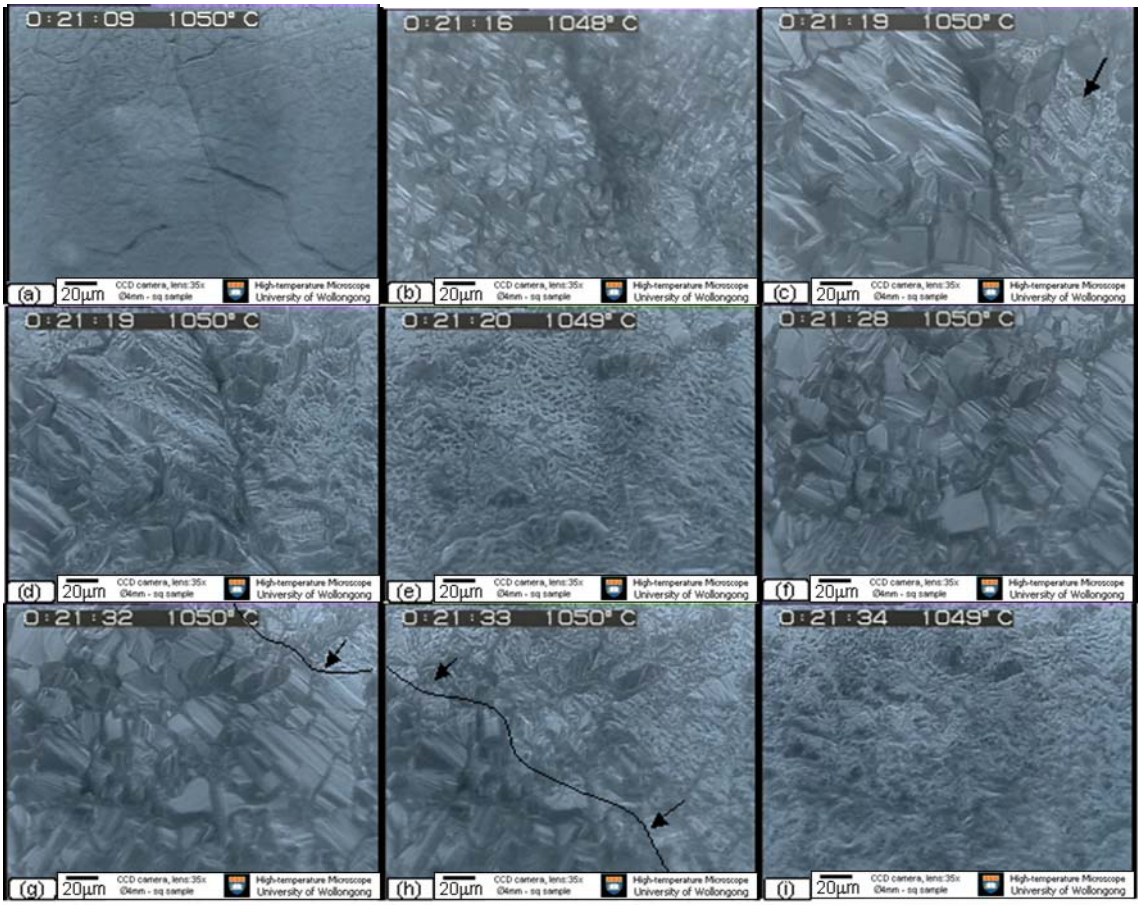

Figure 6.18. Sequential pictures of oxide formation on a low-carbon steel surface. Oxidation was induced at 1050ºC for 30s. Method 1 of progressive air introduction was used with a gas flow rate of $5x10^{-5}m^3.s^{-1}$. The video corresponding to this oxidation is available in the annexed CD.

In Figure 6.18, the following sequence of events can be identified:

Frame (a) Austenite grains and grain boundaries are clearly visible on the surface of the polished sample at 1050ºC under an argon atmosphere before the specimen is exposed to air.

Frame (b) Following introduction of air into the reaction chamber, the growth of an oxide phase around the former austenite grain boundary is detected. It is interesting that the austenite grain boundary remains visible notwithstanding the fact that a significant amount of oxidation has already occurred.

Frames (c) The oxide grains grow much larger with time and the austenite grain boundary still remains intact. Also, a 'new' oxide phase sweeps over the top of the existing oxide, starting at the right hand side of the image.

Frames (d) & (e) The 'new' oxide phase continues to sweep over the initial oxide layer (from right to left in the frames), and continues until the whole

surface is covered by the new phase. Frame (e) shows that the original austenite grain boundary is now covered with oxide.

Frame (f) The morphology of the newly formed phase changes with time and resembles again the oxide phase shown in frame (c). The former austenite grain boundaries have now completely disappeared.

Frames (g) & (h) Another oxide layer seems to nucleate at the top right-hand corner of the frame and it sweeps over the surface until the whole surface is covered by this 'new' phase. (More detail of the morphology of this 3rd oxide formation is depicted in Figure 6.19).

Frame (i) The last phase that formed retains its original morphology. It is experimentally possible to confirm that the oxide is growing continuously as the sample becomes un-focused with time, and has to be refocussed in a way that indicates an increase in thickness. The grain size and morphology of this last phase formed remain unaltered.

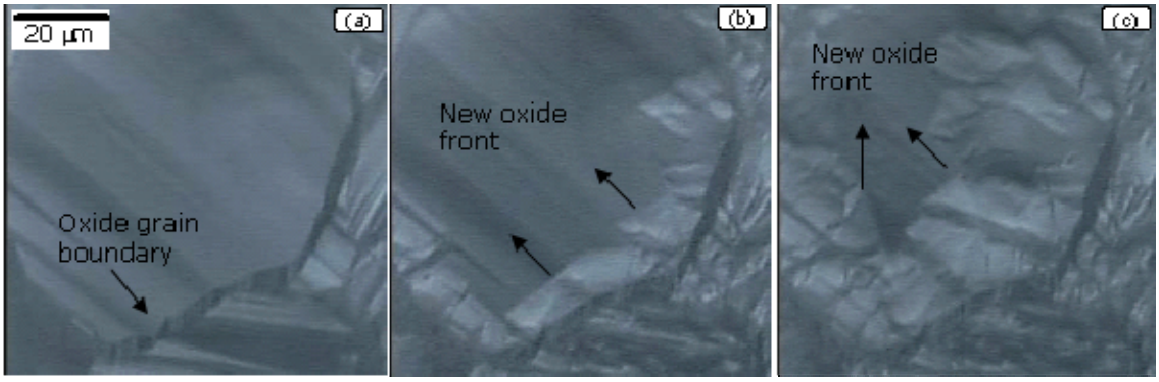

Figure 6.19. The sequence of pictures provide detail of the third oxide formation occurring from the grain boundaries. The new phase nucleates at an oxide grain boundary (the second oxide layer) and growth proceeds into the grain. From the nucleation of new oxide in Frame (a) to the growth state shown in Frame (c) 3.24 sec have elapsed. Method 1 of air insertion was used with an air flow rate of $6x10^{-6}m^3.s^{-1}$ and 1050ºC. The video corresponding to this oxidation is available in the annexed CD.

There is a possibility that the slow growth of oxide grains and the delayed formation of the two other oxide layers might be a consequence of the slow introduction of air into the specimen chamber. The progressive increase of the partial pressure of oxygen might mean that the rate of the reaction is controlled by the supply of the reaction gas to the oxide/gas interface. Moreover, a new oxide phase should not form until the partial pressure of oxygen exceeds the equilibrium value required for the formation of the corresponding higher oxide. It is for this reason that we have introduced Method 2 of air insertion into the reaction chamber. In order to ensure that the formation of the new oxides phases is independent of the oxygen partial

pressure, and that the rate limiting step in oxide formation is not determined by the rate of oxygen supply, we modified the high-temperature microscope to introduce a constant flow of air into the specimen surface. By blowing air directly onto the specimen surface, the influence of a varying oxygen partial pressure on the kinetics of oxidation is minimised. It is therefore more likely that the specimen surface would be exposed to an instantaneous and constant partial pressure of oxygen of 0.21 atm. In Figure 6.21 is depicted the sequence of events observed when air is introduced using Method 2.

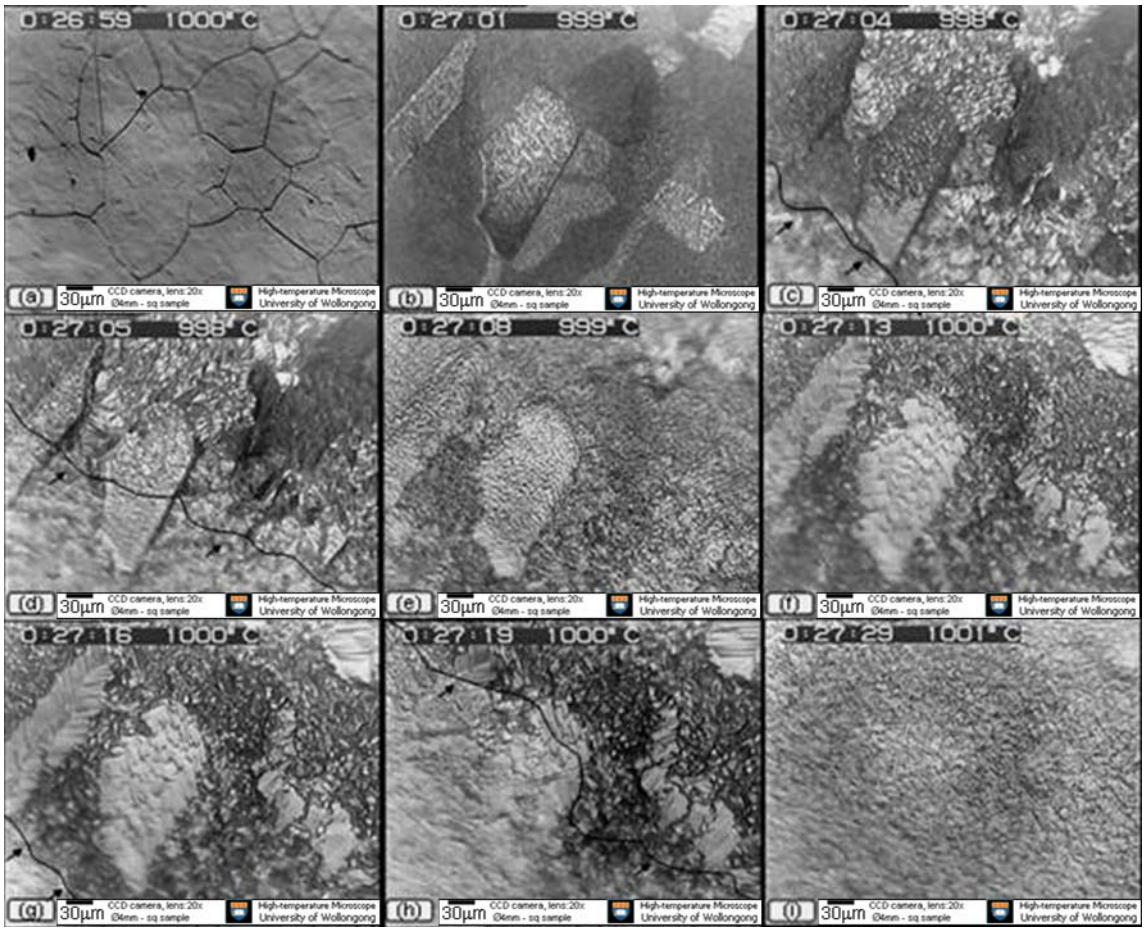

Figure 6.20. A sequence of pictures of oxide formation and oxide phase formation occurring on the surface of low-carbon steel when Method 2 of air insertion is used. Oxidation was induced at 1000°C for 30s. The video corresponding to this oxidation is available in the annexed CD.

Figure 6.20 shows the following sequence of events:

Frame (a) Austenite grain boundaries are clearly delineated on the surface of the polished sample and no visible oxides have formed before the introduction of air into the furnace chamber.

Frame (b) An oxide phase (which we believe is wüstite) nucleates in several areas randomly on the surface and the wüstite grains grow with time until the wüstite ledges are clearly visible

Frames (c), (d) & (e) A 'new' oxide phase appears at the left hand side of the image and continues to grow until the whole surface is covered as shown by the arrows.

Frame (f) The morphology of the newly formed phase changes with time and after a while resembles the phase structure of the initial oxide (wüstite) shown in Frame (c). The former austenite grains have not changed and these boundaries remain clearly visible.

Frames (g) & (h) 'Another' oxide layer forms and sweeps over the former oxides, initiating at the lower left-hand corner of the image and growing until it covers the whole surface.

Frame (i) The last layer of oxide formed, remains intact and retains its original morphology.

Samples of the composite oxide formed on the steel substrate were extracted, grinded and subjected to powder X-ray diffraction analysis. The three oxides of iron are evident in the X-ray spectra of samples oxidised by method 2, as shown in Figure 6.21. A small amount of haematite is detected as a weak peak in 2θ: 33.3º, corresponding to the (121) direction, while the rest of the oxide consists mainly of wüstite and magnetite.

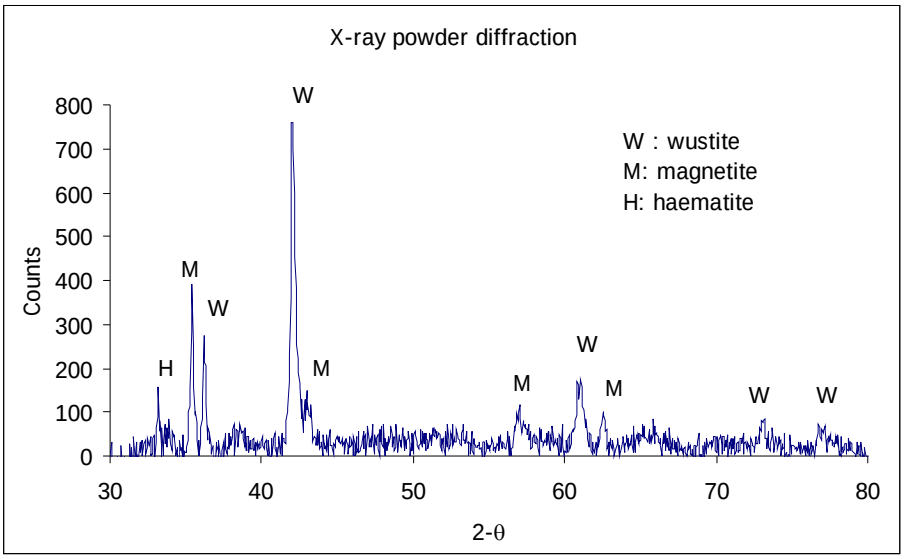

Figure 6.21. X-ray powder diffraction of the oxide layer extracted from samples oxidised by Method 2.

Morphology of the oxide layers

As opposed to the oxide formation observed in silicon steels, the first oxide formed on the surface of low-carbon steels nucleates randomly and covers very quickly, the whole surface. Therefore, it was not possible to 'freeze' a single nucleus during growth as was done with the silicon steels. The study of oxide morphology in this instance was done by scanning electron microscope, and some of the features are detailed in Figure 6.22.

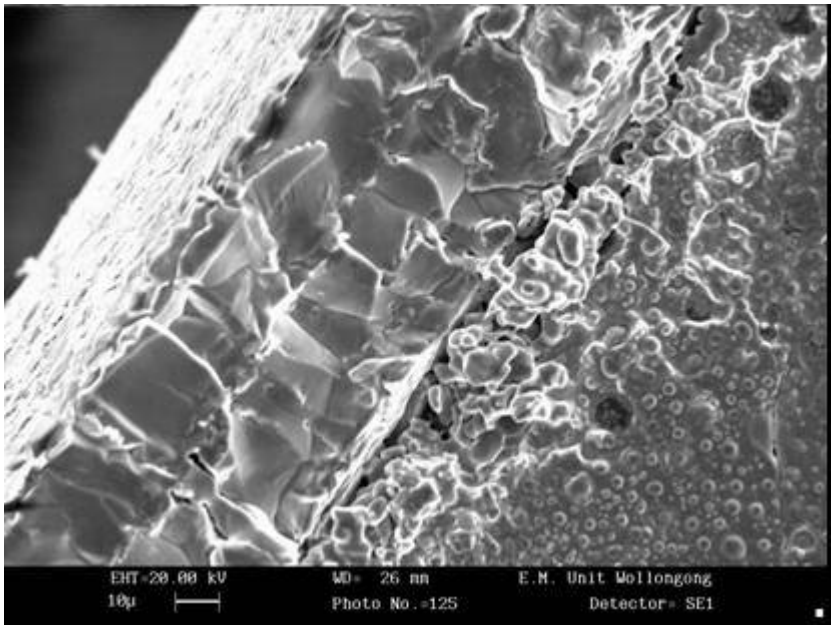

Figure 6.22. Transverse section of a fractured surface of scale formed on the surface of a low-carbon steel at 1000ºC and 30s of oxidation.

The scale shown in Figure 6.22 was detached from the surface and just the lateral scales remain with some detail of the substrate in the low right-hand corner of the image. It appears that some small spots remain on the substrate, perhaps related to the primary oxide nuclei. The fractured scale contains large columnar crystals as shown on the left-hand side of the image.

A cross section of the oxide layer formed on the surface of the low-carbon steels after 30 seconds of oxidation at 1000ºC is shown in Figure 6.23. In this sample, a typical configuration for iron oxides is observed composed of a thick wüstite (Fe_xO) layer that formed over the steel substrate followed of a magnetite (Fe_3O_4) layer and few hematite (Fe_2O_3) spots at the magnetite/gas interface. Chen *et al* (2002) have shown that hematite could comprise 1% of the total oxide thickness and hence,

there is a possibility that hematite may have formed on the gas interface but it is not detectable at the instrument resolution or perhaps damaged during polishing. The picture provides evidence that the cooling rate used, was high enough to retain wüstite metastable at room temperature as there are no indications of the eutectoid decomposition of wüstite into iron and magnetite.

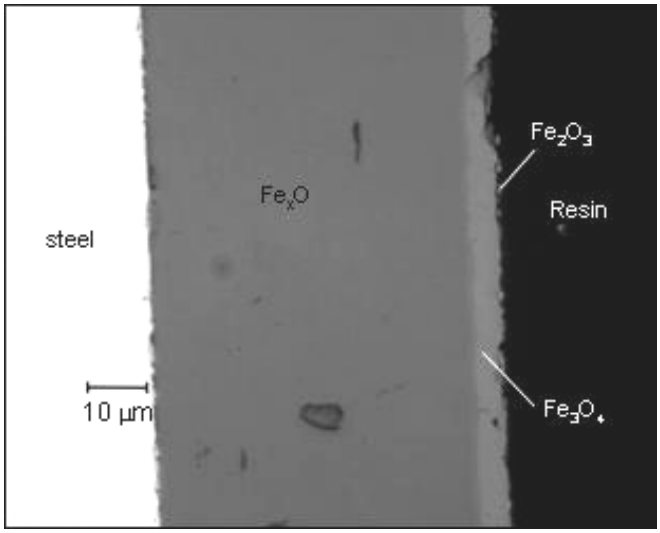

Figure 6.23. Optical image of the oxide layer that formed on the surface of a low-carbon steel oxidized for 30 seconds at 1000ºC.

To gain further insight on the morphology of the layer and interface formed in low-carbon steels, an analysis using EPMA was performed on samples oxidised at 1000ºC for 5 seconds. Maps of the oxide and the interface are shown in Figure 6.24. The oxides are clearly formed by iron and oxygen with some contribution of manganese. The oxide layers of wüstite and magnetite are clearly visible, but no hematite seems to form at these short oxidation times. The steel substrate shows what appear to be grain boundaries of the steel with precipitates of MnS and Al_2O_3. There is evidence of segregation of silicon, phosphorous and even sulphur to the steel/oxides interface during oxidation.

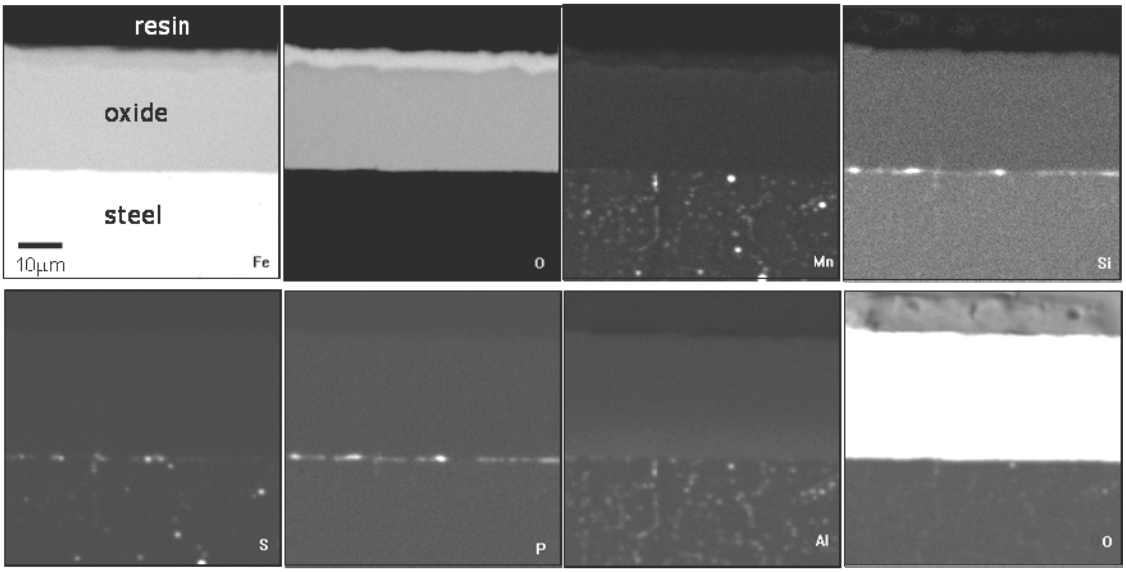

Figure 6.24 EPMA maps of the oxide and interface formed in low-carbon steels oxidised at 1000ºC for 5 seconds.

It is relevant to keep into consideration that the steel oxidised in the sample shown in Figure 6.24 contains small amounts of Si and P (0.005% and 0.012% respectively, see Table 6.2) but nevertheless the segregation of these elements to the interface is clearly evident. Al and S (0.03% and 0.014% respectively) form precipitates of Al_2O_3 and MnS on the grain boundaries. The extent to which silicon and phosphorous segregate to the metal/oxide interface in only 5 seconds is surprising, although the tendency of phosphorous to segregate to the surface is well known.

6.2.3 Kinetics of oxidation

The thickness of the oxide layer formed on the surface of low-carbon steel at constant time, as a function of the temperature of oxidation, is shown in Figure 6.25. A linear relationship is established between the temperature at which oxidation occurs and the thickness of the oxide layer after 30 seconds of oxidation. Some scatter is observed in the values corresponding to oxidation temperatures of 950ºC and 1000ºC respectively, which we presume might be due to the variability in grain size of the steels and also due to the inexact times for opening and closing of air induced by the manual operation of the instrument. In the temperature range 880ºC to 915ºC, the oxide layer tended to separate (spall) from the steel surface and such samples are shown in Figure 6.25.

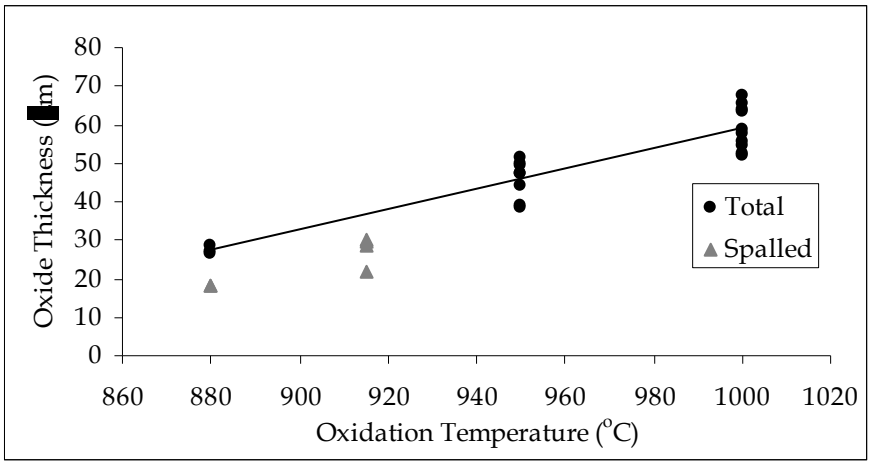

Figure 6.25. Influence of temperature of oxidation on the thickness of the oxide layer formed following 30 seconds of oxidation of a low-carbon steel. The samples that spall during oxidation are also shown in the graph.

Spalling was observed in the HTM as a sudden 'jump' of the oxide by 20 to 30μm above the original focused position of the image. All the samples oxidized at 915ºC and two at 880ºC spalled by separating from the substrate. It is assumed that as the oxide separates from the substrate, iron ions cannot diffuse to the oxide and no further growth of the oxide layer at the metal/oxide interface occurs. However, the oxide layer continues to grow at the oxide/gas interface by consumption of iron from wüstite to form magnetite and, in similar fashion, from magnetite to hematite. The influence of spalling on the relative proportions of wüstite and magnetite in the oxide layer is shown in Figure 6.26. As shown in this figure, wüstite contributes to about 93% of the oxide thickness in situations were the oxide remains adhered to the substrate, with magnetite contributing about 7% irrespective of the oxidation temperature. However, when spalling occurs, new wüstite cannot form because the supply of iron ions is effectively cut off from the oxide layer when it detaches from the iron substrate. Hence, the fraction of magnetite in the oxide layer is higher (50%-98% as opposed to 7% in an oxide layer that adheres to the steel substrate).

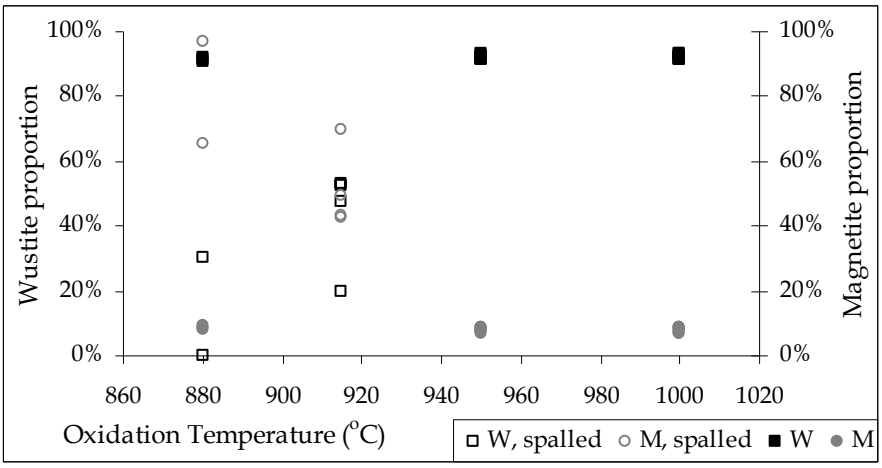

Figure 6.26. Influence of temperature and spalling on the proportions of wüstite and magnetite in the oxide layer that forms on the surface of low-carbon steel.

Figure 6.27 shows the aspect of the morphology in a spalled sample. The oxide is clearly separated from the steel substrate (the vacuum impregnated resin used when mounting the sample for observation gets imbedded in between the substrate and the oxide layer). The oxide layer, when separated from the steel substrate, contains a much higher fraction of magnetite than when the oxide layer adheres to the substrate. On the left-hand side of Figure 6.28 is shown a SEM image of a spalled sample, as opposed to the optical photo on the right-hand side, the hematite is not discernible from the magnetite. This effect on the observation should be carefully taken into consideration when analysing the morphology of oxide samples using SEM.

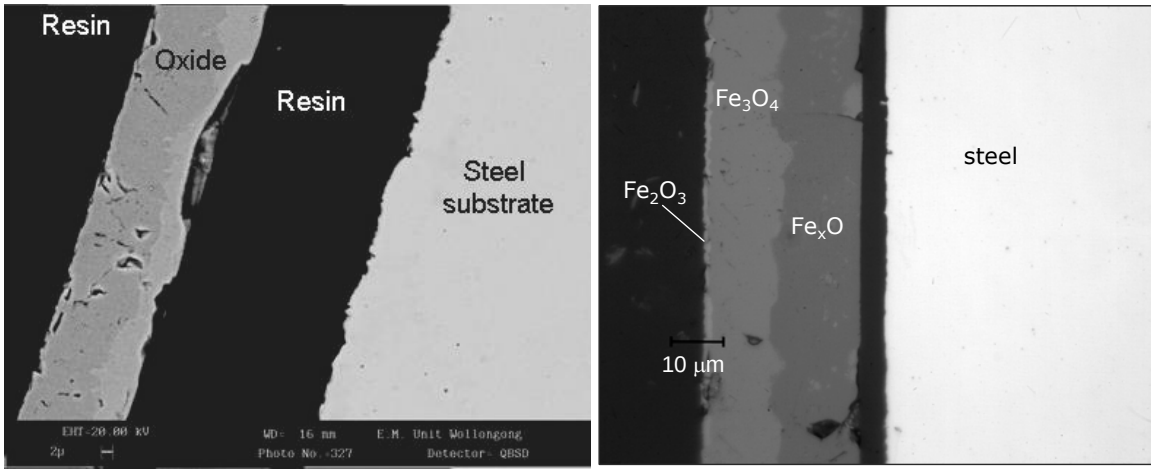

Figure 6.27. Images of a scale spalled from the surface of a low-carbon steel. Left-hand side is an SEM photo and right-hand side is an optical micrograph from a similar sample. Oxidation was induced at 915ºC for 30s using Method 2 of air insertion.

As an attempt to gain a better understanding of the spalling processes, we determined the actual surface temperature during oxidation at 915 and 1000ºC. A thermocouple was welded directly onto the polished sample surface to measure the steel surface temperature while the normal oxidation experiment is conducted. The control temperature, monitored by the thermocouple welded onto the crucible holder (see Figure 6.1) is also measured and in Figure 6.28, these two temperature traces are shown as a function of time of oxidation.

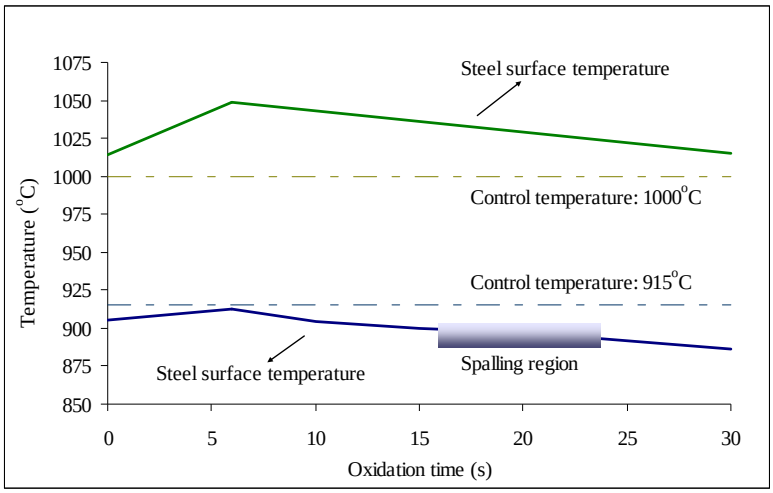

Figure 6.28. Results of the surface and control temperatures of a steel reacting with air at 915ºC and 1000ºC respectively

A comparison between these two temperature measurements shows that at an experimental temperature of 1000ºC, the surface temperature of the sample is slightly higher than the control temperature, being around 1020ºC (this is a typical feature because the reference thermocouple is positioned on the specimen holder far removed from the actual specimen, see Figure 6.1). An increase in the temperature of the steel surface (this is an absolute and accurate temperature) occurs in the first 7 seconds of oxidation, due to the exothermic oxidation reaction. As oxidation proceeds, the surface of the steel is covered by oxide and the temperature slowly reduces to about 1020ºC after 30s of oxidation. At an oxidation temperature of 915ºC, the temperature of the steel surface is about 10ºC below that of the reference thermocouple, it increases with the oxidation reaction and reduces as oxidation proceeds, reaching about 890ºC after 30s. The small differences in temperature between the reference thermocouple and thermocouple at the steel surface before the oxidation is initiated are the result of the complex heat transfer conditions within the infra-red heating furnace. Spalling usually occurs in samples oxidized at a control temperature of 915ºC after 18 to 23s of oxidation as indicated in Figure 8, in other words, around a temperature of 900ºC.

The kinetics of oxidation in the first 30 seconds of exposure to air of low carbon and silicon steels at 950ºC is compared in Figure 6.29 and it follows that a mixed linear-parabolic growth rate would be consistent for oxide growth in both these steels.

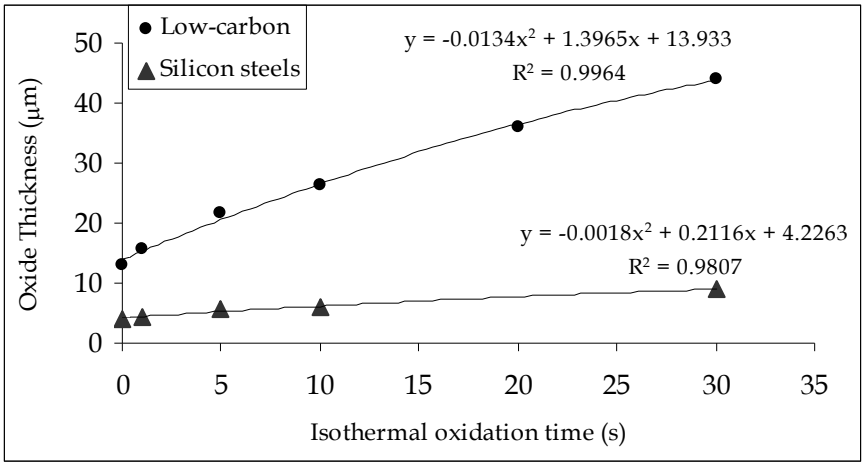

Figure 6.29. Linear-parabolic growth observed in samples oxidized at 950ºC for different times up to 30s for both low-carbon and silicon steels

The results depicted in Figure 6.29 may give the impression that a thin oxide is present on the steel surface before oxidation is initiated but this is merely a consequence of the experimental design and procedure as follows: samples are heated to the pre-selected temperature, followed by the injection of air onto the sample surface and start of oxidation; when the specimen has been reacting with air for a pre-determined length of time, the sample is cooled at the highest possible rate attainable in the instrument (23º $C.s^{-1}$) until the temperature reaches 700ºC when the air source is shut off. In practical terms, this procedure results in the specimen being oxidized on cooling from the reaction temperature (in this case 950ºC) to 700ºC. This experimental procedure was adopted to avoid the reduction of oxides and the concomitant changes in oxide layer morphology when the air supply is cut off, but it does mean that the measured oxide layer thickness is an overestimation. When the air supply is cut off at 700ºC, the rate of reduction is much lower than at the pre-determined oxidation temperature and the oxide morphology is not likely to be subjected to significant changes, or at least small changes, if occurring, will be similar for all samples. As shown in Figure 6.29, the growth rate of the oxide layer is almost linear in the first few seconds of growth and hence, it seems reasonable to assume that the measured oxide layer thickness at zero time corresponds to the extra thickness developed in the time interval of cooling from the isothermal oxidation temperature to 700ºC. The experimental values shown in Figure 6.29 can be corrected to intercept zero by subtracting the

thickness of the oxide layer that will grow in the time when the specimen is cooled from the reaction temperature to 700ºC. These corrected isothermal growth rates are shown in Figure 6.30. The best fit of the experimental values can be obtained by assuming a mixed linear-parabolic rate as suggested by Friedel *et al* (2004),

$$x^2 + jx = k\ t \qquad \text{Eq. 6.1}$$

with j and k as constants. From the trend lines on Figure 6.30, for low-carbon steels j: 47.66μm and k: 77.52μm^2.s^{-1}, while for silicon steels j: 5.53μm and k: 1.75μm^2.s^{-1} at times less than 30 seconds. These graphs indicate that the rate of growth on low-carbon steels is much higher than that of silicon steels.

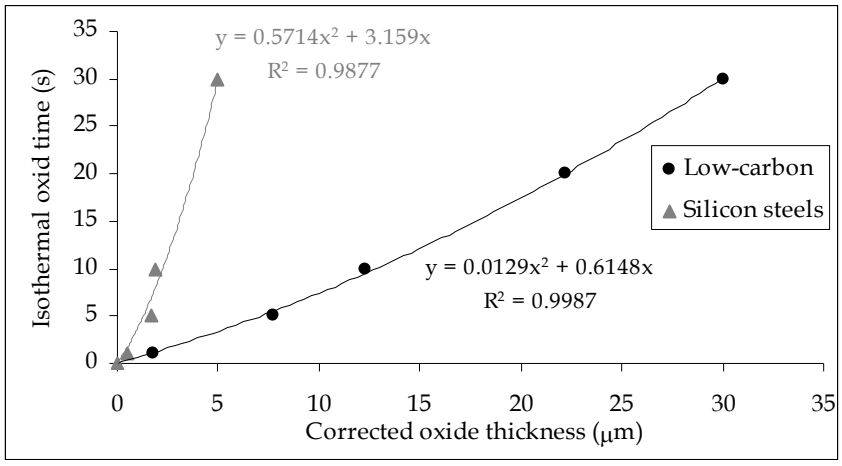

Figure 6.30. Mixed parabolic-linear growth of the oxide thickness, corrected by subtracting the thickness of the oxide layer formed during cooling (see text).

In the course of our experimentation we found that the time taken for the third oxide layer to form, varies from sample to sample. On further investigation, we found that the size of austenite grains before oxidation is initiated, affects time-to-formation of this third oxide. The time-to-formation of the third oxide is shown in Figure 6.31 as a function of austenite grain size for samples in the single austenite phase field in the temperature range 950 –1000ºC.

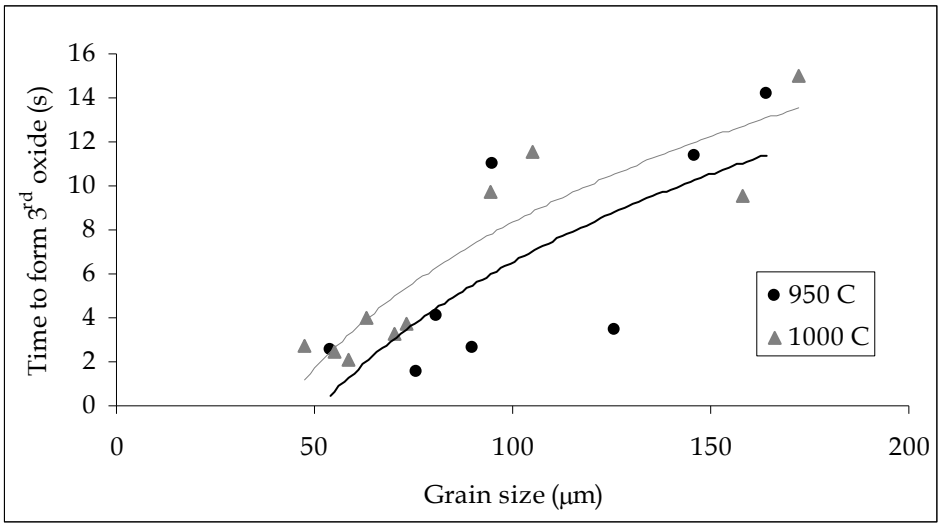

Figure 6.31. Influence of austenite grain size on the time-to-form the third oxide on low carbon steels at temperatures of 950 and 1000ºC

It follows from Figure 6.31 that the time required to form the third oxide is a strong function of the austenite grain size while the temperature of oxidation seems to play a minor role. The scatter in the experimental measurements is mainly due to errors induced during the measurement of grain size, which are an average from a broad range of sizes. Nevertheless, a clear logarithmic trend can be observed with reference to the influence of austenite grain size on the time-to-formation of the third oxide. The curves conform to the following equation:

$$t_{F3} = a \ln g_s + t_{F3}^0 \qquad \text{Eq. 6.2}$$

where t_{F3} is the time-to form the third oxide (s), a: rate constant depending of the temperature of oxidation (s.μm^{-1}), g_s: austenite grain size (μm) and t_{F3}^0 : hypothetical time-to-formation of the third oxide when the grain size is very small (g_s=0).

As the austenite grain size influences t_{F3} we explored the effect that the time required to form the 3rd oxide may have on the thickness of the oxide formed after 30 seconds of oxidation. The results are displayed in Figure 6.32, and it shows that the time required to form the third oxide have slight influence on the corrected thickness of oxide (once growth during cooling is subtracted) after 30s of oxidation.

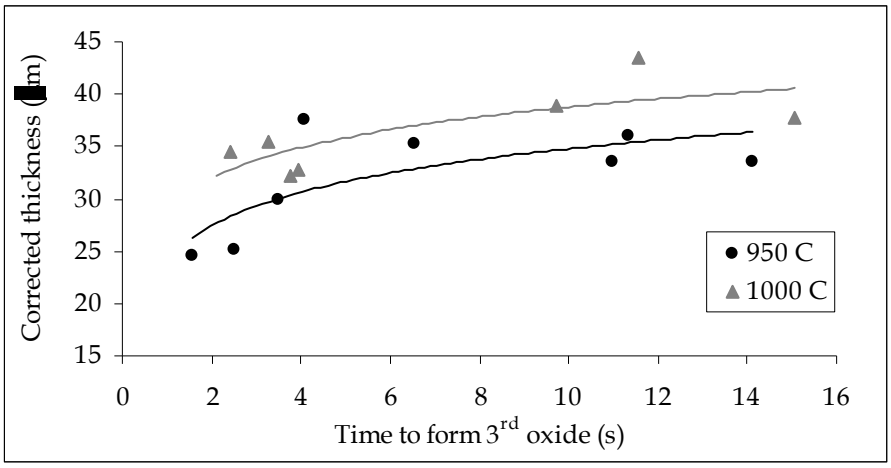

Figure 6.32. Influence of the time to form the 3rd oxide on the thickness of the oxide layer after 30s of oxidation (low-carbon steels)

Figure 6.32 shows that the longer it takes for the 3rd oxide to form, the thicker the oxide layer will be. The curves in Figure 6.32 can be mathematically expressed as:

$$X_{(30s)} = b \ln t_{F3} + X^0 \qquad \text{Eq. 6.3}$$

In where $X_{(30s)}$ is thickness of oxide after 30 seconds of oxidation (μm), b: temperature dependent rate constant ($\mu m.s^{-1}$) and X^0: hypothetical thickness of oxide when the 3rd oxide form simultaneously with the first layer of oxide (t_{F3}=0). Table 6.5 gives the constants determined for Eq. 6.1, 6.2 and 6.3.

Table 6.5. Empirical values of the constants corresponding to Eq. 6.1, 6.2 and 6.3.

	j	k	a	t_{F3}^0	b	X^0
At 950ºC	47.66	77.52	9.8494	-38.823	4.5457	24.35
At 1000ºC	74.93	123.5	9.5756	-35.570	4.243	29.02

6.3 Discussion

Oxidation experiments were conducted in a high-temperature microscope at temperatures, times and atmospheric conditions closely resembling those of finishing-mill operations. We determined the influence of temperature, grain size of the steel substrate, steel composition and oxidation times on oxide formation and morphology on the early stages of oxidation. The main objective of the present study was to compare the oxidation behaviour of low-carbon and silicon steel.

6.3.1 Oxide formation

Oxide formation on silicon steels

Minor additions of elements can have a significant influence on the nature of the oxides formed in the early stages of oxidation. In the commercial silicon steel studied, additions of less than 0.6% Al, Mn and Si are sufficient to form a complex interface between the substrate and the iron oxide, reduce the concentration of oxide nuclei forming at the start of oxidation and consequently reduce the rate of growth of the bulk oxide layer.

Figure 6.33 is a schematic illustration aimed at describing the sequential stages of oxidation of the silicon steel studied.

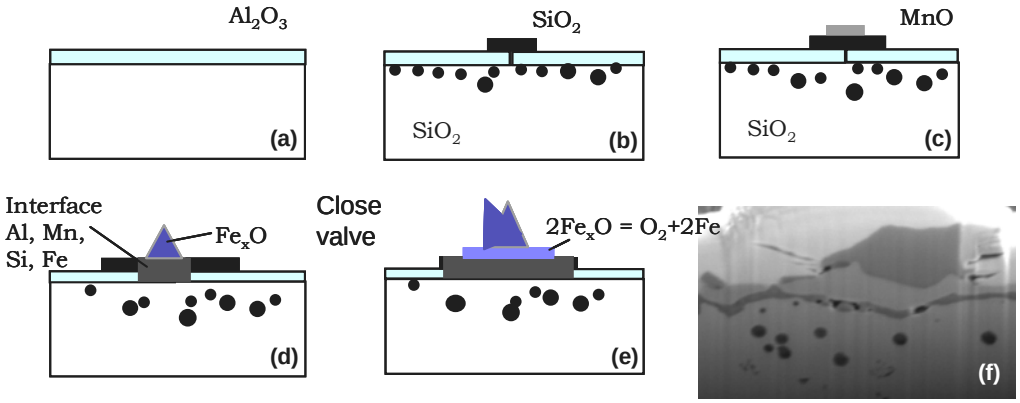

Figure 6.33. Schematic illustration of the nucleation and growth of oxides during oxidation of silicon steel.

In the schematic illustration, Figure 6.33, the following sequence of events during oxide growth is depicted:

(a) The first layer that forms is aluminium oxide (Al_2O_3), which actually forms even before air is introduced into the chamber because of the high reactivity of aluminium. The equilibrium partial pressure of oxygen for the formation of alumina (Al_2O_3) at 900ºC is about 10^{-40} atm (see Ellingham diagram in Figure 2.6) and even at the high-purity argon atmosphere in which the experiments were conducted, the oxygen partial pressure is only $\sim 10^{-21}$ atm. As shown in the phase diagram of this type of steel (Figure 6.4), ferrite is the stable phase below 902ºC, while at higher temperatures austenite and ferrite coexist. Therefore, the selective alumina oxidation depicted by the white and dark grains may result from different crystallographic orientation of the ferrite grains or the presence of austenite grains.

(b) When air is introduced into the chamber, silicon oxide (SiO_2) nucleates. These nuclei formed preferentially on grains that had a darker appearance, presumably because these grains contained a thinner (or no) layer of Al_2O_3. It can be assumed that at this stage the internal SiO_2 precipitates have already formed. Atkinson (1982) explains that precipitates form by diffusion of oxygen into the alloy up to a certain depth, while simultaneously the segregation of Si atoms to the internal oxidation zone increases the concentration of Si near the surface until, at some critical volume fraction of precipitates, a continuous layer of SiO_2 forms on the surface of the metal.

Logani *et al* (1971[a]), observed the same kind of precipitates and scarce nucleation of SiO_2 in steels that contained no significant amounts of aluminium. These nuclei formed preferentially at the grain boundaries of the metal, indicating that the presence of an alumina layer on the surface is not necessarily the limiting factor for the nucleation of silica. Nevertheless, in our samples nucleation initiated in preferred steel grains and the onset of nuclei is not on the grain boundaries. It may be argued that an incoherent scale of alumina formed on grains with certain orientations and that the silica nuclei formed on defect zones of the alumina layer, similar to the mechanism proposed by Erhart *et al* (1984) for steels with much higher aluminium concentration. After internal precipitates and surface nuclei form, the silica continues growing in an isotropic lateral fashion depicted in the experiments on the HTM as circular spots increasing in diameter.

(c) As the partial pressure of oxygen continues to increase Mn irons are transported through the silica layer forming MnO on the surface. The analysis of the interface formed after all the oxides developed, depicts the presence of manganese in a gradient with higher concentration near the steel substrate. These findings show that the presence of manganese might be also influencing the kinetics of oxide formation.

(d) The final layer of oxide is that of wüstite (Fe_xO) which grows laterally and also vertically by the supply of iron ions (Fe^{+2}, Fe^{+3}), being transported through all the oxide layers to the oxide-gas interface. It is known that Al, Fe, Mn and O form spinels like $MnFe_2O_4$, $MnAl_2O_4$ (Lins *et al*, 2004) and Si, Fe and O form fayalite ($2FeO\text{-}SiO_2$) therefore an inner layer of complex oxides might continue forming to the expense of the layer of already formed iron oxides.

(e) During experimentation, the air supply is closed and replaced with argon in order to deter further lateral growth of the oxides so that the composition of the nuclei can be determined. This action gradually reduces the partial pressure of oxygen in the chamber and all the oxides that where forming at the exact moment the partial pressure of oxygen is reduced below the equilibrium for their formation, will regain electrons and form pure metal. Such formation of metal (reduction of oxide) is proportional to the rate of diffusion of species through the oxide. As a consequence, the iron ions that were transported through the oxide, regain their electrons and form a layer of pure iron exactly between the wüstite and the interface formed by the more stable oxides. Furthermore, a thin rim of Si is observed on the EDS maps forming on the border of the growing layer of SiO_2 and a rim of Mn was also observed at the limit of the pure iron zone.

Finally, a photo is shown of one of the transverse cuts made through an oxide nucleus which depicts all the layers formed. The internal silica precipitates located exactly below the wüstite crystals are much bigger and farther from the surface than those that formed close to the first silica layer (see Figure 6.11). It may be argued that the new iron oxides formed on the surface, which are predominantly p-type semiconductors, will deter further transport of oxygen ions (anions) to the steel surface and prevent further formation of precipitates. Hence, the precipitates, which have already formed, combine and grow.

In the next set of experiments with silicon steels the partial pressure of oxygen was kept constant and well above the equilibrium value required for the formation of all the oxides that are likely to form (0.21atm). The main oxides formed are magnetite and hematite, and an interface layer consisting of non-coherent oxides and possibly inter-metallics between the substrate and the iron oxides. The presence of magnetite and hematite and not wüstite indicates that the interface layer is retarding the diffusion of iron-ions to the surface. In-situ observations have shown that higher iron oxides form in the first few seconds of oxidation regardless of the grain size, much faster of what is observed in low-carbon steels.

The interface layer remains proportional in thickness to oxides growing at the gas interface. This indicates that after all the oxide layers are formed and have covered the surface of the metal, the growth in thickness of the products in the interface layer and the iron oxides at the gas interface occur simultaneously.

Oxide formation on low-carbon steels

During the high temperature, isothermal, in-situ observation of oxidation of a low carbon steel surface we have observed that an oxide forms on the surface of the steel substrate, grows as a function of time and that two other oxide phases form within the first 30 seconds of oxidation. We assume that the first layer of oxide that forms on the steel surface is wüstite (Fe_xO) because the wüstite phase should, from thermodynamic considerations, be stoichiometrically more stable than the other iron oxides at higher iron activity. The crystal shape that we observed resembles that reported by Logani *et al* (1969) who found the same kind of pyramidal morphology (typical of rock-salt structure) in wüstite crystals formed on the surface of steel.

The second oxide that nucleates and sweeps across the surface is likely to be magnetite (Fe_3O_4), which nucleates and grows on the surface of wüstite. The nucleation of magnetite appears to initiate at zones of ledge intersection or within an area where there is a high concentration of oxide grain boundaries, not necessarily related to the austenite grain boundaries that still remain visible. It seems that the sequence of events that result in the formation of magnetite on the surface of a wüstite layer could be explained by two different mechanisms. Either the supply of Fe^{+2} and/or Fe^{+3} cations diffusing through the wüstite and reaching the oxide/gas interface is reduced in selected areas of the surface; or oxygen anions might be penetrating into the grain boundaries of the wüstite, creating oxygen enriched areas. Once the nuclei of magnetite are formed, a new oxide phase grows laterally on top of the wüstite.

Once the magnetite (second layer of oxide) has formed, it continues to grow and eventually resembles the appearance of wüstite grains before a third oxide layer is formed on top of the second. Due to the continuous growth of the oxide layer on top of the substrate and the relative low rate of diffusion of iron through magnetite (see Table 2.4), the concentration of iron ions reaching the surface is reduced. For this reason it can be argued that the third oxide layer that forms is hematite (Fe_2O_3), which is oxygen-enriched relative to magnetite. However, we have observed that during the period between the second and third oxide formation, the newly formed oxide layer seems to revert to the morphology of the former wüstite, with its faceted structure. Furthermore, pyramidal pits are also observed after the second oxide formation, similar to those observed by Bahgat *et al* (2004) during wüstite reduction experiments. Besides, the X-ray diffraction patterns and also the

transversal sections of the oxide layer after cooling to room temperature, do not show the presence of a layer of hematite.

We are at present not able to fully explain the sequence of events that culminate in the formation of an ostensibly stable oxide layer on a low-carbon steel surface. However, the limited experimental information at our disposal indicates two possibilities: The first possibility would simply be that the three oxides formed in sequence are wüstite, magnetite and hematite as illustrated on Figure 6.34. Magnetite forms on top of the wüstite and continues to grow in thickness. The magnetite might also in appearance resemble wüstite, with ledges growing in faceted fashion, but this interpretation is not in agreement with the spinel structure of magnetite. Once the magnetite reaches a certain thickness and the concentration of iron ions approaching the oxide/gas interface is reduced, the third oxide layer, hematite (Fe_2O_3), is formed. Further flow of iron ions through the oxide layers will reduce continually the higher oxides on the interface between iron oxides, i.e. magnetite is reduced to wüstite and hematite to magnetite. As the diffusion of iron through wüstite is faster than through magnetite, the reduction of magnetite to wüstite will be faster than the reduction of hematite to magnetite. Furthermore, oxygen diffuses faster through the hematite layer than iron and will reach the Fe_3O_4 /Fe_2O_3 interface to form more Fe_2O_3. This sequence of events will lead to the formation of a thick layer of wüstite, followed by thin layer of magnetite and a much thinner layer of hematite.

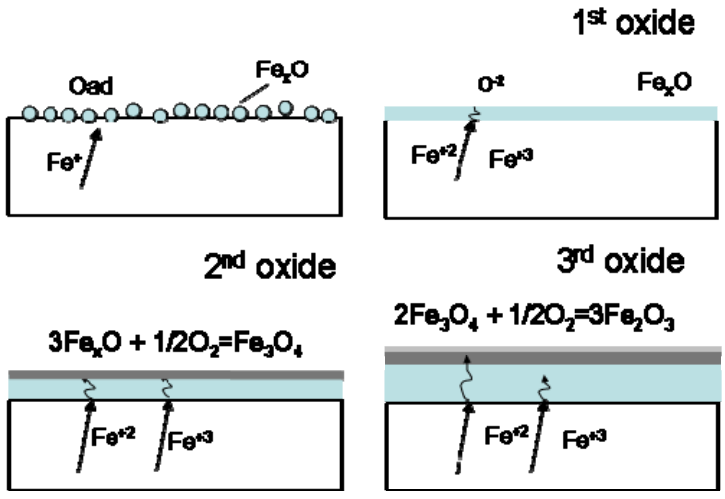

Figure 6.34 Schematic of the oxide formation according to the first proposition

An alternative interpretation is that the second layer that forms is pseudo-stable magnetite, which reduces back to wüstite and, after further exposure to oxygen is re-oxidised to magnetite as a stable oxide layer as shown in Figure 6.35. In this

case, the magnetite formed in the second oxide formation is easily reduced by the continuous supply of iron ions through the oxide grain boundaries or the oxide lattice, and wüstite regains its equilibrium state. Whether wüstite or magnetite is stable, is therefore determined by the balance of iron-ions diffusing through wüstite and reducing the magnetite, and iron ions diffusing through magnetite and reaching the gas interface to form more oxide. Under these conditions, the third layer of oxide sweeping to the surface of the wüstite is again magnetite, which is stable and remains unchanged as the concentration of iron ions reaching the interface oxide/gas has now been diminished to the extent that an oxide with higher oxygen content can remain stable.

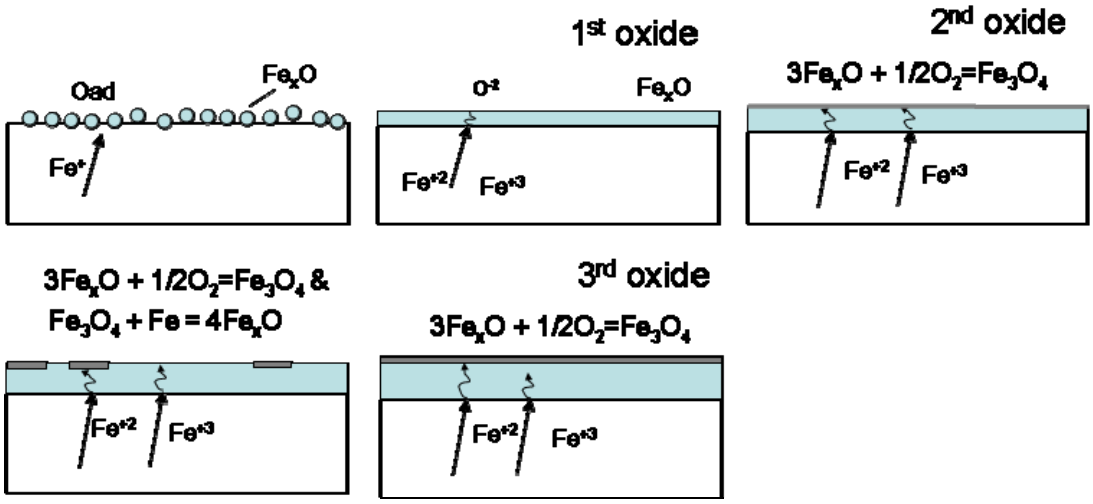

Figure 6.35. Schematic of the oxide formation according to the second proposition

During oxidation of the low carbon steel studied, the phases formed are identical to those formed on pure iron. The minor additions of Mn (0.21% mass) do not seem to influence in the iron-oxide phases formed, and the MnO in all probability, forms a solid solution with the FeO. Nevertheless, the proportion of magnetite (~7%) formed in the short times of oxidation when the oxide remains adhered to the substrate, is higher than the reported for pure iron (4%) in much longer times. The higher proportion of magnetite in our experiments might be product of the unstable or inexistent hematite layer. Once hematite is formed, further oxidation is retarded due to the low diffusivity of iron through it, therefore in experiments in where sufficient time is allowed to form a thick layer of hematite (providing the oxide layer remains adhered to the substrate), the magnetite proportion should be lower as in pure iron oxidation.

6.3.2 Kinetics of oxidation

Spalling

The ratio of magnetite to wüstite in the oxide layer remains constant and equal to 1:13 (M:W) at all the testing temperatures and times up to 30 seconds unless the adhesion of oxide to the substrate is compromised. These observations reinforce the extensive analysis by Bolt (2000); he compiled four main reports describing the types of oxides formed on the steel as a function of temperature, and concludes that the widespread affirmation that at temperatures above 900ºC the relative proportion of magnetite and hematite in the oxide layer is higher that at lower temperatures, is not necessarily correct (Bernard *et al* 1946; Blazevic, 1987; Mascia *et al*, 1998). Although it is possible to detect high proportions of magnetite and hematite on the scale of hot rolled steels, it is likely that they are product of a separation of the scale from the substrate while rolling. Bolt's conclusions corroborate our findings that the fraction of iron oxides formed on low carbon steel, should be constant above 727ºC as long as the oxide layers remain adhered to the substrate.

The occurrence of spalling (also called blisters) at high temperature has been discussed extensively by Matsuno (1980) and Kizu *et al* (2001). Matsuno (1980) demonstrated that spalling occurred between 950 and 1000ºC in low carbon steel samples (0.08%C) and Kizu *et al* (2001) argued that spalling is related to the orientation relationship between the wüstite grains, the oxide rate of growth and the segregation of impurities to the steel/oxide interface. In our experiments we observed a tendency for the oxide layer to spall (or blister) in low carbon steels at temperatures of 880 and 915ºC (Figure 6.25).

The EPMA examination of the oxides formed on low-carbon steel showed that Si and P segregated to the metal/oxide interface (Figure 6.8). Kizu *et al* (2001) argue that the presence of these elements leads to the imminent onset of blisters. Although this is a plausible proposition, we find it difficult to agree completely with this premise. Besides the influence of these elements and the possible eutectic oxides that might form, the phase transformation of the steel substrate might be playing a role on the detachment of oxide. Even though our experiments were conducted under isothermal conditions, the oxidation reaction will initially extract heat from the steel surface and once the oxide layer has reached a certain thickness, the heat transfer rate from the outside of the oxide (where the radiant heat impinges) to the inside of the sample (the steel surface) will diminish. As shown in Figure 6.12, the actual temperature on the sample surface is reduced with

time. It has also to be borne in mind that decarburisation and elemental segregation can occur during heating, annealing and soaking so that the transformation austenite-to-ferrite phase transition temperature (A_3) can change with time. Because this transformation is accompanied by a volume change, it is possible that the phase change could be responsible for spalling. The oxide layer is sufficiently thin at the moment the phase transformation occurs and can deform and separate from the substrate by the effect of the interface movement.

Another cause of accumulated stresses might be differences in the rate of growth of oxides. The presence of combined ferrite and austenite grains, lead to different diffusion rates and account for variable rates of growth.

Comparison between the oxidation kinetics of low-carbon and silicon steels

The previous discussion asserted that the morphology of oxides formed in low-carbon and silicon steels is distinctly different. When the thickness of the oxides is considered it was shown that not only is there a difference the morphology of the oxides formed but also that the effective volume of oxide formed is much smaller in silicon containing steels than in low-carbon steels under identical conditions of oxidation. Following 30 seconds of oxidation, oxides formed on low-carbon steel is 6 times thicker than those formed on silicon steels. This finding provides convincing evidence that minor additions of alloying elements can affect the ion transport through the oxide layer even at very short times of oxidation where the layers are still very thin. The effect of small additions of silicon to steel on the kinetics of oxide formation has already been studied by Marston *et al* (2004) and they observed the same slow growth at the start of oxidation followed by an increase in the thickness after 120 seconds of exposure to the oxidising gas (see Figure 2.14). The findings of Marston *et al* provide evidence that the layer obstructing the diffusion of iron species should disappear with further oxidation. We were not able to detect such a change in our short-time experiments. Nevertheless, we were able to observe in the TEM, a change in morphology of the oxides from a coherent interface layer during the early nucleation stages to a layer formed by porous precipitates once the whole surface of the sample was covered by the oxides and a uniform top layer of iron oxide has formed.

Interpretation of the time for oxide formation

It was found that the time to nucleate the 3rd oxide has an influence on the final oxide thickness, at least at short times of oxidation (less than 30 seconds in our experiments). We have observed that different types of oxide can form in the first seconds of oxidation. It is well known that the diffusion of iron ions through the oxide layer depends upon the morphology of the oxide present (wustite, magnetite and/or hematite); hence the rate of growth of the oxide layer will depend on the type of oxide present. Figure 6.32 and Eq. 6.3 show that the thickness of the oxide formed after 30 seconds depends on the time to form the 3rd oxide. Moreover, the rate of growth might also be influenced by the formation of the second layer of oxide, but unfortunately the times taken for the 2nd oxide to nucleate and form are normally too short to be determined precisely. The difference in rate of growth before and after the 3rd oxide forms can be determined by using the experimental data as explained below.

The theoretical thicknesses of the oxide layer after 30 seconds exposure to air is obtained by substituting into Eq. 6.3 the corresponding constants from Table 6.5 and varying the time-to-form the 3rd oxide (t_{F3}) between 2 and 14 seconds. These values are shown as circles in Figure 6.36. The curve OA represents a constant rate of growth, when all the oxides are present and growing simultaneously; or what is the same, when t_{F3} and t_{F2} equal zero. The thicknesses after 30 seconds of oxidation, represented by the circles, are influenced by t_{F3}; meaning that an oxide of a certain thickness have formed before the third oxide nucleates. To determine the rate of growth of the oxides that formed before the third oxide nucleates, parallel curves to OA are drawn starting at a t_{F3} value and terminating at the corresponding oxide thickness (representing identical rate of growth). As an example, with reference to Figure 6.36: if the third oxide nucleated after 6 seconds, the thickness of the oxide layer(s) that have already formed is 15μm. As soon as the 3rd oxide has formed, the growth rate changes from the slope of curve OC to that of curve CD and after 30 seconds of oxidation the oxide thickness will be 37μm.

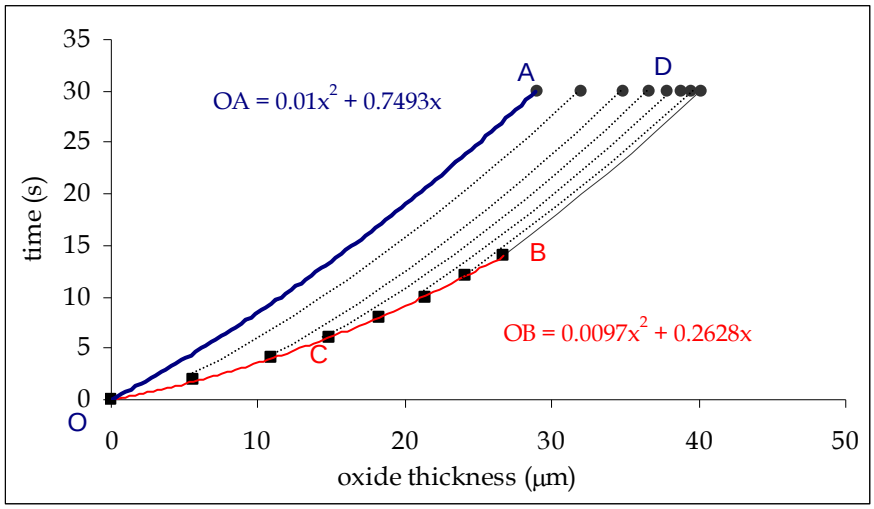

Figure 6.36. Theoretical oxide thickness based on time to form 3rd oxide layer. See text for details.

The information in Figure 6.36 should be interpreted as follows, referring again to the previous example. An oxide layer 15μm thick has formed before the 3rd oxide layer nucleates and the rate of growth of this oxide is given by the tangent to curve OCB at C. The third oxide now nucleates and grows at a rate equal to the tangent to curve CD at D. The fact that there is an abrupt change in growth rate provides evidence that the 3rd oxide that forms is different from the existing one, since the rate of growth of an oxide is a function of the diffusion coefficient or iron ions through that oxide, and it is well known that this diffusion coefficient has different values for wüstite, magnetite and hematite.

Influence of austenite grain boundaries

Because the austenite grain boundaries can still be seen while the oxide film continues to grow as shown in Figure 6.20, our observations suggest that in the early stages of oxidation, diffusion of iron along austenite grain boundaries determines the oxide growth rate. The austenite grain boundaries remain visible up to the occurrence of the second oxide formation when air is progressively increased into the chamber (Method 1), and up to the third oxide growth if the air is blown directly onto the sample surface (Method 2). Moreover, when air is inserted using a very low flow rate, the grain boundaries disappear from vision before the second oxide forms. We presume that a channel is left in the oxide film while it is forming due to the high diffusion rate of iron to the substrate surface through the austenite grain boundaries (see Table 2.4), and the subsequent fast growth of wüstite ledges away from that source of irons, as shown in Figure 6.37. As long as the oxygen potential is lower than the partial pressure of oxygen required for the formation of

the next oxide the high rate of diffusion of iron ions through wüstite will ensure that the oxide continues to grow and will eventually obstruct channels before the oxygen potential is high enough to form the next oxide, as depicted in Figure 6.37 in the case of progressive air introduction.

When the air is blown directly onto the surface of the steel, the thermodynamic conditions are met for the formation of all three iron oxides and hence, wüstite will not grow to such a thickness that it will obstruct these channels before the next oxide forms and therefore, the grain boundary channels remain visible.

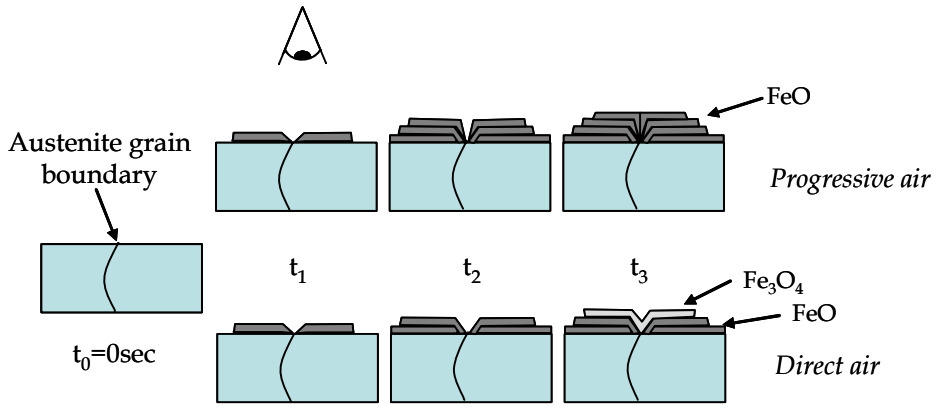

Figure 6.37. Schematic illustration of oxide formation, illustrating the formation of austenite grain boundary channels when using respectively, progressive or direct air insertion.

Logani *et al* (1971[b]) suggested that at high temperature, diffusion in the early stages of oxide formation may preferentially occur along short-circuit paths such as oxide grain boundaries. It is only when these preferred diffusion paths are obstructed by oxide growth that lattice diffusion becomes the dominant transport mechanism. We believe that the austenite grain boundaries act as short-circuit paths for the supply of iron atoms to the steel surface and the consequent transport of ions through to the oxide ledges. In the steel with a small grain size (see Figure 6.38) the number of grain boundaries is larger and therefore, the probability that ledges meet and close the grooves of iron transport is higher than in the case of steel with a large grain size. Once the density of the diffusion path (groove) recedes, the ions coming from the steel have to ionise and transport through the bulk lattice of the existing oxide, slowing down the diffusion rate. At this moment, and as shown in Figure 6.38 the lower concentration of iron ions reaching the surface will cause the transformation of Fe_xO to Fe_3O_4, or Fe_3O_4 to Fe_2O_3 and a stable layer of oxide will grow on top of the former.

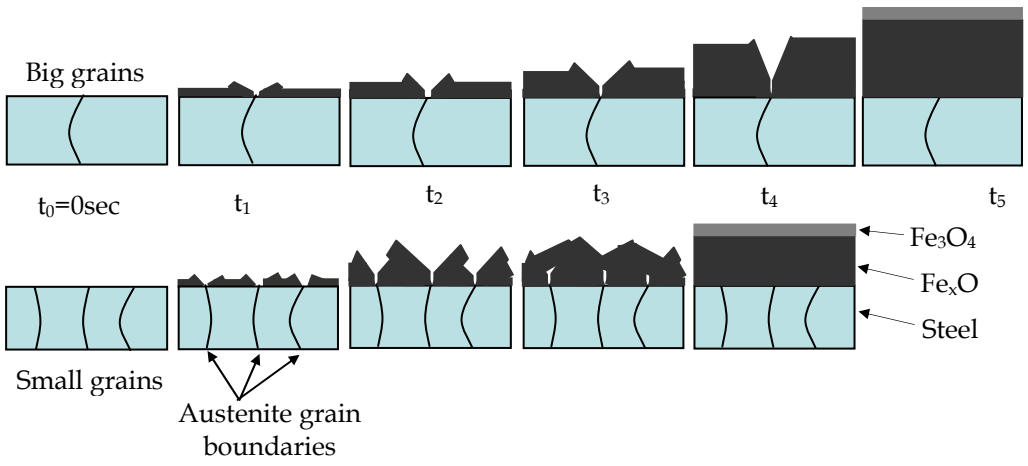

Figure 6.38. Schematic illustration of the process of diffusion and the influence of grain size on the formation of the next oxide layer.

The finding that the thickness of the oxide layer after certain time depends on the number of grain boundaries present in the steel is taken into account in the equation for diffusion proposed by Hart (1957). He expressed the diffusion of species as the weighted sum of the diffusion coefficients for lattice (D_L) and boundary diffusion (D_B) (see Eq. 2.5). According to our results, the fraction of grain boundaries (f) is not related to the grain boundaries of the oxide but to that of the steel. The effective fraction of grain boundaries on the short circuit diffusion is temporal and equals zero after certain time of oxidation (apparently t_{F3} when using method 2 of air insertion). However, in order to predict the real instant that the short-circuit paths of diffusion close due to oxide growth, an atomistic simulation will be required.

Besides a contribution to the fundamental understanding of oxide formation during the early stages of oxidation; the experimental findings detailed in this chapter are relevant to the role tertiary strip scale may play with respect to roll-wear during finishing rolling. In the next chapter consideration is given to the possible effects the nature and behaviour of the oxide could have on the integrity of the tertiary scale, and hence, on uneven roll-wear in the finishing-mill.

Chapter 7
General Discussion

We assessed the possibility that an uneven grain size distribution or crystallographic texture could contribute to the occurrence of ridge-buckle in the cold-rolled strip, but found little evidence of this possibility. Using recrystallization models to predict the austenite grain size in the course of hot-rolling and the ferrite grain size following cooling on the run-out table, we concluded that there is little possibility that measured temperature variations along the width of the strip during rolling can produce a significant change on the final grain size of the strip, notwithstanding the fact that the grain size changes significantly during rolling.

Strong experimental evidence was found that the occurrence of ridges on the hot-rolled strip is related, in the majority of the cases, to uneven wear of the finishing-mill work rolls. Our analysis has also shown that ridges in hot-rolled strips are more likely to form after a certain number of strips have been rolled in a given schedule. The implication of this important finding is that the thermal conditions of the work-rolls have a determining influence on the occurrence of uneven roll-wear.

It is pertinent to mention that in a separate but parallel study, attempts are being made to establish quantitatively, the relationship between ridge, occurring in hot-rolled strip and the occurrence of ridge-buckle defect. Our colleagues at the University of Wollongong, Prof Kiet Tieu and Dr Hongtao Zhu (Zhu *et al*, 2006) have designed a three-dimensional finite element model study by which they have demonstrated that ridge-buckle defect could originate from ridges present in the hot-rolled strip. The excess of material accumulated on the ridge zone will elongate more than the surrounding material in the strip due to the combination of axial compression and longitudinal tension simultaneously applied on the strip during temper rolling. That excess elongation is also influenced by the number of loops in the coil because of the tensile stresses developed during coiling. These relevant findings emphasise the importance of understanding the origin of ridges in hot-rolled strip in order eliminate, or at the very least reduce the incidence of the undesirable ridge-buckle defect.

Our literature analysis on the mechanisms of roll-wear indicated that the nature and integrity of the scale formed during finishing rolling could be playing a role in the uneven wear observed on the work-rolls and further experiments were conducted to elucidate the nature of the oxide formed on strips of two different steels during finishing rolling.

In terms of the oxidation studies, the most relevant findings from the industrial point of view are those that can affect the integrity and nature of the scale and therefore influencing the heat transfer to the work-rolls and the friction during contact between strip and roll in the roll-bite. Of specific interest, and importance, are the significantly slower oxide growth rate of steel containing silicon; the nature of the oxide/metal interface; the occurrence of internal oxidation; the conditions leading to spalling of the oxide and the finding that the type of oxide in contact with the work-rolls in the roll-bite might be a function of the grain size of the steel. In this chapter, an analysis is made of the implications of each of these findings in the behaviour of the scale during rolling and the possible influence on uneven roll wear. These analyses are followed by a discussion on the input that variations in the industrial practice have as indirect factors originating uneven roll-wear.

7.1 Growth rate of oxide

The growth rate of oxide on the steel strip will influence the effective thickness of the scale on the strip entering each roll-bite. We have found that the scale formed on low-carbon steel is six times thicker than the equivalent scale formed on silicon steels after 30 seconds of oxidation. This means that regardless of the extent of compaction the scale can undergo in each roll-bite, the scale formed on silicon steels will be comparatively thinner.

Scale thickness influences inversely the heat-transfer to the roll surface (See Eq. 2.11). Therefore, the surface temperature of the rolls when in contact with a silicon steel strip will be higher than when rolling low-carbon steel. In practical terms, this means that the roll surface will wear much faster, as the upper temperature of the thermal cycle will be higher than normal (as it was demonstrated by Lee *et al*, 1997[b]). An increase in wear occurs because the density of micro-cracks in the surface is augmented and the material on the roll surface can be easily detached. The low rate of growth of oxide on the silicon steel could, at least in part, contribute to the high rate of formation of ridges in this type of steel during finishing rolling. The rolls are likely to deteriorate much faster as the heat transfer rate from the

strip to the work-rolls is much higher than when a thick oxide layers covers the strip. Therefore, when a variation on the integrity of the scale in a certain area of the strip, for whatever reason, leads to uneven roll-wear and a groove develops on the roll surface, such a groove will grow much faster than when the strip was covered by thicker scale. Although this argument provides a plausible explanation for the faster growth of ridges in silicon steel, does not provide an explanation for the origins of a groove on the first place.

The possibility that fayalite might be in liquid phase during the re-heating operation of the silicon steel slabs will affect the nature of the oxidation. Should fayalite melt, the resulting scale will adhere very strongly to the steel strip, because the molten, or partially molten oxide is likely to penetrate the steel grain boundaries and it is extremely unlikely that this strongly adhering scale will be removed in the descaler (Fukagawa *et al*, 1994; Okada *et al* 1995 and Logani *et al*, 1969). Hence, there is a strong likelihood that pockets of fayalite that has not been removed by the descaler, may cause uneven oxidation on the steel surface and may indeed be an important contributing factor to uneven roll-wear.

7.2 Nature of the oxide interface

The nature of the oxide/metal interface plays a major role in the integrity of the scale while the strip is being rolled. Krzyzanowski *et al* (1999) demonstrated in convincing fashion, and Tang's (2006) analysis provided further evidence that a brittle or weak interface is likely to fail under the loads experienced in the roll-bite, causing separation of the scale from the substrate. Once the adhesion between the metal and oxide is compromised, further growth of the scale will occur at the oxide/gas interface and magnetite and hematite, instead of wustite will form because the source of iron ions from the steel substrate has been interrupted. In similar fashion to spalling, once the oxide separates from the iron source, the iron oxides that will continue forming are magnetite and hematite, both of which can be brittle even at the high temperatures of finishing rolling. These brittle oxides may fracture in the following roll-stand, with a consequent increase in the heat transfer rate to the roll.

We have observed a particularly thick interface layer forming in the silicon containing steels. TEM analysis of that interface showed incoherency and porosity, which may be regarded as a source of stress concentration leading to a greater propensity to fracture under load. Furthermore, even at the short times of oxidation

in the finishing mill, the presence of that interface layer affects the diffusion of iron species to the gas/oxide interface and the oxide consists mostly of the more brittle phases of magnetite and hematite.

In low carbon steels the interface between the oxide and the steel substrate is very thin and contain minor amounts of Si, Mn and P, most probably precipitating in the form of complex oxides. Kizu *et al* (2001) found that the presence of these complex oxides can, under certain temperature conditions, enhance spalling, a subject that will be discussed in more detail section 7.4.

The influence of the interface layer in the integrity of the oxides is different whether the steel is tinplate or silicon. While the brittle interface formed in silicon steels can fail under loads, the interface on low carbon steels might induce the separation of the scale from the substrate without any application of loads.

7.3 Internal oxidation and precipitates

Internal oxidation of the steel substrate and formation of precipitates have been observed in both types of steel studied. It seems evident that the main factors affecting the occurrence and concentration of internal oxide precipitation are the activity of the alloying elements, temperature and the prevailing oxygen partial pressure.

In low carbon steel, Al oxides and MnS precipitate preferably on the grain boundaries of the steel. These oxides or sulphides might impede the diffusion of species through the steel grain boundaries. We determined that grain boundary diffusion influences the rate of oxide formation in the early stages; therefore thickness of the oxide formed after certain time might be variable according to the amount of precipitates or oxides formed.

In silicon steels, internal precipitates of silica (SiO_2) were observed up to 3μm below the substrate surface. The conditions of reheating and rolling might have an influence on the concentration of internal precipitates and these precipitates will not be altered by the action of the descaler. Because it is known that a critical volume fraction of precipitates is required to onset the formation of the first SiO_2 layer on the surface of the metal, it can be presumed that when variation in the proportions of precipitates along the strip occurs, the uniformity of the oxide layers forming in the surface should be affected.

7.4 Oxide spalling

The oxide formed on the low carbon steel studied shows a tendency to separate from the substrate at temperatures around 900ºC. This spalling presumably occurs for either of, or a combination of these reasons: ternary oxides of Si-P precipitating at enough concentration in the metal/oxide interface to affect adhesion; a difference in diffusivity between austenite and ferrite grains, when the temperature of oxidation corresponds to two phase structure, will increase internal stresses in the oxide; or a change in volume due to a phase transformation occurring in the steel if oxidation is occurring around A_3 temperature, which can alter the adhesion between oxide and substrate. Therefore, when the conditions are met and the oxide on the strip separates from the substrate, the more brittle magnetite and hematite oxides will form at expense of the wustite and might fracture in following roll-bite. Although spalling would occur if the appropriate temperature and internal stress conditions are met, it is unlikely that the scale will separate from the substrate when it is under compression within the roll-bite. The reasoning is that the compression stress will alter the accumulated internal stresses responsible for spalling in the first place, and simply will contain the expansion of the oxides. Sufficient time should elapse between the moment spalling occurs and the entrance to the following roll in order for spalling be a factor influencing the fracture of the scale into the roll-bite

7.5 Dependence of oxide morphology on grain size of the steel

As shown by the experiments, the grain size of the steel affects the time required for a new iron-oxide, enriched in oxygen, to form on the surface of a pre-existing oxide. It may be argued that the grain size of austenite influences the type and morphology of the oxide formed and hence, the friction experienced in the roll-bite which, in turn, may affect roll-wear. This argument might be valid for the first stand in the finishing mill, where fresh tertiary oxide enters the roll-bite and if the grain size coming from the roughing-mill was different in a band of the strip, then the oxide entering F1 might be of variable morphology. However, once the strip and oxide are compressed in the first stand, regardless of the mechanism of recrystallization, new grains will form and grow with the consequent variability on the number of grain boundaries present. Therefore we can speculate that it is likely that once the first nuclei of new austenite grains form, the rate of oxide growth will increase, the possibility of obstructing the grain boundaries short-circuit paths will also increase and the new layers of higher oxides should form immediately after

exiting the first roll-bite. The morphology of the scale surface in contact with the following roll should not be very variable based solely on this relationship grain size – time to formation.

On the other hand, we demonstrated that the rate of oxide growth is affected by austenite grain size. Therefore, the total thickness of the oxide can vary if the grain size developed during rolling is variable. Due to that difference in rate of growth, accumulated internal stresses might occur and other effects like spalling and variable heat transfer to the roll might come to play a role in increasing the roll wear.

7.6 Possible origins of uneven roll-wear

We have stressed in the arguments above that an increase in the heat transfer rate from the strip to the roll or an increase in the friction between strip oxide and roll surface has to occur in order to produce uneven wear. Besides, and more importantly, the variation in heat transmission or friction should occur in a band or bands of the strip or roll to cause uneven roll-wear. In paragraphs below we are considering operational variables that might produce such variations in specific bands leading to uneven roll wear. Although the arguments are somewhat speculative, principally due to a lack of quantitative information and the complexity of hot-rolling mill operations, it is important to attempt to integrate the experimental findings described above with observations and evidence from the operating hot-strip mill.

7.6.1 Descaling

The descaler 2, located before the finishing mill, is composed by two rows of nozzles distributed along the width of the strip. Supposing that any nozzle on descaler 2 fails sporadically and does not clean completely the surface, leaving some oxide remains; those remaining oxides are likely to be located in a band along the length of the strip. Further oxidation over the pre-existing oxides will be slower than oxidation occurring on the freshly cleaned surface. Moreover, the remaining secondary scale should be more porous because it was formed at longer times than the tertiary scale. In the first roll-pass, the thick secondary scale might fracture easily under the high loads of the first set of rolls of the finishing-mill. Following fracture, there will be a band on the strip surface that is not oxidized and the scale in this band will grow faster than the rest. The accumulation of internal stress due to that uneven rate of growth is likely to assist spallation of the scale.

Once the scale spalls, and if enough time elapses between the separation from the substrate and the next roll-bite, the scale can fracture again under load and create new stresses that possibly lead to new spallation. This combination spalling/fracture might just be occurring in the first three or four rolls of the finishing mill as enough time is required for the more brittle type of iron oxides to grow on the surface after spallation. The fracture of the scale in the roll-bite, as debated before, will lead to an increase in the heat transfer to the roll with the concomitant excess wear in a determined band along the roll-axis.

A second issue in the operating hot-strip mill is that a failure occurring in the descaler will affect the surface temperature of the strip. In a case in where some nozzles of the descaler fail, bands on the surface will remain at higher temperature than the rest of the strip surface; therefore, even if the secondary scale is completely removed during descaling, a failure on the nozzles would cause different rates of growth in the scale and possibly lead to spallation.

7.6.2 Inter-stand cooling

Inter-stand coolers are a single row of nozzles that impinge water at low pressures onto the surface of the strip, on exit of the stands 1, 2, 3 and 4. Those coolers are used to control the exit temperature of the strip and are activated accordingly. As the effect of the inter-stand coolers is uniform on the surface of the strip, again a failure of the system could produce variations of temperature on the strip surface in bands. If that be the case, then it might be inducing differences in the rate of growth of the scale.

7.6.3 Other sources of surface cooling

Sources of concentrated cooling of the surface of the strip before entering the roll-bite can be sweepers, faulty top-roll scrappers and excessive cooling from the loopers.

The sweepers apply a flush of water on the surface of the strip, counter current of the strip movement just before entering the roll-bite. The purpose of the sweepers is to clean the surface from excess water remaining from the inter-stand coolers. The sweeper action has been traditionally discarded as a source of uneven temperature because the pressure of water applied is very low and the water is supposed to evaporate on contact with the strip surface. However, the pressure is high enough to displace the layer of water that remains on the surface of the hot strip. Therefore, we can speculate that the sweeper action, which is localised in the

central zone of the strip, might be causing localised cooling in the scale just before entering the roll. Variations in the water pressure of the sweepers together with a certain temperature of the strip might cause spalling, or direct fracture of the scale due to thermal shock.

Mascia et al (1998) described a modification they implement on their mill consisting of applying water along the width of the strip just before entering the roll bite. The effect of this change is a reduction on the total wear of the rolls and on the incidence of shape defects. In such a modification, as opposed to the use of sweepers, the water is applied uniformly along the width of the strip and exactly before entering the roll-bite. Cooling the scale just before entering the roll-bite will reduce the temperature of the scale and allow sufficient time to reduce the heat transfer rate to the roll and hence, effectively increase the life of the roll material. Mascia's study demonstrated that the position and uniformity of any source of cooling is relevant to the integrity of the strip scale.

Scrappers are used to contain the water applied onto the roll surface by the roll cooling nozzles in order to avoid contact of the water with the strip. They consist on a strip of soft material, located parallel to the roll-axis and just before the roll-bite entry, which is continuously pressed against the roll surface. Faulty scrappers have been reported as a direct cause of uneven roll-wear in the past by BlueScope plant operators. A defect on the scrapper material can let considerable amounts of roll-coolant water to sip through and enter into the roll bite. Faulty scrappers can lead to localised cooling on the strip and also the water sipping through can wash-out the applied lubricant. The lack of lubrication in a band of the roll will increase the friction and cause uneven wear on a band of that set of rolls. Besides, Sun et al (2004) have shown that lack of lubrication causes the scale to increase in roughness and therefore, the scale entering the next roll-bite might affect the new roll by excess friction.

Loopers are small rolls that make contact with the bottom of the strip and keep it at the right tension during rolling. The loopers have to be continuously cooled by water applied to the roll. Any variation in the normal cooling pattern of the loopers can result in uneven cooling leading to spallation of the scale at the bottom of the strip.

7.6.4 Furnace beams

The walking beams used to transport slabs into and through the re-heating furnace, can affect the formation of internal oxides and the segregation of certain elements to the surface. The beams are in contact with the bottom of the slab and can mask the temperature and the exposure of the slab surface to the furnace atmosphere. Rather than the usual thick and porous layer of primary scale (Sheasby *et al*, 1984), a thinner and homogeneous layer of oxide might form at those contact zones which are located parallel to the slab-width. The nature of the scale formed in the furnace depends on the residence time, temperature and the oxidation potential within the furnace and therefore, when the slab leaves the furnace, it is expected that the small temperature variations caused by beam contact be compensated quite quickly due to the large thermal mass of the slab. Nevertheless, the scale is already formed in different a fashion in these zones and although it might be argued that descaling will remove the primary scale and also equalise the differences in the nature of the scale formed, the penetration of the oxides will remain different in the bands coinciding with the furnace beams. The effect of the beams is still evident in the temperature profiles from the landscan temperature measurements, which are taken after the finishing mill; meaning after 7 or 9 roughing passes, coil-box, the action of two de-scalers and the six stands of the finishing-mill. These temperature differences, can however, not be directly linked to the occurrence of uneven roll-wear, which must be due to differences in the longitudinal direction.

This discussion on the origins of uneven wear indicates that a number of conditions need to be met before fracture of scale or a variation on friction can occur. This might explain the sporadic occurrence of ridges. The roll exposure to thermal loads should occur for an extended period so the accumulated effect of the thermal action on the surface renders it more susceptible to changes in temperature; the temperature on the low carbon strip should be below 900ºC to cause spalling, but also the scale formed should not be too thick; the accumulation of segregation elements should be on the right concentration and finally the time from spalling to the application of loads should be long enough to cause fracture in the roll-bite. In silicon steels, fracture might be occurring regularly in the roll-bite due to the nature of the oxides and interface, but again it depends on the temperature of the strip entering the bite and the proportion of iron oxides present to induce the brittle fracture under loads. In addition, variations in strip cooling conditions and/or lubrication are required for the incidence of roll-wear.

Chapter 8
Conclusions and recommendations

8.1 Conclusions

- An analysis of the literature led to two main possible causes of the occurrence of ridge-buckle defect: the hot rolled strip contains a shape defect called ridge; or there are variations in microstructure or crystallographic texture of the strip, leading to uneven deformation during cold rolling.

- No evidence was found of differences in grain size or crystallographic texture along the width of the hot rolled strips at room temperature, in the tinplate and silicon steels analysed. These findings ruled out the possibility that microstructural variations along the width of the strip are the primary origin of ridge-buckle defect formation during subsequent processing.

- Minor variations in temperature influence the development of austenite grain size in the course of hot rolling. It was demonstrated, by using recrystallization models, that the main factor affecting the austenite grain size during rolling, is the type of recrystallization occurring. In the last stands of the finishing mill the strip is likely to undergo static recrystallization, while in the first stands either static or dynamic recrystallization can occur when temperature is varied under constant conditions of strain and strain rate. Austenite grain sizes developed in the steel after static recrystallization and grain growth are larger than those developed when the steel undergoes dynamic recrystallization.

- Calculations, using recrystallization models, confirmed that the ferrite grain size developed after rolling, is essentially independent of temperature when temperature variations of the order of 200ºC are imposed on the steel strip entering the finishing mill.

- The strength of the steel while it is hot rolled is slightly influenced by minor temperature changes along the strip width, experimentally detected at the exit of the finishing mill. This variation in strength due to the temperature changes was too small to be a factor affecting the deformability of the hot steel. Similarly, after rolling and at room temperature, the difference in grain size developed when minor temperature changes affected the strip during hot rolling,

is too small to produce a significant change in the strength of the strip and hence, deformation during cold rolling will not be effected by these small temperature variations.

- Data collected during production of hot-rolled strip indicate that in the majority of the cases when ridges are formed on the strip profile, the rolls in the finishing mill presented uneven wear. Ridges occur more frequently when more than 65 strips have been rolled in the same schedule, indicating that the accumulation of internal stresses on the surface of the roll due to thermal fatigue is a factor influencing the onset of uneven roll-wear.

- A technique was developed to observe in-situ, oxide formation on steel strip. It was possible to simulate oxidation under conditions resembling finishing mill operating conditions. To the author's knowledge, the sequence of oxidation events observed by using this technique has not been reported before.

- Oxidation studies in the first few seconds of exposure of hot steel to air show distinctive behaviour depending on the composition of the steel. Silicon steels contain minor amounts of Al, Si and Mn and these elements oxidise preferentially and before iron oxides are formed on the surface of the steel. The first oxide nucleus consists of an interface layer of complex oxides and possibly inter-metallics of Fe, Mn, Si and Al. This nucleus grows radially followed by the formation of a layer of magnetite and/or a layer of hematite at the nucleus/gas interface. The non-coherent interface layer comprises approximately a quarter of the total thickness of the oxide layer formed and it is consists of spherical precipitates that appear to be brittle in nature.

- Oxides formed in low carbon steels which contain only minor amounts of Mn, consist of wüstite, magnetite and hematite layers. The proportion of the iron oxide types on the layer is almost constant unless the adhesion of oxides to the substrate is compromised. When the oxide separates from the steel substrate, the scale contains higher proportions of magnetite and hematite.

- The main factor affecting the adherence of the scale to the substrate in low carbon steels is the temperature at which oxidation occurs. We found that separation of scale from the substrate is more likely to occur at temperatures in the two-phase field, austenite plus ferrite. The phase transformation from austenite to ferrite occurring at the Ar_3 temperature can be playing a role on the

detachment of scale form the substrate, due to the volume change experienced during transformation. The presence of two types of iron structures (bcc and fcc) with different iron diffusion coefficients could be influencing the rate of formation of the oxides and thus affecting the internal stresses, leading to spallation.

- During the oxidation of low carbon steels, it is possible to observe that three different oxides can nucleate and grow. The first oxide forms on the surface of the steel substrate, while the following oxides form on top of the former ones. However, the nature of the oxides could not be uniquely identified, therefore seems to be two possible explanations for the observed events:
  1) The first oxide that forms is wüstite. Then magnetite nucleates and sweeps over the surface of the wüstite. However, the newly formed oxide is promptly reduced back to wüstite. After certain time of oxidation, a 3rd nucleation and growth event occurs and this last oxide formed is a stable magnetite.
  2) The first oxide formed is wüstite, the 2nd oxidation corresponds to the nucleation and growth of magnetite; and hematite is the oxide sweeping over the surface during the 3rd oxide formation.

- Austenite grain size is influencing the time taken for the 3rd oxide to develop. It is highly probable that the time taken for the 2nd oxide to form is also a function of the austenite grain size but the time to transformation is so short in this case that it could not be accurately measured. We suggested that the presence of grain boundaries increase the diffusion of iron to the surface, essentially acting as short circuit paths. The formation of oxides will be much faster while these paths remain open; however if oxides were to obstruct the shot-circuit diffusion paths, the formation of an iron oxide more deficient in iron, will be induced. Therefore, as larger is the amount of grain boundaries present, faster will be the formation of the 3rd oxide.

- The total oxide layer formed on silicon steel substrates is six times thinner than the oxide layer formed on low carbon steel under the same oxidation conditions. In practical terms, the heat transmission to the roll surface will be much higher when silicon steels are rolled compared to low carbon steels.

- The integrity of the scale could be affected by an external factor impinging variations on a band of the strip in order to modify the heat transmission or friction to the roll and hence, produce uneven roll-wear. An analysis of the mill conditions that can onset that behaviour lead to a series of possible causes:

failure in one or more of the descaler nozzles; failure in one or more nozzles on other sources of cooling such as inter-stand, roll-cooling and loopers cooling; failure on the lubrication system of the roll-bite and/or a defect on the scrapper.

- In summary we found that the ridge-buckle defect is linked mainly to the occurrence of ridge in the hot rolled strip and not to differences in the microstructure or crystallographic texture. Ridge occurs because the strip copies the uneven wear shape of the finishing-mill work-rolls. Uneven wear on rolls originates when changes in mill conditions affect the integrity of the scale during rolling.

8.2 Recommendations for future work

- The experimental technique that was developed in this work proved to be very effective. The *in-situ* observation of initial oxide nucleation and growth is a most powerful technique and it is strongly recommended that this type of observations be extended to the study of the oxidation behaviour of other steel compositions.

- A significant contribution to understand the oxidation occurring in plant conditions will be the simulation of oxidation under humid air.

- Thermodynamic and kinetics modelling should be pursued to develop a predictive model that can be used to predict *a priory* the most likely oxides to form under specified conditions. The *in-situ* oxidation experiments and subsequent analysis of the oxides can be used to validate the models.

- In order to determine the nature of the oxides forming on low carbon steel substrates, it is recommended that high temperature X-ray diffraction experiments be conducted under similar conditions used in the experimental part of this thesis.

- In-depth plant studies which include the effect of modifying parameters and practices on the finishing mill, such as side-shifting of the rolls or descaling pressure, are recommended in order to integrate the results of theory with practice.

References

Adachi T and G H Meier. 1987. “Oxidation of iron-silicon alloys” Oxidation of metals. 27(5/6): 347-366

Atkinson A. 1982. “A theoretical analysis of the oxidation of Fe-Si alloys” Corrosion science 22(2): 87-102.

Bahgat M., Y. Sasaki, S. Hijino, M. Iguchi, K Ishii, 2004."The effect of grain boundaries on iron nucleation during wustite reduction process". *ISIJ International.* 44 (12):2023-2028.

Ballufi R. W., S. M. Allen and W. C. Carter. 2005. "Kinetics of materials". *Wiley-Interscience*, USA.

Basabe V V and J A Szpunar. 2004. “Growth rate and phase composition of oxide scales during hot rolling of low carbon steel” *ISIJ Intern*. 44(9): 1554-1559

Baud J, A Ferrier, L Manec and J Benard. 1975. “The oxidation and decarburising of Fe-C alloys in air and the influence of relative humidity” *Oxidation of metals*, 9(1): 69-97

Bernard J and O Coquelle. 1946. “Nouvelle recherches sur l’oxydation du fer aux températures élevées par la méthode micrographique”, *Compte Rendus* 222: 796.

Birks N. and G. H. Meier. 1983. "Introduction to high temperature oxidation of metals". *Ed.,* Edward Arnold, London.

Blazevic D. 2002. “Build up or ridges” Hot Strip mill operations Volume IV. Hot rolling Consultants.

Blazevic D T. 1987. “Rolled-in scale – the consistent problem”. *Proceedings 4th International steel rolling conference, Deauville, France* : A38.1-A38.13.

Boelen R, P F Thomson and A Brownrigg. 2002. “Controlled oxidation rolling”. *International conference on thermomechanical processing: mechanics, microstructure and control*, 23-26 June 2002, Sheffield, UK. : 94-102

Bolt P H. 2000. “The properties of oxide scales on hot rolled steels: a literature review”. *Published into the 2004 ECSC Research project 7210.PR/153.* " Investigation of the formation, constitution and properties of scale formed during the finishing, rolling, cooling and coiling of thin hot strips" by Friedel F., H. Bolt, X. Cornet, G. Bourdon, X. Vanden, E. Zeimetz, S. Ehlers and F. Steinert.

Bolt P. H. 2004. “Understanding the properties of oxide scales on hot rolled steel strip”. *Steel research international.* 75 (6): 399-404.

Bunge H J, H R Wenk and J Pannetier. 1982. “Neutron diffraction texture analysis using a position sensitive detector” *Textures microstructure*, 5: 153-170.

Cabrera N and N F Mott. 1948-1949. Report progress in Physics, 163 (12).

Callister W. D. 2003. “Materials science and engineering – an introduction”. *John Wiley & Sons, Inc*. USA.

Carter C. 2002. “Ridge investigation – Technical note”. *BHP Mill operations Integrated Steel Division Port Kembla Steelworks*

Chao H. 1967. “The mechanism of ridging in ferritic stainless steel” *Transactions of the ASM*. 60 :37-50.

Chen R Y and W Y D Yuen. 2002. “Oxidation of low-carbon, low-silicon mild steel at 450-900ºC under conditions relevant to hot-strip processing”. *Oxidation of metals*. 57(1/2): 53-79.

Chen R Y and W Y D Yuen. 2003. “Review of the high-temperature oxidation of iron and carbon steels in air or oxygen. *Oxidation of metals*. 59(5/6): 433-468.

Christoph G R and J F Griffin. 1959. “Influence of hot strip profile on subsequent operations”. Flat rolled products: rolling and treatment. *Interscience publishers*, Vol 1.

Colás R. 1996. “A model for the hot deformation of low-carbon steel”. *Journal of Mat. Processing Tech*. 62: 180-184.

Colás R. 1998. “Mathematical modelling of hot rolling steel strip” *Mat Sc. Tech*. 14(5): 388-393

Das S, E J Palmiere and I C Howard. 2004. “The cut-groove technique to infer interfacial effects during hot rolling” Met and Mat transactions A. 35A (3): 1087-1095.

Devadas C and I V Samarasekera. 1986. “Heat transfer during hot rolling of steel strip” *Ironmaking and steelmaking*. 13(6): 311-321

Devadas C, I V Samarasekera and E B Hawbolt. 1991a. “The thermal and metallurgical state of steel strip during hot rolling: Part I. Characterization of heat transfer” *Metal. Trans* A. 22A(2): 307-319.

Devadas C, I V Samarasekera and E B Hawbolt. 1991b. “The thermal and metallurgical state of steel strip during hot rolling: Part II. Factors influencing rolling loads” *Metal. Trans A*. 22A(2): 321-333.

Devadas C, I V Samarasekera and E B Hawbolt. 1991c. “The thermal and metallurgical state of steel strip during hot rolling: Part III. Microstructural evolution” *Metal. Trans A*. 22A(2): 335-349.

Dingley D J and Randle V. 1992. “Review: Microtexture determination by electron back-scatter diffraction”. *Journal of Materials Science*. 27: 4545-4566

Echsler H, S Ito and M Schutze. 2003. “Mechanical properties of oxide scales on mild steel at 800 to 1000ºC”. *Oxidation of metals*. 60(3/4): 241-269

Erhart H., R. Wang and R. A. Rapp. 1983."In Situ SEM study of the high-temperature oxidation of an Fe-Mn-Al-Si alloy". *Oxidation of metals.* 21 (1/2):81-88.

Fehlner F P and N F Mott. 1970. "Oxidation in the thin-film range". *Oxidation of metals and alloys. American Society for Metals*, Ohio, Ch.3: 37-62.

Friedel F., H. Bolt, X. Cornet, G. Bourdon, X. Vanden, E. Zeimetz, S. Ehlers and F. Steinert. 2004." Investigation of the formation, constitution and properties of scale formed during the finishing, rolling, cooling and coiling of thin hot strips". *ECSC Research project 7210.PR/153.*

Fukagawa T, H Okada and Y Maehara. 1994. "Mechanism of red scale defect formation in Si-added hot-rolled steel sheets. ISIJ Intern. 34(11): 906-911.

Garnaud G. and R. A. Rapp. 1977."Thickness of the oxide layers formed during the oxidation of iron". *Oxidation of metals.* 11 (4): 193-198.

Gibbs G. B. and J. E. Harris. 1969. "Diffusion at solid-solid interfaces". *Interfaces conference, Melbourne, Edit. R. C. Gifkins*; Butterworks: 53-76.

Gilbertson W F. 1965. "Hot rolled strip abnormalities leading to ridge in cold reduced sheets and tinplate". *Journal of the Iron and Steel Institute*. (6): 553-561

Griffits R. 1934. *J. Iron and Steel Inst*. 130: 377-388

Guthrie R I L. and J J Jonas. 1990. "Steel processing technology". *Metals Handbook*, 10th edn. *ASM*, Materials Park, OH, US. 1: 107-125

Guy A G. 1960. "Elements of physical metallurgy". Addison-Wesley, USA.

Hall E. O. 1951. *Proceedings physics society*. B64: 747

Hanlon D N, J Sietsma and S van der Zwaag. 2001. "The effect of plastic deformation of Austenite on the kinetics of subsequent ferrite formation" *ISIJ International*. 41(9): 1028-1036.

Hart E W. 1957. Acta Metallurgica 5: 597.

Hidaka Y, T Anraku and N Otsuka. 2002. "Tensile deformation of iron oxides at 600-1250ºC. Oxidation of metals. 58 (5/6): 469-485

Hodgson P D and R K Gibbs. 1992. "A mathematical model to predict the mechanical properties of hot rolled C-Mn and microalloyed steels". *ISIJ International* 32(12): 1329-1338.

Horsky J and M Raudensky. 1996. "Mathematical modelling and experimental study of heat transfer on roll cooled by water nozzles". Institute of Materials UK. 288-298.

Humphreys F J. 1999. "A new analysis of recovery, recrystallisation and grain growth". Materials science and technology. 15(1): 37-44.

Humphreys FJ and Hatherly M. 1996. "Recrystallization and related annealing phenomena" *Pergamon press UK*

Jonas J J. 1997. “Dynamic recrystallisation in strip mills-industrial fact or metallurgical fiction?. *Thermec’97 Edited by T. Chandra and T Sakai. TMS*. 1: 31-45.

Jonas J J. 2001. “The hot strip mill as an experimental tool”. *Ironmaking and Steelmaking*. 28(2): 133-137.

Jungling T. L. and R. A. Rapp. 1984."High temperature oxidation of iron at 1200C in a hot-stage environmental scanning electron microscope". *Metallurgical transactions A.* 15A (12): 231-2240.

Kato O, H Yamamoto, M Ataka and K Nakajima. 1992. “Mechanisms of surface deterioration of roll for hot strip rolling”. *ISIJ International*. 32(11): 1216-1220.

Katrakova D and F Mucklich. 2001. “Specimen preparation for electron backscatter diffraction – Part 1: Metals”. *Prakt. Metallogr*. 38 (10): 547-565.

Key-to-steel webpage. Silicon Steels and Their Applications. http://www.key-to-steel.com/ViewArticle.asp?ID=101. 8 Dec 2005.

Kiessling R. 1997. “Non-metallic inclusions in steel”. Part IV. *The institute of Materials*. London.

Kizu T, Y Hagataki, T Inazumi and Y Hosoya. 2002. “Intergranular and internal oxidation during hot-rolling process in ultra-low carbon steel” *ISIJ Intern*. 42(2): 206-214.

Kolchenko GI and N P Kuznetsova. 1984. Izy. VUZ Chernaja Metall. 11113-125.

Krzyzanowski M and J H Beynon. 1999. “The tensile failure of mild steel oxides under hot rolling conditions” *Steel research* 70(1): 22-27.

Krzyzanowski M and J H Beynon. 2002. “Measurement of oxide properties for numerical evaluation of their failure under hot rolling conditions” *Journal of materials processing technology* 125-126: 398-404.

Kubaschewski O. and B. E. Hopkins. 1962. "Oxidation of metals and alloys". *2nd Ed.,* Butterworths, London.

Laasraoui A and J J Jonas. 1991. “Prediction of temperature distribution, flow stress and microstructure during the multipass hot rolling of steel plate and strip”. *ISIJ Intern*. 31(1): 95-105.

Leduc L A. 1980. *PhD thesis.* University of Sheffield, UK.

Lee D. B. and J. W.Choi. 2005."High temperature oxidation of steels in air and CO_2-O_2 atmosphere". *Oxidation of metals.* 64 (5/6): 319-329.

Lee J H, J C Oh, J W Park, H C Lee and S Lee. 2001. “Effects or tempering temperature on wear resistance and surface roughness of a high speed steel roll” *ISIJ Intern*. 41(8): 859-865.

Lee M. and R. A. Rapp. 1988."Development of scale morphology during wustite growth on iron at high temperature". *Oxidation of metals.* 30 (1/2): 125-138.

Lee S, D H Kim, J H Ryu and K Shin. 1997[b]. “Correlation of microstructure and thermal fatigue property of three work rolls”. *Met and Mat Trans. A*. 28A(12): 2595-2608.

Lee S, K-S Sohn, C G Lee and B I Jung. 1997[a]. “Correlation of microstructure and fracture toughness in three high-speed steel rolls”. *Met and Mat Trans. A*. 28A(1): 123-134

Li Y H and C M Sellars. 2001. “Behaviour of surface oxide scale before roll bite in hot rolling of steel”. Materials science and technology. 18(3): 304-311.

Logani RC and W W Smeltzer. 1969. “Kinetics of wüstite-fayalite scale formation on iron-silicon alloys” Oxidation of metals 1(1):3-21

Logani RC and W W Smeltzer. 1971[a]. “The development of the wüstite-fayalite scale on an iron-1.5% silicon alloy at 1000ºC” Oxidation of metals 3(1):15-32

Logani RC and W W Smeltzer. 1971[b]. “Principles of metal oxidation” Canadian metallurgical quarterly. 10(3): 149-163

Lu C, A K Tieu, Z Jiang. 2002. “A design of a third-order CVC roll profile”. *Journal of materials processing technology*. 125-126 : 645-648

Lundberg S-E. 1997.”Evaluation of roll surface temperature and heat transfer in the roll gap by temperature measurements in the rolls”. *Scand. J. of Metall*. 26(1):20-26

Maccagno TM, J J Jonas, S Yue, B J McCrady, R Slobodian and D Deeks. 1994. “Determination of recrystallization stop temperature from rolling mill logs and comparison with laboratory simulation results” ISIJ Intern 34(11): 917-922.

Manohar P A, M Ferry and T Chandra. 2001. “Recrystallisation of ferrite and Austenite” Encyclopaedia of Materials: Science and Technology, Elsevier Science, UK 4:3019-3024

Marston H F, PH Bolt, G Leprince, M Roder, R Klima, J Niska and M Jarl. 2004. “Challenges in the modelling of scale formation and decarburisation of high carbon, special and general steels” *Ironmaking and steelmaking*. 31(1): 57-65.

Mascia J C, O C Marini, E Ubici. 1998. “Reduction of work roll wear by controlling tertiary scale growth” *Iron and steel engineering*. (6): 48-51.

Matsuno F. 1980.”Blistering and hydraulic removal of scale films of rimmed steel at high temperature” Transactions ISIJ. 20: 413-421.

Misaka Y and T Yoshimoto. 1967. *Journal of Japan society technology of plasticity*. 8:414

Morrison W B. 1966. “The effect of grain size on the stress-strain relationship in low-carbon steel” ASM Trans quart. 59(4): 824-846.

Muojekwu C A, D Q Jin, I V Samarasekera and J K Brimacombe. 1997. “Thermomechanical history of steel strip during hot rolling – A comparison of conventional cold-charge rolling and hot-direct rolling of thin slabs”. *TMS-ISS J K Brimacombe –Reflections and perspectives. Samarasekera I and Henein H editors*.

Nohara K and K Hirano. 1977. “Self-diffusion of Fe in Fe-Mn alloys.Chern. Metall. (2):110-113.

Norton J. F., S. Canetoli and P. Pex. 1993. "The use of a hot-stage microscope in high-temperature corrosion studies". *Proceedings of the second international conference on microscopy of oxidation,* University of Cambridge, 29-31 March 1993.*Edit. S. Newcomb and Bennett M. J.*; The institute of materials, 23-35.

Oh J M, M J McNallan and W E King. 1986. “Microstructural development in the surface region during oxidation of iron-manganese-nickel-silicon alloys” J. Electrochemical society. 133(5): 1042-1048.

Ohata T, Zuccarelli J P, Sorano H and Noda A. 2002. “New grade CPC roll and a centrifugal cast HSS roll with CPC outer shell chemistries”. *44th MWSP Conference proceedings*. Vol XL. pg 92

Okada H, T Fukagawa, H Ishihsra, A Okamoto, M Azuma and Y Matsuda. 1995. “Prevention of red scale formation during hot rolling of steels” ISIJ International. 35(7): 886-891.

Park H D, I J Kim, J J Yi and J K Kim. 1994. “Effect of the hot-coil profile on the flatness and profile of cold-rolled strip”. *Journal of Materials Processing Technology*. 41 : 349-360.

Park S, K Y Kim, Y D Lee and C G Park. 2002. “Evolution of microstructure and texture associated with ridging in ferritic stainless steel”. *ISIJ Inter*. 42 (1): 100-105.

Pelton A and C Bale. 2000. “Thermodynamics”. *Direct reduced iron.* Ed. Jerome Feinman and Donald MacRae. *ISS Society*.

Perez A., R. L. Corral, R Fuentes, R. Colas, 2004. “Computer simulation of the thermal behaviour of a work roll during hot rolling of steel strip”. *Journal of Materials Processing Technology.* 153/154:894-899.

Petch N. J. 1953. *Journal of the Iron and Steel Institute*. 174: 25

Phelan D. J., M. H. Reid and R. J. Dippenaar. 2005."Experimental and modelling studies into high temperature phase transformations". *Computational Materials Science.* 34: 282-289.

Rabinowicz, E. 1965. “Friction and wear of materials”. John Wiley & Sons, USA.

Rapp R. A. 1984."The high temperature oxidation of metals forming cation-diffusing scales". *Metallurgical transactions A.* 15A (5): 765-782.

Raudensky M Horsky J and Pohanka M. 2002. “Optimal cooling of rolls in hot rolling” Journal of Material Processing Technology. 125-126: 700-705.

Ray R K, J J Jonas, M P Butron-Guillen, J Savoie. 1994 “Transformation textures in steels” *ISIJ International* 34(12): 927-942.

Riesz C H. 1970. “Friction, lubrication and wear mechanisms”. Metal deformation processes: friction and lubrication, Edit: John A. Schey. *Marcel Dekker, Inc* USA. Ch3: 102.

Roberts W L. 1983. “Hot rolling of steel”. *Marcel Dekker, Inc*. USA

Rocquet P, G Jegaden and J Voinchet. 1965. “Study of the origin of ridges occurring during cold rolling” *Mechanical working of steel*. Pt. 2 AIME metallurgical society conferences. 26: 401-418

Saboonchi A and M Abbaspour. 2004. “Changing the geometry of water spray on milling work roll and its effect on work roll temperature”. Journal of Materials Processing Technology. 148: 35-49.

Sakai T and J J Jonas. 1984. “Dynamic recrystallisation: Mechanical and microstructural considerations”. *Acta Metall*. 32(2): 189-209.

Samarasekera I V, D Q Jin and J K Brimacombe. 1997. “The application of microstructural engineering to the hot rolling of steel”. *TMS-ISS J K Brimacombe –Reflections and perspectives. Samarasekera I and Henein H editors*.

Sano Y, T Hattori and M Haga. 1992. “Characteristics of high-carbon high speed steel rolls for hot strip mill” . *ISIJ International*. 32(11): 1194-1201.

Schmid B., N. Aas, O. Grong and R. Odegard. 2002."High-temperature oxidation of iron and the decay of wustite studied with in situ ESEM". *Oxidation of metals.* 57 (1/2): 115-130.

Sellars C M . 1980. “ The physical metallurgy of hot working”. Proceedings of the international conference on hot working and forming processes. Sellars CM and G J Davies editors. The Metals Society London. Pg 3-15

Sellars C M and J A Whiteman. 1979. “Recrystallisation and grain growth in hot rolling”. *Metal Science* March-April: 187-194.

Senk D, S Sridhar, M Safi, N J McDonald and M Krings. 2004.”Oxidation and characterization of As-cast TRIP steel surfaces” Steel research Int 75(10): 680-685.

Sheasby J. S., W. E. Boggs and E. T. Turkdogan. 1984."Scale growth on steels at 1200^{o}C: rationale of rate and morphology". *Metal Science.* 18 (3): 127-136.

Siciliano F and J Jonas. 2000. “Mathematical modelling of the hot strip rolling of microalloyed Nb, multiply-alloyed Cr-Mo, and plain C-Mn steels”. Metallurgical and Materials Trans A. 31A(2): 511-530

Siebert C A. 1939. *Transaction Amer Soc Met*. 27: 752-757.

Sims R B. 1954. *Proceedings Institute Mechanical Engineers*. 168: 191

Stevens PG, K P Ivens and P Harper. 1971. “Increasing work-roll life by improved roll-cooling practice” *Journal of the Iron and Steel Institute*. (1): 1-11

Stumpf W. 2003. “Grain size modelling of a low carbon strip steel during hot rolling in a compact strip production (CSP) plant using the hot charge route” *The Journal of the South African Institute of mining and metallurgy*. (12): 617-631

Sun W, A K Tieu, Z Jiang and C Lu. 2004[a]. “High temperature oxide scale characteristics of low carbon steel in hot rolling” Journal of Materials Processing Technology. Vol. 155-156, pp. 1307-1312. 30 Nov. 2004

Sun W, A K Tieu, Z Jiang, H Zhu and C Lu. 2004[b]. “Oxide scales growth of low-carbon steel at high temperatures” *Journal of Materials Processing Technology*. Vol. 155-156, pp. 1300-1306.

Sun W, A K Tieu, Z Jiang and H Zhu. 2004[c]. “Effect of hot rolling conditions on deformation behaviour of oxide scale at high temperatures” *Key Engineering Materials* 274-276: 511-516.

Sun W, A K Tieu, Z Jiang, C Lu and B de Jong. 2003. “Morphology of mild steel oxide scale” *EMAC 2003 proceedings*: 277-281.

Sun W. 2005. “A study on the characteristics of oxide scale in hot rolling of steel” *PhD Thesis University of Wollongong*.

Takechi H, H Kato, T Sunami and T Nakayama. 1967. “The mechanism of ridging formation in 17%-chromium stainless steel sheets. *Trans JIM* (8): 233-239

Takeda M, T Ohnishi and Y Mukai. 2003. “Influence of silicon content on the structure and adhesion of the primary scales on Si containing steels” *Current advances in materials and processes-ISIJ meeting*. 16(6): 1360-1363

Tamura I, C Ouchi, T Tanaka and H Sekine. 1988. “Thermomechanical processing of high strength low alloy steels”. *Butterworths.* Ch. 9.

Tan K, M Krzyzanowski and J H Beynon. 2001. “Effect of steel composition on failure of oxide scales in tension under hot rolling conditions” *Steel Research* 72(7): 250-258.

Tang J. 2006."A study of oxide scale deformation and surface roughness transformation in hot strip rolling". *PhD thesis University of Wollongong*, Australia.

Thorning C. and S. Sridhar. 2005. "Oxide scale formation on TRIP steel surfaces". *Proceedings of the AISTech'05, Charlotte, NC, USA*; Association for Iron and Steel Technology, 2: 415-424.

Tseng A A, Chang J G, Raudensky M and Horsky J. 1995. “An inverse finite element evaluation of roll cooling in hot rolling of steels” Journal of Materials Process & Manufacturing Science. 3 (4): 387-408.

Van Leeuwen Y, J Sieltsma and S van der Zwaag. 2003. “The influence of carbon diffusion on the character of the g-a phase transformation in steel” ISIJ International. 43(5): 767-773.

Van Leeuwen Y. 2000. “Moving interfaces in low-carbon steel: A phase transformation model” *Research thesis Technical University of Delft*, The Nederlands.

Vander G F.1986. “Applied metallography” *Van Nostrand Reinhold*. New York

Wagner C. 1933."Beitrag zur theorie des anlaufvorgangs". *Z. Physik. Chem.* 21: 25-41.

Williams R V and G M Boxall. 1965. “Roll surface deterioration in hot strip mills” *Journal of the Iron and Steel Institute*. (4): 369-377

Yuen W Y D. 1994. “The thermal boundary layer in a rotating cylinder subject to prescribed surface heat fluxes” *Int. J. Heat Mass Transfer*. 37(4): 605-618.

Zaluzec N J. 1979. “Quantitative X-ray microanalysis: instrumental considerations and applications to materials science”. *Introduction to analytical microscopy Ed. JJ Hren, J I Goldstein and D C Joy*. Plenum press, pp. 149-167

Zambrano P C, Delgado A L, Guerrero-Mata M P, Colás R and Leduc L A. 2003. “Hot rolling of light gauge steel strip”. *ISIJ Intern*. 43 (7): 1030-1035

Zener C and J H Hollomon. 1944. “Efect of strain rate upon plastic flow of steel*”. J. Appl. Phys*. 15: 22-32.

Zhu H and A K Tieu. 2006. Private communication on study of ridge-buckle defect, part of the ARC linkage grant # LP 0348927 to the University of Wollongong.

Appendix A

Program for the fitting of a parabola to real values of strip thickness

From -350 to +350mm of the width in a given strip, sections of 50mm were selected and the median values of the sections grouped in column x in Table A.1. The square values of that width position are calculated in column x^2. Minimum values of strip thickness corresponding to each section are determined in Yn column, and its standard deviation in STD column. The half of the minimum standard deviation from all of the calculated thickness values is added to the Yn values. Finally the trend or parabolic regression fit is calculated between x, x2 and Yn +STD/2 and displayed in Y column.

Table A.1. Excel table to calculate the ideal parabola fitting in the profile shapes of the strip

x	x^2	Yn	STD	Yn+STD/2	Y
-325	105625	2285	1.10	2286.06	2283.47
-275	75625	2285	2.25	2286.06	2287.08
-225	50625	2289	1.42	2290.06	2290.02
-175	30625	2289	1.62	2290.06	2292.29
-125	15625	2289	1.83	2290.06	2293.89
-75	5625	2294	1.06	2295.06	2294.82
-25	625	2296	2.07	2297.06	2295.07
25	625	2296	2.00	2297.06	2294.65
75	5625	2295	2.66	2296.06	2293.56
125	15625	2290	1.57	2291.06	2291.80
175	30625	2288	1.90	2289.06	2289.37
225	50625	2283	2.95	2284.06	2286.27
275	75625	2282	1.52	2283.06	2282.49
325	105625	2277	2.83	2278.06	2278.04

a	b	c
-0.00013	-0.00835	2294.95

As the rows Y, x^2 and x in Table A.1 represent a point in the ideal parabola of the form:

$$Y = ax^2 + bx + c$$

Selecting any three points in the parabola is enough to calculate the values of a, b and c in the equation and construct the fitting parabola with all the included values of strip width.

Once the fitting parabola is constructed, the real thickness values are subtracted from the corresponding ideal parabola values. Consecutive sections of the

difference between the ideal parabola and real values that are above or below the parabola are grouped and the maximum difference is calculated, which correspond to the height of the ridge.

Visual and numerical data are generated from that difference in groups of 10 consecutive strips at the time as shown in the example of Figure A.2. The graphic data allow for a rapid detection of heights above 6µm and the numerical data permits to collect values corresponding to the maximum height of the ridge, its width and position in the strip width. Ridges with widths above 300mm or below 30mm are not considered.

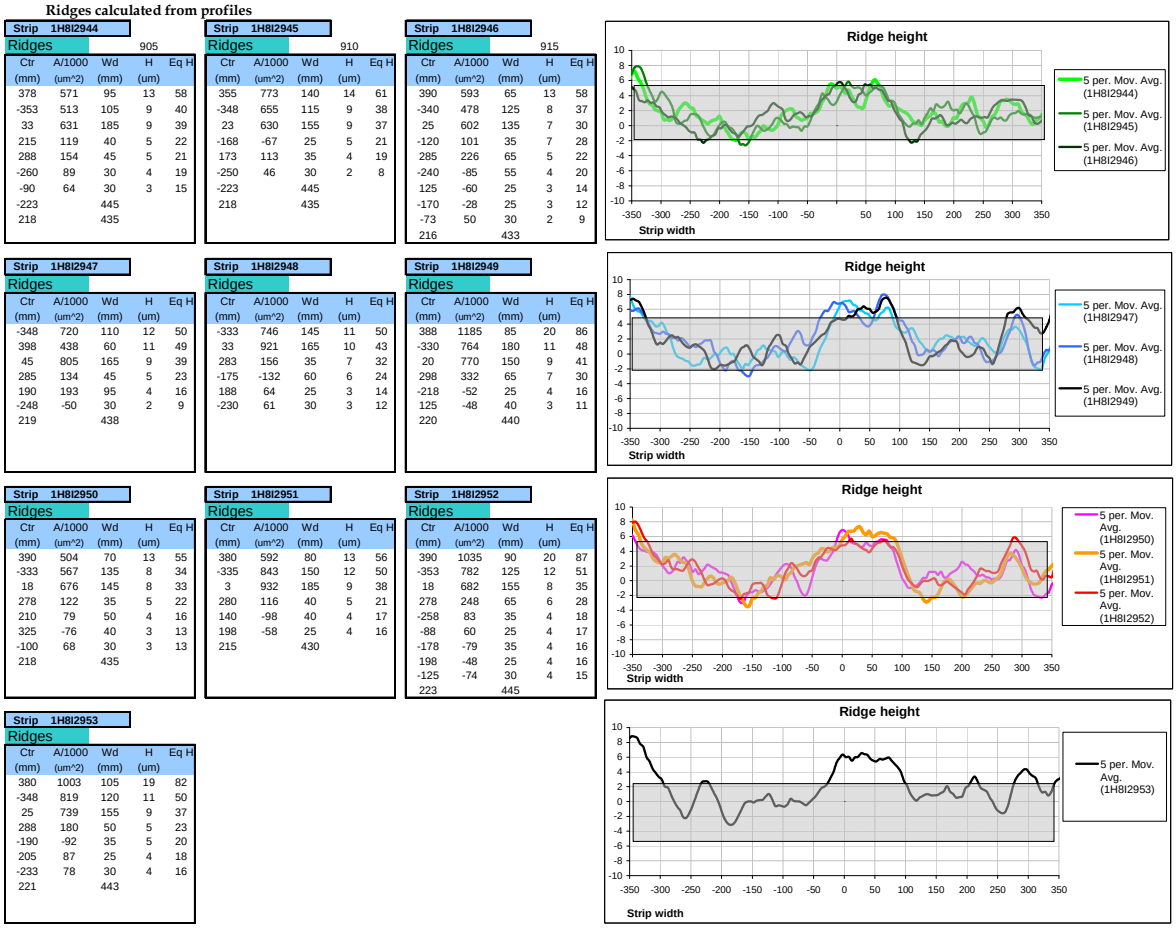

Figure A.2. Representation of the numerical and visual ridge detection program developed by using MS Excel program.

Appendix B

Relevant publications

Melfo W. M., R. J. Dippenaar and C. D. Carter. 2005. "Ridge-Buckle defects in thin rolled steel strip". *Proceedings of the AISTech'05,* Charlotte, NC, USA; Association of Iron and Steel Technology, 2: 367-375.
Selected for publication in the Iron and Steel Technology Magazine. August 2006 p.54-61.

Melfo W. M. and R. J. Dippenaar. 2005. "Ridges in hot rolled strip: microstructural development as a function of temperature variations in the strip". *Proceedings of the AISTech'05,* Charlotte, NC, USA; Association of Iron and Steel Technology, 2: 295-306.

Melfo W. M., R. J. Dippenaar and M. H. Reid. 2006. "In-Situ Study of Scale Formation under Finishing-Mill Operating Conditions". *Proceedings of the AISTech'06 Conference,* 1-4 May. Cleveland, Ohio, USA, 2: 25-35.

Melfo W. M. and R. J. Dippenaar. 2006."In-situ observations of early oxide formation in steel under hot-rolling conditions". *Journal of Microscopy.* In Press.

Index of Figures

Index of Tables